https://doi.org/10.15388/vu.thesis.311
https://orcid.org/0000-0002-8918-9473

VILNIUS UNIVERSITY

Vytenis Šumskas

Finite volume ADI schemes for hybrid dimension heat conduction models

DOCTORAL DISSERTATION

Natural Sciences,
Mathematics (N 001)

VILNIUS 2022

The dissertation was prepared between 2017 and 2021 at Vilnius University.

Academic supervisor – Prof. Habil. Dr. Raimondas Čiegis (Vilnius Gediminas Technical University, Natural Sciences, Mathematics – N 001).
Academic consultant – Prof. Dr. Olga Štikonienė (Vilnius University, Natural Sciences, Mathematics – N 001).

This doctoral dissertation will be defended in a public meeting of the Dissertation Defence Panel:

Chairman – Prof. Habil. Dr. Artūras Štikonas (Vilnius University, Natural Sciences, Mathematics – N001).
Members:
Prof. Dr. Jaan Janno (Tallinn University of Technology, Natural Sciences, Mathematics – N001),
Prof. Dr. Arnas Kačeniauskas (Vilnius Gediminas Technical University, Natural Sciences, Mathematics – N001),
Prof. Dr. Pranas Katauskis (Vilnius University, Natural Sciences, Mathematics – N001),
Doc. Dr. Kristina Kaulakytė (Vilnius University, Natural Sciences, Mathematics – N001).

The dissertation shall be defended at a public meeting of the Dissertation Defence Panel at 4 p.m. on 6th June 2022 in Room 102 of the Faculty of Mathematics and Informatics, Vilnius University.
Address: Naugarduko st. 24, Vilnius, Lithuania.
Tel.: +370 5 219 3050; e-mail: mif@mif.vu.lt.
The text of this dissertation can be accessed at the Library of Vilnius University, as well as on the website of Vilnius University: *www.vu.lt/lt/naujienos/ivykiu-kalendorius*

https://doi.org/10.15388/vu.thesis.311
https://orcid.org/0000-0002-8918-9473

VILNIAUS UNIVERSITETAS

Vytenis Šumskas

Baigtinių tūrių kintamųjų krypčių schemos hibridinės dimensijos šilumos laidumo modeliams

DAKTARO DISERTACIJA

Gamtos mokslai,
Matematika (N 001)

VILNIUS 2022

Disertacija rengta 2017–2021 metais Vilniaus universitete.

Mokslinis vadovas – prof. habil. dr. Raimondas Čiegis (Vilniaus Gedimino technikos universitetas, gamtos mokslai, matematika – N 001).
Mokslinė konsultantė – prof. dr. Olga Štikonienė (Vilniaus universitetas, gamtos mokslai, matematika – N 001).

Gynimo taryba:
Pirmininkas – prof. habil. dr. Artūras Štikonas (Vilniaus universitetas, gamtos mokslai, matematika – N001).
Nariai:
prof. dr. Jaan Janno (Talino technikos universitetas, gamtos mokslai, matematika – N001),
prof. dr. Arnas Kačeniauskas (Vilniaus Gedimino technikos universitetas, gamtos mokslai, matematika – N001),
prof. dr. Pranas Katauskis (Vilniaus universitetas, gamtos mokslai, matematika – N001),
doc. dr. Kristina Kaulakytė (Vilniaus universitetas, gamtos mokslai, matematika – N001).

Disertacija ginama viešame Gynimo tarybos posėdyje 2022 m. birželio mėn. 6 d. 16 val. Vilniaus universiteto Matematikos ir informatikos fakulteto 102 auditorijoje. Adresas: Naugarduko g. 24, Vilnius, Lietuva, tel. +370 5 219 3050; el. paštas mif@mif.vu.lt.

Disertaciją galima peržiūrėti Vilniaus universiteto bibliotekoje ir VU interneto svetainėje adresu:
www.vu.lt/lt/naujienos/ivykiu-kalendorius

Contents

Notation

$\mathbb{R}$	set of real numbers
Δ	Laplace operator
∂	boundary
∂_D	boundary with Dirichlet boundary condition
∂_N	boundary with Neumann boundary condition
$\frac{\partial}{\partial x}$	partial derivative with respect to x
∂_r	discrete partial derivative with respect to r
Ω	domain
$\overline{\Omega}_h$	numerical mesh with endpoints included
Ω_h	numerical mesh without endpoints
$\Omega_{h,RD}$	numerical mesh of reduced dimension model
A_1^h	discrete 2nd derivative operator
$\mathcal{A}_1^h$	discrete 2nd derivative operator of hybrid dimension
S	averaging operator
δ	distance at which dimension is reduced
$\delta = \delta^*$	notation for the case of full dimension model
$e(\delta)$	error with respect to dimension reduction parameter δ
$e(\tau)$	error with respect to time step τ
e_r	relational error
$\rho(\tau)$	experimental convergence rate in time

Introduction

Research topic

The focus of this dissertation is on reduced dimension models of partial differential equations (PDEs) that are solved using numerical methods. The method of dimension reduction is applied to heat conduction models to reduce the number of dimensions in a part of domain, thus reducing computational time at the cost of some accuracy. Efficient numerical algorithms based on the alternating direction implicit (ADI) schemes are derived to solve obtained hybrid dimension models that couple 1-dimensional (1D) zones with 2D or 3D zones.

On the side, some numerical schemes are constructed and discussed for a problem originating from a model of fluid-structure interaction, where a 3D model has been completely reduced to 1D in the whole domain. A fourth order PDE is solved numerically to analyse some aspects of viscous fluid travelling through an elastic vessel.

This research contributes to the topics of PDE systems with nonlocal boundary conditions, reduced dimension models and their applications to problems of mathematical medicine in thin domains. This dissertation relates to these topics in the sense of numerical and computational mathematics, as the schemes are programmed and analysed from the perspective of their stability, accuracy and computational time.

Actuality

Modelling physical phenomena in domains containing thin structures of rods or plates has been of great interest in industry and medicine [14, 40, 79]. The methods that reduce computational costs of such models are also of big importance [13,43,61,70], as

accurate computations for complex geometries may require a lot of computational resources.

As has been widely researched, the selection of boundary conditions can have a huge impact on mathematical models [5, 31]. They can also greatly depend on nonclassical conditions defined at places of domain where, e.g., coefficients are discontinuous or some surface processes should be included into the model [71,82]. In our case, some nonclassical and nonlocal conjugation conditions are included. From the perspective of a numerical solution, this requires to develop special techniques and to modify the implementation of classical algorithms.

Sensitivity to mentioned conditions is also a case of concern for many models of reduced dimension, where some important properties of a full model are preserved and the approximate solution is close to the solution of a full model [2, 7]. In this dissertation, a partial dimension reduction method is considered, where the dimension of a full model is reduced in a big part of initial domain to increase the speed of numerical computations.

This method was first introduced in [52] by G. Panasenko and is based on the asymptotic analysis of a solution of a partial differential equation set in a domain containing thin tubes and on the analysis of variational formulation. The method of asymptotic partial decomposition of the domain was compared to some existing methods of dimension reduction with respect to precision and computational cost, its effectiveness was confirmed in [1]. Some types of conjugation conditions for the 1D-2D coupling for the heat equation were investigated and compared in [78]. However, the question about the most effective numerical solvers for such problems of hybrid dimension is an important ongoing topic.

One such solver is considered here – an efficient ADI scheme to numerically solve partial dimension reduction problems for nonstationary heat transfer. In the presented research, a general convergence analysis template was applied, which is based on two main properties of discrete schemes – the approximation error and the stability analysis. The main task is to modify these

estimates and some properties of discrete differential operators in the case of nonclassical and nonlocal conjugation conditions.

The numerical time-stepping Peaceman-Rachford ADI method [58] is one of the very first splitting methods. The ADI methods were introduced in the 1950's and 1960's by Douglas, Gunn, Peaceman and Rachford in the USA with some important applications to parabolic problems, e.g. reservoir models [65]. It has been successfully applied to solve a 2D heat equation with Bitsadze-Samarskii type nonlocal boundary condition [67], as well as other problems with some nonclassical conditions [68, 69, 76]. The ADI method was effectively applied to some interesting practical electrochemistry problems in [6,41]. Although the ADI method is somewhat limited to 2D problems (except for 3D models that can be simplified to 2D, e.g., see [38]), it is powerful due to its unconditional stability and high efficiency. For what is considered to be the closest candidate to the extension from 2D to 3D of the ADI splitting, we refer the reader to the method of stabilizing corrections [28, 31].

The heat equation is itself of big practical importance in modelling [36, 72]. An interesting parallelisation of temperature distribution problem was done in [34]. An interesting example of hyperbolic heat equation was solved in [33]. The heat equation can also be encountered in other models, e.g., while solving the Navier-Stokes equation in a cross section of a vessel [22]. As Navier-Stokes equations describe the flow of fluids, they are also of big importance in problems concerning mathematical medicine.

The knowledge acquired by using these methods extends the author's expertise for further participation in the research of multiscale mathematical and computer modeling[1]. Chapter 3 here is provided as a supplementary example of ongoing further research. In this chapter, a fourth order PDE with constant coefficients originating from a reduced dimension model of fluid-structure interaction [56] was solved numerically to analyse some aspects of fluid flowing through an elastic tube. Here the aver-

[1] `www.hemodynamics.mif.vu.lt`

aged velocity of fluid is analysed instead of a full 3D solution. Therefore, a numerical solution can be acquired faster with the cost of lower accuracy. For practical simulations of fluid dynamics, efficient numerical strategies and methods with reasonable computational times are an important ongoing research topic.

Aims

The main goal of this dissertation is to develop easy-to-implement comprehensive numerical methods for the hybrid dimension problems, when a smaller part of the model is left full-dimensional, while in the main part of the domain the number of dimensions is reduced to one.

Methods

The process of heat conduction is modelled by a classical parabolic heat conduction PDE for a temperature variable U with a heating function f.

Then, following the results of G. Panasenko, the method of partial dimension reduction (see, e.g., [57]) is used to formulate an approximate problem with hybrid dimensions. For example, in some part of domain the Laplace operator Δ, which consists of the sum of second order spatial derivatives, only retains one spatial variable.

A reasonable gluing of zones of different dimensions is achieved by including the classical conjugation condition that describes the continuity of a solution (for example, at truncation $x = \delta$)

$$U|_{x=\delta-0} = U|_{x=\delta+0}$$

and the nonclassical conjugation condition that describes conservation of full fluxes along the separation

$$\left.\frac{\partial S(U)}{\partial x}\right|_{x=\delta-0} = \left.\frac{\partial U}{\partial x}\right|_{x=\delta+0},$$

here S in an averaging operator that averages the values of a larger dimension zone to be used as a single point in calculations.

Numerical methods are introduced to solve the approximate model of hybrid dimensions – the spatial derivatives are approximated using the finite volume method (FVM [18]) and the time derivative is approximated using the ADI method (for further reading see, e.g., [31]), thus for a 2D case the scheme to advance from time level n to $n+1$ consists of 2 time substeps and reads

$$\begin{aligned} &\frac{U_{jk}^{n+\frac{1}{2}} - U_{jk}^{n}}{\tau/2} + A_1 U_{jk}^{n+\frac{1}{2}} + A_2 U_{jk}^{n} = f_{jk}^{n+\frac{1}{2}}, \\ &\frac{U_{jk}^{n+1} - U_{jk}^{n+\frac{1}{2}}}{\tau/2} + A_1 U_{jk}^{n+\frac{1}{2}} + A_2 U_{jk}^{n+1} = f_{jk}^{n+\frac{1}{2}}. \end{aligned} \tag{1}$$

with the spatial discretization operators defined by

$$\begin{aligned} \partial_x U_{jk}^{n} &= \frac{U_{jk}^{n} - U_{j-1,k}^{n}}{h}, \\ A_1^h U_{jk} &= \frac{1}{V_{jk}} \left(-s_{j+\frac{1}{2},k}^{j} \partial_x U_{j+1,k}^{n} + s_{j-\frac{1}{2},k}^{j} \partial_x U_{jk}^{n} \right) \end{aligned}$$

and

$$\begin{aligned} \partial_y U_{jk}^{n} &= \frac{U_{jk}^{n} - U_{j,k-1}^{n}}{H}, \\ A_2^h U_{jk} &= \frac{1}{V_{jk}} \left(-s_{j,k+\frac{1}{2}}^{k} \partial_y U_{j,k+1}^{n} + s_{j,k-\frac{1}{2}}^{k} \partial_y U_{jk}^{n} \right), \end{aligned}$$

here s, V are some constants related to the FVM and h, H are the spatial step sizes in directions x and y. The scheme (1) is implicit and in each substep of it, only one operator is treated implicitly.

Applying this scheme at points of numerical mesh, the classical model results in a well-behaved tridiagonal matrix, however, for the hybrid dimension case the classical tridiagonal matrix algorithm has to be modified to include nonclassical conjugation conditions. The latter form a system of conditions for the points of truncation zones and the corresponding matrix is shown to be diagonally dominant, thus a unique numerical solution exists for the FVM ADI scheme, finding the solution to the hybrid dimension problem.

The implementation of numerical tests was achieved by using MATLAB and C++ programming languages. The well-known Runge test was applied to inspect the accuracy of time integration. Experimental convergence rates were computed to confirm the theoretical error estimates. The maximum norm was used in error analysis to confirm the efficiency of dimension reduction technique.

Novelty

Few studies focus on the partial dimension reduction for PDEs. A more common approach is the full dimension reduction, which gives larger errors but has a greater effect on the reduction of computational costs. This dissertation might be best seen as an offshoot of some recent research of partial dimension reduction for the heat equation models [3, 57] that later went off to some more practical applications for the fluid flow problems [7, 12, 54, 56].

One of the most important contributions of this dissertation is the implementation of the ADI method for the hybrid dimension models. The finite volume method is considered in this field naturally, however, the standard methods to step in time are often numerical Euler schemes with the first order accuracy in time. In this dissertation, a second order accuracy in time was achieved with the efficient ADI scheme. Furthermore, some important properties for the operators of discrete derivatives were proven for the partially reduced dimension geometries.

Defended propositions

1. Partial dimension reduction is an effective method to reduce computational costs of finding a numerical solution, while preserving high accuracy for the heat conduction models.

2. The constructed FVM ADI scheme is well compatible with the partial dimension reduction technique for the models of

heat conduction. It possesses a unique numerical solution which can be computed efficiently, with the error of second order in space and time.

Dissemination of results

Conferences

1. 8th European Congress of Mathematics, 20-26 June 2021, online: ADI scheme for partially dimension reduced heat conduction models.

2. Lithuanian Mathematical Society LXII Conference, 16-17 June 2021, online: FVM ADI scheme for hybrid dimension heat conduction models.

3. Young Researchers for Smart Society, 13 May 2021, online: Solution of hybrid dimension heat conduction models with FVM ADI scheme.

4. International Conference on Mathematical Sciences, 7-9 October 2021, online: Numerical analysis of a FDM solution to a fluid-structure interaction problem.

Publications

1. R. Čiegis, G. Panasenko, K. Pileckas, V. Šumskas, *ADI scheme for partially dimension reduced heat conduction models*, Comput. Math. with Appl., **80** (2020), 1275-1286.

2. V. Šumskas, R. Čiegis, *Finite volume ADI scheme for hybrid dimension heat conduction problems set in a cross-shaped domain*, Lith. Math. J. (2022).

Structure of the dissertation

The primary part of this thesis consists of introduction, two main chapters, one supplementary chapter, conclusions and a list of references.

Chapter 1 considers a model of heat conduction set in a 3D tube with a radial symmetry condition. In Section 1.1 the nonstationary heat conduction equation is formulated in a cylindrical tube and the initial and boundary conditions are specified. In Section 1.2 the FVM ADI scheme is constructed for the full problem in the cylindrical tube. In Section 1.3 the convergence of the FVM ADI scheme is considered. The approximation error is shown to be of order $O(\tau^2+h^2+H^2)$, the unconditional stability of ADI scheme and some properties of spatial discretization operators are proven. In Section 1.4 the approximate solution is defined by considering a reduced model, where the domain is simplified by coupling 3D regions with 1D reduced dimension tube. The nonclassical and nonlocal conjugation conditions are defined at the truncations of the tube. In Section 1.5 the backward Euler scheme for the reduced model is considered as a side problem and some properties of spatial discretization operators in the hybrid dimension case are proven. In Section 1.6 the unique existence of the FVM ADI numerical solution to the hybrid dimension model is proven, along a constructive algorithm of how the classical tridiagonal solver has to be modified to include nonclassical conjugation conditions. In Section 1.7 the convergence of the FVM ADI scheme for the hybrid model is considered. The stability of proposed scheme is investigated in a special energy norm. Section 1.8 discusses some computational experiments with 1 or 2 reduced zones. The experimental convergence rates agree well with the theoretical convergence estimates. Some conclusions of Chapter 1 are stated in Section 1.9.

Chapter 2 investigates a similar 2D problem. In Section 2.1 the nonstationary heat transfer problem is set up in a cross-shaped domain. In Section 2.2 FVM is formulated for this problem. In Section 2.3 the convergence of the ADI scheme is analysed. In Section 2.4 the dimension reduction technique is established and a reduced model is presented. In Section 2.5 an algorithm is constructed to modify the classical Thomas method to preserve a unique solution with reduced dimension zones. In

Section 2.6 the convergence of the constructed scheme for the hybrid model is considered. In Section 2.7 results of computational experiments are presented. Section 2.8 states some conclusions of the Chapter 2.

Chapter 3 briefly covers author's contribution to one of the problems that were encountered in further scientific research. In Section 3.1, a 4th order PDE problem is formulated and some aspects of dimensional analysis are presented. The equation is discussed from the perspective of mathematical physics, as including multiple physical phenomena. Some recommendations for the numerical solver are noted there. In Section 3.2, a numerical scheme is constructed using forward and central finite differences. Its stability is analysed in Section 3.3 and accuracy is analysed in Section 3.4. Section 3.5 discusses some issues of initial and boundary conditions. Computational tests of the accuracy of constructed solver are provided in Section 3.6. In Section 3.7, an alternative scheme is constructed using central finite differences instead of forward finite differences. Its stability and accuracy are briefly analysed. Section 3.8 discusses some conclusions that arise from comparing these two schemes, as well as comparing different boundary conditions.

The final Chapter 4 summarizes some general conclusions.

1 FVM ADI scheme for 3D models set in a rod with radial symmetry

In this chapter, a heat conduction problem is considered in a 3-dimensional rod that satisfies the radial symmetry condition. Due to it, the 3D cylinder can be considered as a spin of a 2D plate. Then the dimension of this 2D problem is reduced to 1 in some parts of the domain, thus losing some accuracy, but also reducing computational costs to acquire a solution.

Perhaps the closest ideological analogue for speeding-up the solution is the adaptive grid method [46, 74]. At places where the solution does not differ much along the radius, we reduce the dimension from 2 to 1, while an adaptive grid method would take the opportunity to increase the size of grid elements, thus also requiring less computational resources to obtain a solution.

While the theory regarding the reduction of dimension has been well established in numerous works of G. Panasenko [3, 52, 57], here we aim to effectively implement it numerically and the proposed suggestion is the Peaceman-Rachford alternating direction implicit (ADI) method. Its robustness for 2D problems is well-known [31]. Furthermore, as will be seen in this chapter, some specifications of presented model are quite reasonable in terms of numerical analysis, if the ADI method is used.

1.1 Formulation of the classical model

Let us consider a tube $\mathcal{T} \subset \mathbb{R}^3$, which has the following form in cylindrical coordinates (r, ϕ, z): $\mathcal{T} = D \times (0, l)$, where D is a disc of radius R: $D = \{(r, \phi) : 0 < r < R, 0 \leqslant \phi < 2\pi\}$. Here l is the length of the cylindrical tube.

We are interested in solving a linear heat equation in $\mathcal{T} \times (0,T)$. Let us assume that the initial and boundary conditions and all coefficients satisfy the radial symmetry condition (that is, they are independent of ϕ), thus the following problem is acquired

$$\begin{cases} \dfrac{\partial u}{\partial t} = \dfrac{1}{r}\dfrac{\partial}{\partial r}\Big(r\dfrac{\partial u}{\partial r}\Big) + \dfrac{\partial^2 u}{\partial z^2} + f(r,z,t), (r,z,t) \in Q_T = \Omega \times (0,T], \\ u(r,0,t) = g_1(r,t), \quad u(r,l,t) = g_2(r,t),\ (r,t) \in (0,R] \times (0,T], \\ r\dfrac{\partial u}{\partial r} = 0, \quad 0 < z < l, r = 0 \text{ and } r = R,\ 0 < t \leqslant T, \\ u(r,z,0) = u^0(r,z), \quad (r,z) \in \Omega. \end{cases} \tag{1.1}$$

Here $\Omega = \{(r,z) \in (0,R) \times (0,l)\}$.

The implementation of radial symmetry assumption gives rise to the problem (1.1) with only two spatial variables. The specifications of this transformation are a well-known result (see, e.g., [17]).

1.2 FVM ADI scheme

The spatial discretization is implemented using the finite volume method (FVM, also known as the subdomain method, e.g., see [60]).

In general, the finite volume method can be considered as a way to construct an advanced scheme of finite difference method (FDM). More precisely, schemes of finite differences whose derivation roots in a conservation law, are also called finite volume schemes. In FDM discretizations, the unknowns are considered as points in grid, while the FVM framework considers cells (also called control volumes) and the unknowns are fundamentally considered as averages over cells. An analogue to FVM is a set of neighbouring body cells that can exchange some quantities over the walls in such a way that overall the conservation law must hold. The formulation of FVM uses fluxes through cell walls and it is a natural approach, especially in models with

Neumann boundary conditions. It gives rise to a better intuitive understanding of the physical interpretation of some operations.

The finite volume method might be a better choice than FDM to approximate some stiff terms more accurately, as an average over cell is taken instead of a value at one point. However, for most problems there is little practical difference, since cell midpoints can be viewed as somewhat good approximations of averages over the cells and vice versa. Overall, the FVM framework should be seen as a somewhat core virtue to understanding advanced numerical methods rather than a competitor to FDM.

Now, let us define the uniform spatial mesh as $\bar{\Omega}_h = \bar{\omega}_r \times \bar{\omega}_z$ with

$$\bar{\omega}_r = \{r_j : \quad r_j = jh, \quad j = 0, \dots, J\}, \quad r_J = R,$$
$$\bar{\omega}_z = \{z_k : \quad z_k = kH, \quad k = 0, \dots, K\}, \quad z_K = l.$$

Here h and H are the space step sizes. We are using the so-called cell-centred finite volume method (see, e.g., [31]). Each discrete unknown is defined at a point (r_j, z_k) and is associated with a control volume $\mathcal{K}_{j,k}$. For simplicity of notations, we also consider a uniform time mesh:

$$\bar{\omega}_t = \{t^n : \quad t^n = n\tau, \qquad n = 0, \dots, N\}, \quad t^N = T,$$

here τ is the time step size.

Let U^n_{jk} be a numerical approximation to the exact solution $u(r_j, z_k, t^n)$ of problem (1.1) at the grid point (r_j, z_k, t^n).

For functions defined on the grid $\Omega_h \times \omega_t$, we introduce the discrete operators with respect to z and r:

$$\partial_z U^n_{jk} := \frac{U^n_{jk} - U^n_{j,k-1}}{H},$$
$$A^h_2 U^n_{jk} := -\frac{1}{H}\Big(\partial_z U^n_{j,k+1} - \partial_z U^n_{jk}\Big)$$

and

$$\partial_r U^n_{jk} := \frac{U^n_{jk} - U^n_{j-1,k}}{h},$$
$$A^h_1 U^n_{jk} := -\frac{1}{\widetilde{r}_j h}\Big(r_{j+\frac{1}{2}} \partial_r U^n_{j+1,k} - r_{j-\frac{1}{2}} \partial_r U^n_{jk}\Big),$$

where

$$\widetilde{r}_0 = \frac{1}{8}h,\ \widetilde{r}_j = r_j,\ 1 \leqslant j < J,\ \widetilde{r}_J = \frac{1}{2}\big(R - \frac{h}{4}\big), r_{-\frac{1}{2}} = 0, r_{J+\frac{1}{2}} = 0.$$

Note that here almost all coefficients of derivative terms coincide with coefficients of analogous simplest scheme of FDM. Only the first and last coefficients differ, as the grid is equidistant and discrete approximation of diffusion operators is obtained by using FVM.

Then the heat conduction problem (1.1) is approximated by the following Peaceman-Rachford ADI [31] scheme

$$\begin{aligned}
&\frac{U_{jk}^{n+\frac{1}{2}} - U_{jk}^{n}}{\tau/2} + A_1^h U_{jk}^{n+\frac{1}{2}} + A_2^h U_{jk}^{n} = f_{jk}^{n+\frac{1}{2}},\ \ (r_j, z_k) \in \bar{\omega}_r \times \omega_z,\\
&\frac{U_{jk}^{n+1} - U_{jk}^{n+\frac{1}{2}}}{\tau/2} + A_1^h U_{jk}^{n+\frac{1}{2}} + A_2^h U_{jk}^{n+1} = f_{jk}^{n+\frac{1}{2}},\ \ (r_j, z_k) \in \bar{\omega}_r \times \omega_z.
\end{aligned} \tag{1.2}$$

At the first step, the 2D system to implicitly obtain $U^{n+\frac{1}{2}}$ is split into a set of implicit 1D problems along the r coordinate and each subproblem is solved by using the classical fast factorization algorithm. At the second step, the 1D subproblems to find U^{n+1} are solved along the z coordinate.

1.3 Convergence of the FVM ADI scheme

In this section some classical substantial results of the ADI scheme are merely fit to our case and formulated in the notations of yet nonreduced model.

Lemma 1.1. *If a solution of the problem* (1.1) *is sufficiently smooth, then the approximation error of ADI scheme* (1.2) *is* $O(\tau^2 + h^2 + H^2)$.

Proof. Taking into account the boundary conditions of ADI scheme (1.2), we get that

$$U_{jk}^{n+\frac{1}{2}} = \frac{U_{jk}^{n+1} + U_{jk}^{n}}{2} + \frac{\tau}{4} A_2^h (U_{jk}^{n+1} - U_{jk}^{n}),$$
$$\frac{U_{jk}^{n+1} - U_{jk}^{n}}{\tau} + A_1^h U_{jk}^{n+\frac{1}{2}} + A_2^h \Big(\frac{U_{jk}^{n+1} + U_{jk}^{n}}{2} \Big) = f_{jk}^{n+\frac{1}{2}}.$$

After substitution of the first equation into the second one, it follows that the solution of ADI scheme (1.2) satisfies the scheme

$$\frac{U_{jk}^{n+1} - U_{jk}^{n}}{\tau} + A_1^h \Big(\frac{U_{jk}^{n+1} + U_{jk}^{n}}{2} \Big) + A_2^h \Big(\frac{U_{jk}^{n+1} + U_{jk}^{n}}{2} \Big)$$
$$+ \frac{\tau^2}{4} A_1^h A_2^h \Big(\frac{U_{jk}^{n+1} - U_{jk}^{n}}{\tau} \Big) = f_{jk}^{n+\frac{1}{2}}.$$

which is equivalent to the classical symmetrical finite difference scheme up to order $O(\tau^2)$ term. The approximation error of the discrete space operators A_1^h and A_2^h is estimated by using the Taylor expansions. □

Let us consider discrete functions $u_k = u(z_k), v_k = v(z_k)$ defined on the spatial mesh $\bar{\omega}_z$, such that $u_0 = u_K = 0$, $v_0 = v_K = 0$. Then the formulas

$$(u, v) = \sum_{k=1}^{K-1} u_k v_k H, \quad \|u\| = (u, u)^{1/2}$$

define an inner product and a norm in this vector space. We also define one more inner product

$$(\partial_z u, \partial_z v] = \sum_{k=1}^{K} \partial_z u_k \partial_z v_k H.$$

In a similar way, for functions $u_j = u(r_j), v_j = v(r_j)$ defined on the spatial mesh $\bar{\omega}_r$, the formulas

$$[u, v]_r = \sum_{j=0}^{J} \widetilde{r}_j u_j v_j h, \ \ \|u\|_r = [u, u]_r^{1/2},$$
$$(\partial_r u, \partial_r v]_r = \sum_{j=1}^{J} r_{j-\frac{1}{2}} \partial_r u_j \partial_r v_j h$$

define two inner products and a norm in this vector space.

Lemma 1.2. *The discrete operators A_1^h and A_2^h are symmetric and positive semi-definite and positive definite operators, respectively.*

Proof. First, the operator A_2^h is investigated. Applying the summation by parts formula and taking into account the boundary conditions for vectors u and v, we get [66]

$$(A_2^h u, v) = \sum_{k=1}^{K-1} (A_2^h u)_k v_k H = (\partial_z u, \partial_z v].$$

It follows from the obtained equality that A_2^h is a symmetric operator. It is also well-known that the eigenvalue problem

$$A_2^h \phi_l = \lambda_l \phi_l$$

has a complete set of eigenvectors ϕ_l, $l = 1, \ldots, K-1$, and all eigenvalues are positive $\lambda_l > 0$ (see [66]). Thus A_2^h is a positive-definite operator.

Now consider the operator A_1^h. Applying the summation by parts formula, we get

$$\begin{aligned}
[A_1^h u, v]_r &= \sum_{j=0}^{J} \widetilde{r}_j (A_1^h u)_j v_j h \\
&= -r_{\frac{1}{2}} \frac{u_1 - u_0}{h} v_0 - \sum_{j=1}^{J-1} \Big(r_{j+\frac{1}{2}} \frac{u_{j+1} - u_j}{h} r_{j-\frac{1}{2}} \frac{u_j - u_{j-1}}{h} \Big) v_j \\
&- r_{J-\frac{1}{2}} \frac{u_J - u_{J-1}}{h} v_J = r_{\frac{1}{2}} \frac{u_1 - u_0}{h} (v_1 - v_0) \\
&+ \sum_{j=2}^{J-1} r_{j-\frac{1}{2}} \frac{u_j - u_{j-1}}{h} (v_j - v_{j-1}) + r_{J-\frac{1}{2}} \frac{u_J - u_{J-1}}{h} (v_J - v_{J-1}) \\
&= (\partial_r u, \partial_r v]_r.
\end{aligned}$$

It follows from the obtained equality that A_1^h is a symmetric operator. From

$$[A_1^h u, u]_r = (\partial_r u, \partial_r u]_r \geqslant 0$$

we see that A_1^h is a positive semi-definite operator.

The eigenvalue problem

$$A_1^h \psi_l = \mu_l \psi_l$$

has a complete set of eigenvectors ψ_l, $l = 0, \ldots, J$, one eigenvalue $\mu_0 = 0$ and the remaining eigenvalues are positive $\mu_l > 0$. □

Proposition 1.3. *ADI scheme* (1.2) *is unconditionally stable.*

Proof. The Fourier stability analysis is used. Let us consider the solution of ADI scheme (1.2) in the case when boundary conditions $g_j = 0$, $j = 1, 2$. Since operators A_1^h and A_2^h commute, the solution to (1.2) can be written as

$$U_{jk}^{n+1} = \sum_{l=0}^{J} \sum_{r=1}^{K-1} c_{lr}^{n+1} \psi_l(r_j) \phi_r(z_k).$$

Substituting this formula into equations (1.2), we obtain the stability equations for each mode

$$c_{lr}^{n+1} = q_{lr} c_{lr}^{n}, \quad q_{lr} = \frac{(1 - 0.5\tau\lambda_r)(1 - 0.5\tau\mu_l)}{(1 + 0.5\tau\lambda_r)(1 + 0.5\tau\mu_l)}.$$

Since eigenvalues $\lambda_r > 0$, $\mu_l \geqslant 0$, it implies that the ADI scheme (1.2) is unconditionally stable in the L_2 norm. □

Note that here the classical stability analysis is valid because the operators A_1^h and A_2^h commute.

1.4 A hybrid dimension model

Following the approach of A. Amosov and G. Panasenko [3], in this section we consider a modified approximate problem that approximates the classical heat conduction model (1.1). This approach makes use of the observation that in long tubes, the values of heat along the radius tend to smoothen while diffusing through externally unheated parts of domain. Therefore, at places that are sufficiently far from the heating sources, only the average (along the radius) values of heat might be considered and the error made by this approximation is expected to be relatively low.

Let the averaging operator $S(u)$ be defined by

$$S(u) = \frac{2}{R^2}\int_0^R ru(r,z,t)\mathrm{d}r.$$

It is derived by integrating u over a circle and dividing the result by its area, thus finding the averaged value of u.

Next, we assume that the initial condition u^0 and source function f satisfy the relations

$$u^0(r,z) = S(u^0), \quad f(r,z,t) = S(f), \quad (z,t) \in (0,l)\times(0,T].$$

It means that u^0 and f do not depend on r within the tube $\mathcal{T}$.

Denote a reduced tube by $\mathcal{T}_\delta = D\times(\delta, l-\delta)$ and $\Omega_\delta = \{(r,z)\in(0,R)\times(\delta,l-\delta)\}$. Function U is called an approximate solution to problem (1.1) if it satisfies the following problem (for justification see [3])

$$\begin{cases} \dfrac{\partial U}{\partial t} = \dfrac{1}{r}\dfrac{\partial}{\partial r}\Big(r\dfrac{\partial U}{\partial r}\Big) + \dfrac{\partial^2 U}{\partial z^2} + f(z,t), (r,z,t)\in(\Omega\setminus\Omega_\delta)\times(0,T], \\ \dfrac{\partial U}{\partial t} = \dfrac{\partial^2 U}{\partial z^2} + f(z,t), \quad (r,z,t)\in\Omega_\delta\times(0,T], \\ U(r,0,t) = g_1(r,t), \quad U(r,l,t) = g_2(r,t), \ (r,t)\in(0,R]\times(0,T], \\ r\dfrac{\partial U}{\partial r} = 0, \quad z\in(0,\delta)\cup(l-\delta,l), r=0 \text{ and } r=R, \ 0<t\leqslant T, \\ U(r,z,0) = u^0(r,z), \quad (r,z)\in\Omega. \end{cases} \tag{1.3}$$

In $\Omega_\delta\times(0,T]$ the solution U does not depend on r, i.e.

$$U(r,z,t) = S(U), \quad (r,z,t)\in\Omega_\delta\times(0,T].$$

Thus in the reduced tube it is sufficient to find 1D space function $U(0,z,t)$.

By analysing the weak form of the heat equation, it is shown in [3] that the following conjugation conditions are valid at the truncations of the tube

$$U\big|_{z=\delta-0} = U\big|_{z=\delta+0}, \quad U\big|_{z=l-\delta-0} = U\big|_{z=l-\delta+0}, \tag{1.4}$$

$$\frac{\partial S(U)}{\partial z}\Big|_{z=\delta-0} = \frac{\partial U}{\partial z}\Big|_{z=\delta+0}, \quad \frac{\partial U}{\partial z}\Big|_{z=l-\delta-0} = \frac{\partial S(U)}{\partial z}\Big|_{z=l-\delta+0}. \tag{1.5}$$

Conditions (1.4) are classical and mean that U is continuous at the truncation points, while the remaining two conditions (1.5) are nonlocal and they define the conservation of full fluxes along the separation lines.

1.5 The backward Euler scheme for problem (1.3)–(1.5)

Besides some outcomes and notations that contribute to the later results, this section might also be considered as a supplementary example of how to implement the dimension reduction technique numerically using one of the most straightforward schemes, that is, the backward Euler scheme.

Let K_1 and K_2 define the truncation points of the domain $z_{K_1} = \delta$, $z_{K_2} = l - \delta$. Then the spatial mesh ω_z is split into three parts:

$$\begin{aligned}
\omega_{z1} &= \{z_k : \quad z_k = kH, \quad k = 1, \dots, K_1 - 1\}, \\
\omega_{z2} &= \{z_k : \quad z_k = kH, \quad k = K_1 + 1, \dots, K_2 - 1\}, \\
\omega_{z3} &= \{z_k : \quad z_k = kH, \quad k = K_2 + 1, \dots, K - 1\}.
\end{aligned}$$

We define two discrete meshes $\Omega_{h,RD} = (\bar{\omega}_r \times (\omega_{z1} \cup \omega_{z3})) \cup \bar{\omega}_{z2}$ and $\bar{\Omega}_{h,RD} = \Omega_{h,RD} \cup \big(\bar{\omega}_r \times (z_0 \cup z_K)\big)$.

Note that in ω_{z2}, one point along the radius is sufficient for each k, as only one point represents the whole cross section. Therefore, the index notation $*$ will be used for such cases instead of j. The same holds for points on truncation lines between different dimension zones, that is, for $k \in \{K_1, K_2\}$.

We also note that more general meshes are used in [57, 77], where some atypical cells along the interface are constructed that give a nonadmissible mesh. In this paper we use the same finite volume approach. Since the constructed mesh in the full dimension subregions is regular and compact, the obtained discrete problem can be solved efficiently by using the ADI method. We also note a general framework of finite element and finite difference schemes for construction of discrete approximations on

nonmatching grids [18, 19]. A numerical comparison of these methods for 1D-2D discrete schemes is done in [77].

The heat conduction problem (1.3)–(1.5) is approximated by the backward Euler scheme

$$\frac{U_{jk}^{n+1}-U_{jk}^{n}}{\tau}+A_1^hU_{jk}^{n+1}+A_2^hU_{jk}^{n+1}=f_{jk}^{n+1},$$
$$(r_j,z_k)\in\bar\omega_r\times(\omega_{z1}\cup\omega_{z3}),\quad(1.6)$$
$$\frac{U_{*k}^{n+1}-U_{*k}^{n}}{\tau}+A_2^hU_{*k}^{n+1}=f_{*k}^{n+1},\quad z_k\in\omega_{z2},$$
$$\frac{U_{*K_1}^{n+1}-U_{*K_1}^{n}}{\tau}+\frac{1}{H^2}\Big(-S_h(U_{K_1-1}^{n+1})+2U_{*K_1}^{n+1}-U_{*,K_1+1}^{n+1}\Big)=f_{*K_1}^{n+1},$$
$$(1.7)$$
$$\frac{U_{*K_2}^{n+1}-U_{*K_2}^{n}}{\tau}+\frac{1}{H^2}\Big(-S_h(U_{K_2+1}^{n+1})+2U_{*K_2}^{n+1}-U_{*,K_2-1}^{n+1}\Big)=f_{*K_2}^{n+1},$$
$$U_{j0}^{n+1}=g_1(r_j,t^{n+1}),\quad U_{jK}^{n+1}=g_2(r_j,t^{n+1}).\quad(1.8)$$

Here S_h denotes the discrete averaging operator

$$S_h(U_k^n)=\frac{2}{R^2}\sum_{j=0}^{J}\widetilde r_jU_{jk}^nh.$$

Note that equations (1.7) approximate the nonlocal flux conjugation conditions:

$$\sum_{j=0}^{J}\widetilde r_j\Big(\frac{U_{*,K_1+1}^{n+1}-U_{*K_1}^{n+1}}{H}-\frac{H}{2}\Big(\frac{U_{*K_1}^{n+1}-U_{*K_1}^{n}}{\tau}-f_{*K_1}^{n+1}\Big)\Big)h$$
$$=\sum_{j=0}^{J}\widetilde r_j\Big(\frac{U_{*K_1}^{n+1}-U_{j,K_1-1}^{n+1}}{H}+\frac{H}{2}\Big(\frac{U_{*K_1}^{n+1}-U_{*K_1}^{n}}{\tau}-f_{*K_1}^{n+1}\Big)\Big)h,$$
$$(1.9)$$

Now let us consider 2D discrete functions $U_{jk}=U(r_j,z_k),V_{jk}=V(r_j,z_k)$ defined on the spatial mesh $\bar\Omega_{h,RD}$. We denote the set of such vectors by D_h.

For $U,V\in D_h$, such that $U_{j0}=U_{jK}=0$, $V_{j0}=V_{jK}=0$, $r_j\in\bar\omega_r$ the formulas

$$(U,V)=\sum_{j=0}^{J}\widetilde{r}_j\Big(\sum_{k=1}^{K_1-1}U_{jk}V_{jk}H+\sum_{k=K_2+1}^{K-1}U_{jk}V_{jk}H\Big)h$$
$$+\frac{R^2}{2}\sum_{k=K_1}^{K_2}U_{*k}V_{*k}h,\quad \|U\|=(U,U)^{1/2}$$

define an inner product and a norm in this 2D vector space.

Our main aim is to investigate the solvability of the discrete scheme (1.6)–(1.8). The second aim is to demonstrate that efficient algorithms based on MG methods can be used to compute the solution of this nonlocal problem.

Let us define two operators for $U\in D_h$:

$$\mathcal{A}_1^hU=\begin{cases}A_1^hU_{jk}, & (r_j,z_k)\in\bar{\omega}_r\times(\omega_{z1}\cup\omega_{z3}),\\ 0, & z_k\in\bar{\omega}_{z2},\end{cases}$$

$$\mathcal{A}_2^hU=\begin{cases}A_2^hU_{jk}, & (r_j,z_k)\in\bar{\omega}_r\times(\omega_{z1}\cup\omega_{z3}),\\ A_2^hU_{*k}, & z_k\in\omega_{z2},\\ \frac{1}{H^2}\big(-S_h(U_{K_1-1})+2U_{*K_1}-U_{*,K_1+1}\big), & k=K_1,\\ \frac{1}{H^2}\big(-S_h(U_{K_2+1})+2U_{*K_2}-U_{*,K_2-1}\big), & k=K_2.\end{cases}$$

Then we can write the backward Euler scheme as

$$\frac{U^{n+1}-U^n}{\tau}+(\mathcal{A}_1^h+\mathcal{A}_2^h)U^{n+1}=f^{n+1},\quad (r_j,z_k)\in\Omega_{h,RD}.$$

Considering the conjugation conditions, the current spatial approximation ensures some important properties of the discrete operators $\mathcal{A}_1^h$ and $\mathcal{A}_2^h$ that are presented in the lemma below. In general, other approximations might not necessarily result in the same properties.

Lemma 1.4. *The discrete operators $\mathcal{A}_1^h$ and $\mathcal{A}_2^h$ are symmetric and positive semi-definite and positive definite operators, respectively.*

Proof. Let us consider $U,V\in D_h$, such that $U_{j0}=U_{jK}=0$, $V_{j0}=V_{jK}=0$, $r_j\in\bar{\omega}_r$.

First, the operator $\mathcal{A}_1^h$ is investigated. Applying the summation by part formula, we get

$$(\mathcal{A}_1^h U, V) = \sum_{j=1}^{J} r_{j-\frac{1}{2}} \Big(\sum_{k=1}^{K_1-1} \partial_r U_{jk} \partial_r V_{jk} H + \sum_{k=K_2+1}^{K-1} \partial_r U_{jk} \partial_r V_{jk} H \Big) h$$
$$= (U, \mathcal{A}_1^h V), \ (\mathcal{A}_1^h U, U) \geqslant 0.$$

It follows from the obtained estimates that $\mathcal{A}_1^h$ is a symmetric and positive semi-definite operator.

Next, the operator $\mathcal{A}_2^h$ is investigated. Applying the summation by parts formula and taking into account the boundary conditions for vectors U, V, we get

$$(\mathcal{A}_2^h U, V) = \sum_{j=0}^{J} \widetilde{r}_j \Big(\sum_{k=1}^{K_1-1} \big(A_2^h U\big)_{jk} V_{jk} H + \sum_{k=K_2+1}^{K-1} \big(A_2^h U\big)_{jk} V_{jk} H \Big) h$$
$$+ \frac{R^2}{2} \Big(\frac{1}{H} \big(- S_h(U_{K_1-1}) + 2U_{*K_1} - U_{*,K_1+1} \big) V_{*K_1}$$
$$+ \sum_{k=K_1+1}^{K_2-1} \big(A_2^h U\big)_{*k} V_{*k} H - \frac{1}{H} \big(S_h(U_{K_2+1}) - 2U_{*K_2} + U_{*,K_2-1} \big) V_{*K_2} \Big)$$
$$= \sum_{j=0}^{J} \widetilde{r}_j \Big(\sum_{k=1}^{K_1} \partial_z U_{jk} \, \partial_z V_{jk} H - \partial_z U_{jK_1} V_{*K_1} + \sum_{k=K_2+1}^{K} \partial_z U_{jk} \, \partial_z V_{jk} H$$
$$+ \partial_z U_{j,K_2+1} V_{*K_2} \Big) h + \frac{R^2}{2} \Big(\sum_{k=K_1+1}^{K_2} \partial_z U_{*k} \, \partial_z V_{*k} H - \partial_z U_{*K_2} V_{*K_2}$$
$$+ \partial_z U_{*,K_1+1} V_{*K_1} - \partial_z U_{*,K_1+1} V_{*K_1} + \frac{U_{*K_1} - S_h(U_{K_1-1})}{H} V_{*K_1}$$
$$+ \partial_z U_{*K_2} V_{*K_2} - \frac{S_h(U_{K_2+1}) - U_{*K_2}}{H} V_{*K_2} \Big)$$
$$= \sum_{j=0}^{J} \widetilde{r}_j \Big(\sum_{k=1}^{K_1} \partial_z U_{jk} \, \partial_z V_{jk} H + \sum_{k=K_2+1}^{K} \partial_z U_{jk} \, \partial_z V_{jk} H \Big) h$$
$$+ \frac{R^2}{2} \sum_{k=K_1+1}^{K_2} \partial_z U_{*k} \, \partial_z V_{*k} H = (U, \mathcal{A}_2^h V),$$
$$(\mathcal{A}_2^h U, U) \geqslant 0.$$

The nonlocal conjugation conditions (1.9) are used to derive these equalities.

It follows from the obtained estimates that $\mathcal{A}_2^h$ is a symmetric and positive semi-definite operator. From the ellipticity condition it follows that $\mathcal{A}_2^h$ is positive definite. □

1.6 Unique existence of the ADI numerical solution to the hybrid model

In this section, we return to the ADI method to numerically integrate in time, instead of the backward Euler scheme. The definition of operators $\mathcal{A}_1^h$ and $\mathcal{A}_2^h$ is the same as in the latter section. The heat conduction problem (1.3)–(1.5) is approximated by the ADI scheme for $(r_j, z_k) \in \Omega_{h,RD}$ in the following compact form:

$$\frac{U^{n+\frac{1}{2}} - U^n}{\tau/2} + \mathcal{A}_1^h U^{n+\frac{1}{2}} + \mathcal{A}_2^h U^n = f^{n+\frac{1}{2}},$$
$$\frac{U^{n+1} - U^{n+\frac{1}{2}}}{\tau/2} + \mathcal{A}_1^h U^{n+\frac{1}{2}} + \mathcal{A}_2^h U^{n+1} = f^{n+\frac{1}{2}}.$$

For the sake of convenience, the detailed form is also presented. For the first substep it is

$$\frac{U_{jk}^{n+\frac{1}{2}} - U_{jk}^n}{\tau/2} + A_1^h U_{jk}^{n+\frac{1}{2}} + A_2^h U_{jk}^n = f_{jk}^{n+\frac{1}{2}},$$
$$(r_j, z_k) \in \bar{\omega}_r \times (\omega_{z1} \cup \omega_{z3}), \qquad (1.10)$$
$$\frac{U_{*k}^{n+\frac{1}{2}} - U_{*k}^n}{\tau/2} + A_2^h U_{*k}^n = f_{*k}^{n+\frac{1}{2}}, \quad z_k \in \omega_{z2},$$
$$\frac{U_{*K_1}^{n+\frac{1}{2}} - U_{*K_1}^n}{\tau/2} + \frac{1}{H^2}\Big(- S_h(U_{K_1-1}^n) + 2U_{*K_1}^n - U_{*,K_1+1}^n \Big) = f_{*K_1}^{n+\frac{1}{2}},$$
$$\frac{U_{*K_2}^{n+\frac{1}{2}} - U_{*K_2}^n}{\tau/2} + \frac{1}{H^2}\Big(- S_h(U_{K_2+1}^n) + 2U_{*K_2}^n - U_{*,K_2-1}^n \Big) = f_{*K_2}^{n+\frac{1}{2}}$$

and for the second substep it is

$$\frac{U_{jk}^{n+1}-U_{jk}^{n+\frac{1}{2}}}{\tau/2}+A_1^h U_{jk}^{n+\frac{1}{2}}+A_2^h U_{jk}^{n+1}=f_{jk}^{n+\frac{1}{2}},$$

$$(r_j,z_k)\in\bar{\omega}_r\times(\omega_{z1}\cup\omega_{z3}), \qquad (1.11)$$

$$\frac{U_{*k}^{n+1}-U_{*k}^{n+\frac{1}{2}}}{\tau/2}+A_2^h U_{*k}^{n+1}=f_{*k}^{n+\frac{1}{2}},\quad z_k\in\omega_{z2}, \qquad (1.12)$$

$$\frac{U_{*K_1}^{n+1}-U_{*K_1}^{n+\frac{1}{2}}}{\tau/2}+\frac{1}{H^2}\Big(-S_h(U_{K_1-1}^{n+1})+2U_{*K_1}^{n+1}-U_{*,K_1+1}^{n+1}\Big)=f_{*K_1}^{n+\frac{1}{2}}, \qquad (1.13)$$

$$\frac{U_{*K_2}^{n+1}-U_{*K_2}^{n+\frac{1}{2}}}{\tau/2}+\frac{1}{H^2}\Big(-S_h(U_{K_2+1}^{n+1})+2U_{*K_2}^{n+1}-U_{*,K_2-1}^{n+1}\Big)=f_{*K_2}^{n+\frac{1}{2}}. \qquad (1.14)$$

Due to nonlocal conjugation conditions (1.13) and (1.14), the classical factorization algorithm has to be modified in order to solve the 1D subproblems (1.11), (1.12).

Lemma 1.5. *A unique solution of the linear system of equations* (1.11)–(1.14) *exists and it can be computed by using the efficient factorization algorithm.*

Proof. The given proof also defines the constructive algorithm to solve (1.11)–(1.14). For each $r_j\in\omega_r$, the solution is factorized separately in each subdomain ω_{z1}, ω_{z2} and ω_{z3}. Let us rewrite (1.11),(1.12) as

$$-a_{jk}U_{j,k-1}^{n+1}+c_{jk}U_{jk}^{n+1}-b_{jk}U_{j,k+1}^{n+1}=d_{jk},$$
$$a_{jk},\ b_{jk},\ c_{jk}\geqslant 0,\quad c_{jk}\geqslant a_{jk}+b_{jk}.$$

1. *Domain* ω_{z1}. The solution is presented in the following form:

$$U_{jk}^{n+1}=\alpha_{jk}U_{j,k+1}^{n+1}+\gamma_{jk},\quad 0\leqslant k<K_1, \qquad (1.15)$$
$$\alpha_{j0}=0,\ \alpha_{jk}=\frac{b_{jk}}{c_{jk}-a_{jk}\alpha_{j,k-1}},$$
$$\gamma_{j0}=g_1(r_j,t^{n+1}),\ \gamma_{jk}=\frac{d_{jk}+a_{jk}\gamma_{j,k-1}}{c_{jk}-a_{jk}\alpha_{j,k-1}}.$$

By induction it can be proved that the estimates $0 \leqslant \alpha_{jk} \leqslant 1$ are valid.

2. *Domain* ω_{z2}. The solution is presented in the following form:

$$U_{*k}^{n+1} = \alpha_{*k} U_{*K_1}^{n+1} + \beta_{*k} U_{*K_2}^{n+1} + \gamma_{*k}, \quad K_1 < k < K_2. \tag{1.16}$$

This factorization is done in two steps. First, the solution is written in the form

$$U_{*k}^{n+1} = \widetilde{\alpha}_{*k} U_{*K_1}^{n+1} + \widetilde{\beta}_{*k} U_{*,k+1}^{n+1} + \widetilde{\gamma}_{*k}, \quad K_1 < k < K_2, \tag{1.17}$$

$$\widetilde{\alpha}_{*,K_1+1} = \frac{a_{*,K_1+1}}{c_{*,K_1+1}}, \quad \widetilde{\alpha}_{*k} = \frac{a_{*k}}{c_{*k} - a_{*k}\widetilde{\beta}_{*,k-1}} \widetilde{\alpha}_{*,k-1},$$

$$\widetilde{\beta}_{*,K_1+1} = \frac{b_{*,K_1+1}}{c_{*,K_1+1}}, \quad \widetilde{\beta}_{*k} = \frac{b_{*k}}{c_{*k} - a_{*k}\widetilde{\beta}_{*,k-1}},$$

$$\widetilde{\gamma}_{*,K_1+1} = \frac{d_{*,K_1+1}}{c_{*,K_1+1}}, \quad \widetilde{\gamma}_{*k} = \frac{a_{*k}\widetilde{\gamma}_{*,k-1} + d_{*k}}{c_{*k} - a_{*k}\widetilde{\beta}_{*,k-1}}.$$

Let us assume that $0 \leqslant \widetilde{\alpha}_{*,k-1}, \widetilde{\beta}_{*,k-1} \leqslant 1$ and $\widetilde{\alpha}_{*,k-1} + \widetilde{\beta}_{*,k-1} \leqslant 1$. Then it follows from the given formulas that $0 \leqslant \widetilde{\beta}_{*k} \leqslant 1$ and $\widetilde{\alpha}_{*k} \geqslant 0$. It remains to prove that $\widetilde{\alpha}_{*k} \leqslant 1$ and $\widetilde{\alpha}_{*k} + \widetilde{\beta}_{*k} \leqslant 1$. It follows from simple inequalities

$$\begin{aligned} &a_{*k}\widetilde{\alpha}_{*,k-1} + b_{*k} + a_{*k}\widetilde{\beta}_{*,k-1} \\ &= a_{*k}(\widetilde{\alpha}_{*,k-1} + \widetilde{\beta}_{*,k-1}) + b_{*k} \leqslant a_{*k} + b_{*k} \leqslant c_{*k}, \end{aligned}$$

that

$$a_{*k}\widetilde{\alpha}_{*,k-1} + b_{*k} \leqslant c_{*k} - a_{*k}\widetilde{\beta}_{*,k-1}.$$

Thus we get the estimate

$$0 \leqslant \widetilde{\alpha}_{*k} + \widetilde{\beta}_{*k} \leqslant 1. \tag{1.18}$$

The proof by induction is completed.

Next, we compute coefficients α_{*k}, β_{*k} and γ_{*k} in formula (1.16)

$$\alpha_{*,K_2-1} = \widetilde{\alpha}_{*,K_2-1}, \quad \beta_{*,K_2-1} = \widetilde{\beta}_{*,K_2-1}, \quad \alpha_{*k} = \widetilde{\alpha}_{*k} + \widetilde{\beta}_{*k}\alpha_{*,k+1}, \tag{1.19}$$

$$\beta_{*k} = \widetilde{\beta}_{*k}\beta_{*,k+1}, \quad \gamma_{*k} = \widetilde{\gamma}_{*k} + \widetilde{\beta}_{*k}\gamma_{*,k+1}, \quad k = K_2 - 2, \ldots, K_1 + 1.$$

From estimates for $\widetilde{\alpha}_{*k}$, $\widetilde{\beta}_{*k}$ and from (1.19) it follows that

$$0 \leqslant \alpha_{*k}, \beta_{*k} \leqslant 1, \quad 0 \leqslant \alpha_{*k} + \beta_{*k} \leqslant 1.$$

3. *Domain* ω_{z3}. For each $j = 0, \ldots, J$, the solution is presented in the following form:

$$\begin{aligned} & U_{jk}^{n+1} = \beta_{jk} U_{j,k-1}^{n+1} + \gamma_{jk}, \quad K_2 < k \leqslant K, \\ & \beta_{jK} = 0, \ \ \beta_{jk} = \frac{a_{jk}}{c_{jk} - b_{jk}\beta_{j,k+1}}, \\ & \gamma_{jK} = g_2(r_j, t^{n+1}), \ \ \gamma_{jk} = \frac{d_{jk} + b_{jk}\gamma_{j,k+1}}{c_{jk} - b_{jk}\beta_{j,k+1}}. \end{aligned} \tag{1.20}$$

By induction it can be proved that the estimates $0 \leqslant \beta_{jk} \leqslant 1$ are valid.

Substituting (1.15)–(1.20) into equations (1.13) and (1.14), we get a linear system of two equations to find $U_{*K_1}^{n+1}$, $U_{*K_2}^{n+1}$:

$$\begin{cases} A_{11} U_{*K_1}^{n+1} + A_{12} U_{*K_2}^{n+1} = B_1 \\ A_{21} U_{*K_1}^{n+1} + A_{22} U_{*K_2}^{n+1} = B_2, \end{cases} \tag{1.21}$$

where coefficients are defined by

$$\begin{aligned} A_{11} &= \frac{2}{\tau} + \frac{1}{H^2}\Big(2 - \alpha_{*,K_1+1} - \frac{2h}{R^2}\sum_{j=0}^{J} \widetilde{r}_j \alpha_{j,K_1-1}\Big), \\ A_{12} &= -\frac{1}{H^2}\beta_{*,K_1+1}, \ \ A_{21} = -\frac{1}{H^2}\alpha_{*,K_2-1}, \\ A_{22} &= \frac{2}{\tau} + \frac{1}{H^2}\Big(2 - \beta_{*,K_2-1} - \frac{2h}{R^2}\sum_{j=0}^{J} \widetilde{r}_j \beta_{j,K_2+1}\Big). \end{aligned}$$

From the estimates given above we have that

$$\begin{aligned} & 2 - \alpha_{*,K_1+1} - \frac{2h}{R^2}\sum_{j=0}^{J} \widetilde{r}_j \alpha_{j,K_1-1} \geqslant \beta_{*,K_1+1}, \\ & 2 - \beta_{*,K_2-1} - \frac{2h}{R^2}\sum_{j=0}^{J} \widetilde{r}_j \beta_{j,K_2+1} \geqslant \alpha_{*,K_2-1}, \end{aligned}$$

thus the determinant of the matrix of system (1.21) is positive and the unique solution $U_{*K_1}^{n+1}$, $U_{*K_2}^{n+1}$ exists. Then the backward factorization step is applied and the rest of values U_{jk}^{n+1} are computed. $\square$

We wish to emphasize that the classical Thomas algorithm, which is widely used in numerical solvers, can be modified using this constructive proof to include nonclassical conjugation conditions. Thus the formulae derived in Lemma 1.5 also contribute to the benefit of users with interest to expand their computational libraries of customized algorithms.

1.7 Convergence of the FVM ADI scheme for the hybrid model

Since the operators $\mathcal{A}_1^h$ and A_2^h do not commute, we can't apply the spectral stability analysis which was used in the classical case. Here we restrict to showing stability estimates in one particular energy norm.

Proposition 1.6. *If U^n is the solution of ADI scheme* (1.10)–(1.14)*, when $f^n \equiv 0$ and $g_1^n = g_2^n \equiv 0$, then the following stability estimate is valid*

$$\|(I + \frac{\tau}{2}\mathcal{A}_2^h)U^n\| \leqslant \|(I + \frac{\tau}{2}\mathcal{A}_2^h)U^0\|. \tag{1.22}$$

Proof. The proof technique of (1.22) is well known, see e.g. [31]. The ADI scheme equations (1.10),(1.11) give $U^{n+1} = RU^n$ with

$$R = \Big(I + \frac{\tau}{2}\mathcal{A}_2^h\Big)^{-1}\Big(I - \frac{\tau}{2}\mathcal{A}_1^h\Big)\Big(I + \frac{\tau}{2}\mathcal{A}_1^h\Big)^{-1}\Big(I - \frac{\tau}{2}\mathcal{A}_2^h\Big)$$

We rewrite this relation as

$$\Big(I + \frac{\tau}{2}\mathcal{A}_2^h\Big)U^{n+1} = \widetilde{R}\Big(I + \frac{\tau}{2}\mathcal{A}_2^h\Big)U^n$$

with operator $\widetilde{R}$ defined by

$$\widetilde{R} = \Big(I - \frac{\tau}{2}\mathcal{A}_1^h\Big)\Big(I + \frac{\tau}{2}\mathcal{A}_1^h\Big)^{-1}\Big(I - \frac{\tau}{2}\mathcal{A}_2^h\Big)\Big(I + \frac{\tau}{2}\mathcal{A}_2^h\Big)^{-1}.$$

By induction we prove that

$$\Big(I + \frac{\tau}{2}\mathcal{A}_2^h\Big)U^n = \widetilde{R}^n\Big(I + \frac{\tau}{2}\mathcal{A}_2^h\Big)U^0.$$

It follows from Lemma 1.2 that $\|\widetilde{R}\| \leqslant 1$, thus

$$\|\widetilde{R}^n\| \leqslant \|\widetilde{R}\|^n \leqslant 1.$$

The proposition is proved. □

It is interesting to note that analogous proof of stability estimate would not work in the case of 3 spatial operators.

The presented stability estimate is with respect to the initial condition. From it, the stability with respect to the right-hand side can also be derived, for example, see [66].

1.8 Computational experiments

Two nodes and one edge

In the first example, a domain with two nodes and one edge is investigated. Consider the problem (1.1) in the tube with geometry parameters $l = 1$, $R = 0.1$. We solve this problem till $T = 1$ with given initial, boundary conditions and the zero source function

$$u^0(r,z) = 0,\ g_1(r,t) = (1+3t)e^{-(r/R)^2},$$
$$g_2(r,t) = 4te^{-(2r/R)^2},\ f(r,z,t) = 0.$$

The accuracy of time integration of ADI schemes
First, we have tested the time integration accuracy of the ADI solver for the full dimension model. A uniform space grid Ω_h with $J = 100$, $K = 400$ is used. Table 1.1 shows correspondence between a given sequence of decreasing time step widths τ, errors $e(\tau)$ and experimental convergence rates $\rho(\tau)$ of the discrete solution for the ADI scheme (1.2) in the maximum norm

$$e(\tau) = \max_{(r_j,z_k)\in\Omega_h} \left|U_{jk}^N - U(r_j,z_k,T)\right|, \quad \rho(\tau) = \log_2\left(e(2\tau)/e(\tau)\right),$$

where $U(r_j,z_k,T)$ is computed by using the very small time step $\tau = 5\cdot 10^{-5}$. Then the integration error that is introduced by the ADI scheme can be measured accurately.

It follows from the presented results that the accuracy of the ADI scheme agrees well with the theoretical prediction.

The accuracy of the reduced dimension model
Next, we investigate the accuracy of the reduced dimension model

Table 1.1: Errors $e(\tau)$ and experimental convergence rates $\rho(\tau)$ for the discrete solution of ADI scheme (1.2) for a sequence of time steps τ.

τ	$e(\tau)$	$\rho(\tau)$
0.0025	$5.215{\cdot}10^{-3}$	1.631
0.00125	$1.334{\cdot}10^{-3}$	1.958
0.000625	$3.343{\cdot}10^{-4}$	2.006
0.0003125	$8.194{\cdot}10^{-5}$	2.028

(1.3)–(1.5). For the space discretization, a uniform grid Ω_h with $J = 100$, $K = 1600$ is used and integration in time is done with $\tau = 0.0005$. For a sequence of reduction parameters δ, Table 1.2 gives errors $e(\delta)$

$$e(\delta) = \max_{(r_j, z_k) \in \Omega_h} \left| U_{jk}^N - U_{jk}^N(\delta) \right|$$

and relative errors e_r

$$e_r = \frac{e(\delta)}{\left| U_{j^*k^*}^N \right|} \cdot 100\%$$

of the reduced dimension model (1.3)–(1.5) solution in the maximum norm. Here j^*, k^* are indices of the grid point at which the error $e(\delta)$ is found.

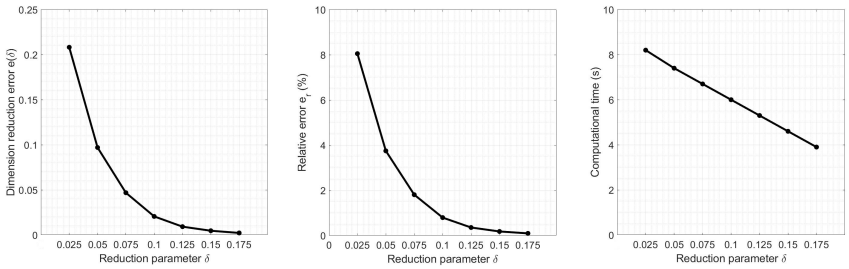

(a) δ vs $e(\delta)$ (b) δ vs e_r (c) δ vs CPU time

Figure 1.1: Graphs of results from Table 1.2, showing correspondence between δ and other data.

It follows from the presented results that starting from $\delta = 0.1$, the accuracy of the reduced dimension model is sufficient

Table 1.2: Errors $e(\delta)$, relative errors e_r and computational times (in seconds) of the discrete solution of the reduced dimension model (1.3)–(1.5) for a sequence of truncation parameters δ. Notation $\delta = \delta^*$ corresponds to the full model

δ	$e(\delta)$	e_r	time
δ^*	–	–	11.4
0.25	0.00013	0.0070%	5.9
0.20	0.00083	0.0421%	4.8
0.15	0.0056	0.2653%	3.7
0.10	0.0377	1.6537%	2.5
0.05	0.2471	9.3954%	1.4

for most real world applications. More generally, we found that for most calculations, starting from δ equal to the radius of the cylinder, the results of hybrid dimension model are visually indistinguishable from the full model.

Three nodes and two edges

In order to show the robustness of the proposed discrete scheme, consider a domain consisting of three full dimension nodes and two edges with a problem defined for $0 \leqslant z \leqslant 2$. One additional node takes into account the influence of the source function. Therefore, the reduced tube is given by $\mathcal{T}_\delta = D \times (\delta, 0.9 - \delta) \cup (1.1 + \delta, l - \delta)$ and $\Omega_\delta = \{(r, z) \in (0, R) \times (\delta, 0.9 - \delta) \cup (1.1 + \delta, l - \delta)\}$. In general, it is assumed that f is a regular function and does not depend on r. But in the central part of the tube $0.9 \leqslant z \leqslant 1.1$, let f still depend on r:

$$f(r, z, t) = 150t \exp(-(r/R)^2) \exp\big(-((z-1)/0.05)^2\big).$$

The implementation of the ADI scheme remains the same. In the new full dimension node, for each $j = 0, \ldots, J$ the solution is presented in the following form:

$$U_{jk}^{n+1} = \alpha_{jk} U_{jK_2}^{n+1} + \beta_{jk} U_{jK_3}^{n+1} + \gamma_{jk}, \quad K_2 < k < K_3.$$

Then we can apply the same factorization algorithm as presented earlier for the ADI scheme in the domain ω_{z2}.

For this test problem, we get a linear system of four equations to find $U^{n+1}_{*K_1}$, $U^{n+1}_{*K_2}$, $U^{n+1}_{*K_3}$, $U^{n+1}_{*K_4}$. A matrix of this system is tridiagonal, thus the standard factorization algorithm can be used to solve it.

The accuracy of time integration of the ADI scheme for the reduced dimension model

Next we have tested the time integration accuracy of the ADI scheme (1.10)–(1.14). For the spacial discretization, the uniform grid Ω_h is used with $J = 100$, $K = 1600$ and the truncation parameter $\delta = 0.1$. Table 1.3 shows correspondence between the given set of decreasing time step widths τ, the errors $e(\tau)$ and the experimental convergence rates $\rho(\tau)$ of the discrete solution for ADI scheme (1.10)–(1.14) in the maximum norm. Here the benchmark solution $U(r_j, z_k, T)$ again is computed by using a very small time step $\tau = 5 \cdot 10^{-5}$.

Table 1.3: Errors $e(\tau)$ and experimental convergence rates $\rho(\tau)$ for the discrete solution of ADI scheme (1.10)–(1.14) in accordance with a sequence of time steps τ and $\delta = 0.1$

τ	$e(\tau)$	$\rho(\tau)$
0.0025	$6.997 \cdot 10^{-3}$	1.279
0.00125	$2.106 \cdot 10^{-3}$	1.732
0.000625	$5.368 \cdot 10^{-4}$	1.972
0.0003125	$1.337 \cdot 10^{-4}$	2.005

The second order convergence rate is clearly seen from the presented results.

Results of computational experiments show that the solution errors $e(\delta)$ of reduced dimension model are almost the same as for the two-noded case. Table 1.4 gives CPU times for different values of truncation parameter δ.

In order to demonstrate accuracy of the reduced dimension model, let us compare solutions of the full and reduced models

Table 1.4: CPU time (in seconds) for computing the reduced dimension model (1.3)–(1.5) solution for a sequence of truncation parameters δ. The column δ^* gives CPU time for computing the full model solution.

	$\delta = \delta^*$	$\delta = 0.25$	$\delta = 0.2$	$\delta = 0.15$	$\delta = 0.1$
CPU time (δ)	24.9	17.0	14.6	12.2	9.8

for truncation parameters $\delta = 0.05$, $\delta = 0.1$ and $\delta = 0.15$. The test problem of three nodes and two edges is solved and all parameters are the same as given above in previous computational experiment, except for $K = 400$. The graphs of solutions are presented in Figures 1.2 – 1.5 (note that for the reduced dimension model, the values of U in reduced one-dimensional zones are replicated vertically to cover the reduced domain).

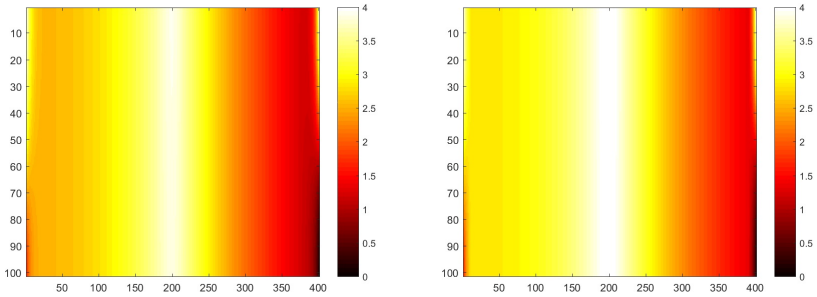

Figure 1.2: Full model and reduced dimension model with $\delta = 0.05$

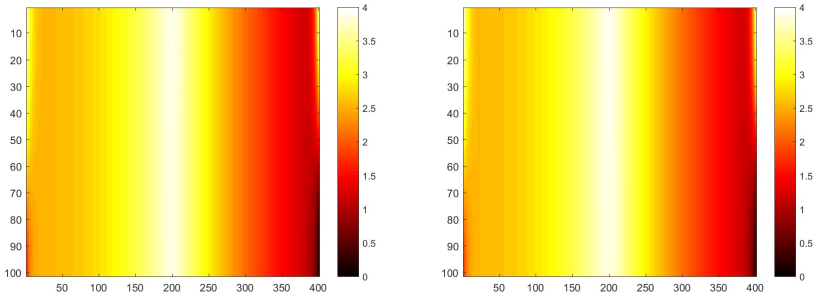

Figure 1.3: Full model and reduced dimension model with $\delta = 0.1$

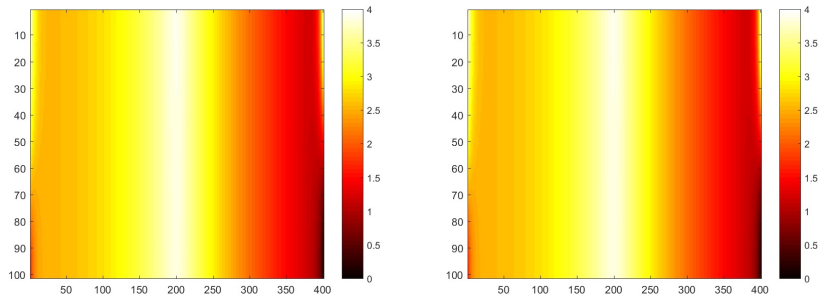

Figure 1.4: Full model and reduced dimension model with $\delta = 0.15$

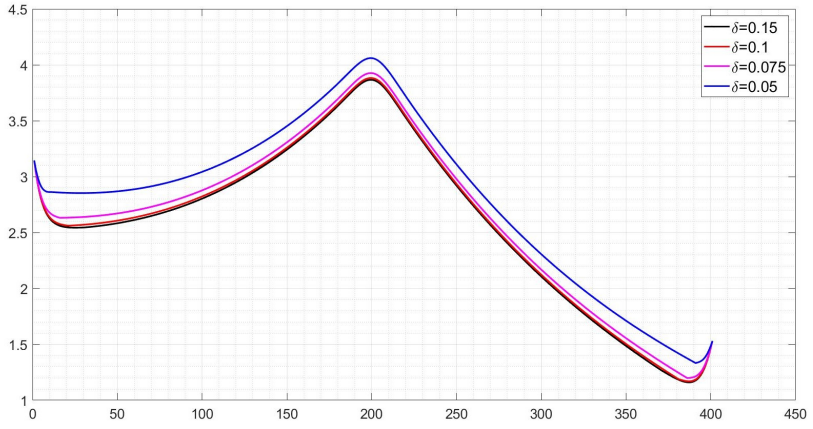

Figure 1.5: Values of solution to hybrid dimension model with different values of δ at cross section $r = R/2$ for two reduced dimension zones.

From the presented results, again a conclusion can be made that starting from $\delta = 0.1$, the accuracy of the reduced dimension model is sufficient for most real world applications.

1.9 Conclusions

The ADI type scheme is constructed to solve the hybrid dimension heat conduction equation. The finite volume method is used to approximate space differential operators with nonclassical conjugation conditions between the parts of different dimensions. The ADI scheme leads to a noniterative implementation

algorithm and a set of one-dimensional linear systems is solved by using the factorization algorithm. An efficient modification of the basic factorization algorithm is developed to resolve nonlocal conjugation conditions. It is proved that the proposed discrete scheme is unconditionally stable. The presented results of numerical experiments confirm the theoretical conclusion that hybrid mathematical models can be used to simulate heat conduction models for a quite broad set of domains and coefficients (also see [3] for an interesting discussion of this topic).

2 FVM ADI scheme for 2D models set in a cross-section domain

In this chapter, the heat conduction problem is considered for a 2D domain that is a cross-section of some plates (see Figure 2.1). Here, the dimension reduction is again the main aspect of results. Although some definitions might be simpler than in the previous case, the current chapter faces new challenges. From the perspective of finite volume method, a new type of computational cell is taken into consideration at inner corners of domain (type #3 in Figure 2.2). Around these corners, the discrete operators of derivatives do not commute. Furthermore, in some zones the x dimension is reduced, while in others the y dimension is reduced. Therefore, some new ideas have to be applied to achieve similar results.

2.1 Formulation of the classical model

Let us consider a cross-shaped domain $\Omega \subset \mathbb{R}^2$. The Dirichlet boundary conditions are defined at the inlets/outlets and we refer to this part of boundary as $\partial_D\Omega$, while the rest of boundary is insulated with a zero Neumann boundary condition and denoted by $\partial_N\Omega = \partial\Omega \setminus \partial_D\Omega$. Given that the length of Ω equals X and the height equals Y, the Dirichlet boundary $\partial_D\Omega = \partial_1\Omega \cup \partial_2\Omega \cup \partial_3\Omega \cup \partial_4\Omega$ is defined by (also see Figure 2.1 below)

$$\partial_1\Omega = \{(x,y) : x = 0,\ Y_1 \leqslant y \leqslant Y_2\},$$
$$\partial_2\Omega = \{(x,y) : y = 0,\ X_1 \leqslant x \leqslant X_2\},$$
$$\partial_3\Omega = \{(x,y) : x = X,\ Y_1 \leqslant y \leqslant Y_2\},$$
$$\partial_4\Omega = \{(x,y) : y = Y,\ X_1 \leqslant x \leqslant X_2\},$$

with real constants X_1, X_2, Y_1 and Y_2 satisfying $0 < X_1 < X_2 < X$ and $0 < Y_1 < Y_2 < Y$.

Let us denote by L_1, L_2, L_3 and L_4 the rods of domain Ω and by L_0 the central part of $\Omega = L_0 \cup L_1 \cup L_2 \cup L_3 \cup L_4$:

$$L_1 = \{(x,y) : 0 \leqslant x \leqslant X_1,\ Y_1 \leqslant y \leqslant Y_2\},$$
$$L_2 = \{(x,y) : X_1 \leqslant x \leqslant X_2,\ 0 \leqslant y \leqslant Y_1\},$$
$$L_3 = \{(x,y) : X_2 \leqslant x \leqslant X,\ Y_1 \leqslant y \leqslant Y_2\},$$
$$L_4 = \{(x,y) : X_1 \leqslant x \leqslant X_2,\ Y_2 \leqslant y \leqslant Y\},$$
$$L_0 = \{(x,y) : X_1 < x < X_2,\ Y_1 < y < Y_2\}.$$

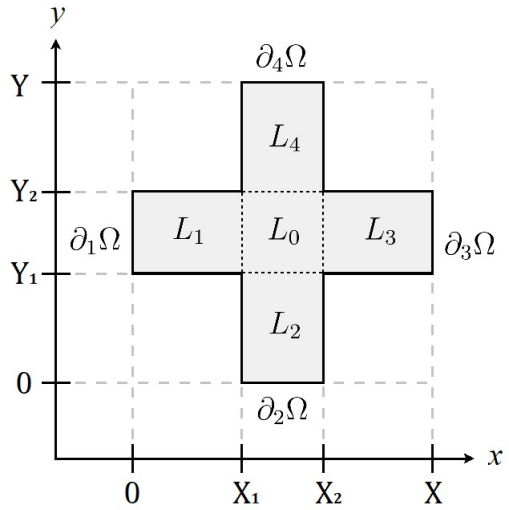

Figure 2.1: Domain Ω (shaded) with located outer boundary layers and rods.

We are interested in solving a linear heat equation with constant coefficients in $\Omega_T = \Omega \times (0,T]$ with Dirichlet boundary

conditions on $\partial_D\Omega$ and Neumann boundary condition on $\partial_N\Omega$, thus the following problem is acquired:

$$\begin{cases} \dfrac{\partial u}{\partial t} = \dfrac{\partial^2 u}{\partial x^2} + \dfrac{\partial^2 u}{\partial y^2} + f(x,y,t), & (x,y,t) \in \Omega_T, \\ u(0,y,t) = g_1(y,t), & (y,t) \in [Y_1, Y_2] \times (0,T], \\ u(x,0,t) = g_2(x,t), & (x,t) \in [X_1, X_2] \times (0,T], \\ u(X,y,t) = g_3(y,t), & (y,t) \in [Y_1, Y_2] \times (0,T], \\ u(x,Y,t) = g_4(x,t), & (x,t) \in [X_1, X_2] \times (0,T], \\ \dfrac{\partial u}{\partial \mathbf{n}} = 0, & (x,y,t) \in \partial_N\Omega \times (0,T], \\ u(x,y,0) = u^0(x,y), & (x,y) \in \Omega, \end{cases} \tag{2.1}$$

here f is a source function and $\mathbf{n}$ denotes the outer normal to $\partial_N\Omega$. The model is presented in a nondimensional form.

2.2 FVM ADI scheme

As in the previous chapter, we are using the so-called cell-centred finite volume method (see, e.g., [31]). Each discrete unknown is defined at a point (x_j, y_k) and is associated with a control volume $\mathcal{K}_{jk}$. Denoting the step size in x direction by h, the step size in y direction by H, an admissible finite volume mesh of Ω is then denoted by $\Omega_h = (\overline{\omega}_x \times \overline{\omega}_y) \cap \Omega$ with

$$\begin{aligned} \overline{\omega}_x &= \{x_j : x_j = jh,\ j = 0,\ \ldots, J\},\ x_J = X, \\ \overline{\omega}_y &= \{y_k : y_k = kH,\ k = 0,\ \ldots, K\},\ y_K = Y. \end{aligned}$$

Furthermore, we will use notations $x_{J_1} = X_1$, $x_{J_2} = X_2$ and $y_{K_1} = Y_1$, $y_{K_2} = Y_2$. Recall that X_1, X_2, Y_1 and Y_2 are the positions of inner walls of domain, where the Neumann boundary condition is formulated.

Therefore, three types of control volumes occur for a cross-shaped domain (see Figure 2.2).

For simplicity of notations, we also consider a uniform time mesh

$$\overline{\omega}_t = \{t^n : t^n = n\tau,\ n = 0,\ \ldots, N\},\ t^N = T.$$

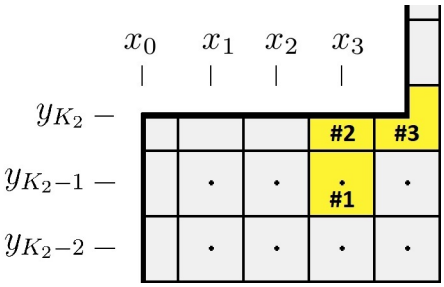

Figure 2.2: Example of celling of the top border of L_1.

Let us now define the following measures: area of control volume as $V_{jk} = m(\mathcal{K}_{jk})$ and length of the border σ_{jk} of control volume as $s_{\alpha\beta} = m(\sigma_{\alpha\beta})$. Figure 2.3 shows how these values vary for three types of control volumes.

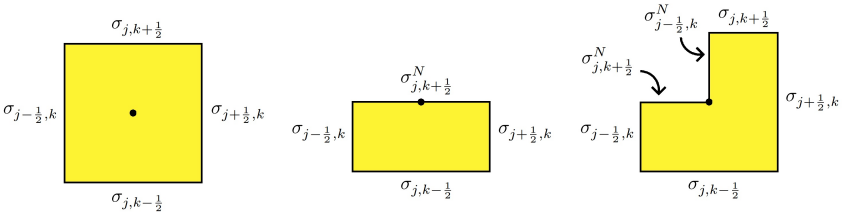

(a) Type#1:$V_{jk} = hH$ (b) Type#2:$V_{jk} = h\dfrac{H}{2}$ (c) Type#3:$V_{jk} = \dfrac{3hH}{4}$

Figure 2.3: Borders of three types of control volumes $\mathcal{K}_{jk}$ defined at (x_j, y_k). Here the upper index N corresponds to the notation of Neumann type boundary.

Consider, for example, the left-side borders of Figure 2.3 (c), namely $\sigma_{j-\frac{1}{2},k}$ and $\sigma^N_{j-\frac{1}{2},k}$. Regarding a flux through the left side of such cell, in general we take into account all left-facing walls, be it of type σ or σ^N, at whatever position they are defined for the cell. In our case, all terms corresponding to σ^N vanish due to the zero-flux condition imposed on the Neumann-type boundary, while for $\sigma_{j-\frac{1}{2},k}$ the length measure s is equal to $H/2$ and the flux through it depends on the neighbour cells on its left and right.

Next, let U^n_{jk} be a numerical approximation to the exact solution $u(x_j, y_k, t^n)$ of problem (2.1). Upon introducing the stan-

dard FVM notations

$$U_{jk}(t) = \frac{1}{V_{jk}} \iint\limits_{\mathcal{K}_{jk}} u(x,y,t)\mathrm{d}x\mathrm{d}y,$$
$$f_{jk}(t) = \frac{1}{V_{jk}} \iint\limits_{\mathcal{K}_{jk}} f(x,y,t)\mathrm{d}x\mathrm{d}y,$$

the finite volume scheme is defined by the equation

$$\frac{\mathrm{d}U_{jk}}{\mathrm{d}t} = -A_1^h U_{jk} - A_2^h U_{jk} + f_{jk} \tag{2.2}$$

with the discrete operators A_1^h and A_2^h redefined by

$$\begin{aligned}
\partial_x U_{jk}^n &= \frac{U_{jk}^n - U_{j-1,k}^n}{h}, \\
A_1^h U_{jk} &= \frac{1}{V_{jk}} \left(-s_{j+\frac{1}{2},k}^j \partial_x U_{j+1,k}^n + s_{j-\frac{1}{2},k}^j \partial_x U_{jk}^n \right), \\
\partial_y U_{jk}^n &= \frac{U_{jk}^n - U_{j,k-1}^n}{H}, \\
A_2^h U_{jk} &= \frac{1}{V_{jk}} \left(-s_{j,k+\frac{1}{2}}^k \partial_y U_{j,k+1}^n + s_{j,k-\frac{1}{2}}^k \partial_y U_{jk}^n \right),
\end{aligned} \tag{2.3}$$

where the implementation of Neumann boundary conditions is included naturally, while for the cells on Dirichlet boundaries, corresponding values of given functions g_i are taken. Furthermore, note that the operators have varying coefficients s. To define them more precisely,

$$\begin{aligned}
s_{j-\frac{1}{2},k}^j &= \frac{H}{2} \text{ if } k \in \{K_1, K_2\} \text{ and } j \in [1, J_1] \cup [J_2 + 1, J], \\
s_{j-\frac{1}{2},k}^j &= H \text{ elsewhere in } \Omega_h, \\
s_{j,k-\frac{1}{2}}^k &= \frac{h}{2} \text{ if } j \in \{J_1, J_2\} \text{ and } k \in [1, K_1] \cup [K_2 + 1, K], \\
s_{j,k-\frac{1}{2}}^k &= h \text{ elsewhere in } \Omega_h,
\end{aligned} \tag{2.4}$$

while for the cells outside Ω_h, the coefficients s are considered to be zero.

Having defined the spatial discretization, we are now in a position to apply the ADI method to integrate in time, thus from

(2.2) the following ADI scheme is obtained for $(x_j, y_k) \in \Omega_h \setminus \partial_D$:

$$\begin{aligned} &\frac{U_{jk}^{n+\frac{1}{2}} - U_{jk}^{n}}{\tau/2} + A_1^h U_{jk}^{n+\frac{1}{2}} + A_2^h U_{jk}^{n} = f_{jk}^{n+\frac{1}{2}}, \\ &\frac{U_{jk}^{n+1} - U_{jk}^{n+\frac{1}{2}}}{\tau/2} + A_1^h U_{jk}^{n+\frac{1}{2}} + A_2^h U_{jk}^{n+1} = f_{jk}^{n+\frac{1}{2}}. \end{aligned} \tag{2.5}$$

Note that in the first substep the x derivative is taken implicitly and in the second substep the y derivative is taken implicitly. Due to this alternate implicit use of operators, the method is called alternating directions implicit from the perspective of dimension splitting. Furthermore, note that the ADI method is locally one-dimensional (LOD) and in contrast to other LOD methods (such as LOD Crank-Nicolson or the trapezoidal splitting), the approximations at intermediate-time stages are consistent with the full problem.

2.3 Convergence of the FVM ADI scheme

Now, let us recall some classical properties of the ADI scheme (2.5), as they will have to be re-evaluated for the hybrid dimension model.

Lemma 2.1. *If a solution of* (2.1) *is sufficiently smooth, then the approximation error of ADI scheme* (2.5) *is* $O(\tau^2+h^2+H^2)$.

Proof. Let us rewrite (2.5) without the intermediate-time value $U^{n+\frac{1}{2}}$. From the difference $(2.5)_1 - (2.5)_2$ we get

$$U_{jk}^{n+\frac{1}{2}} = \frac{U_{jk}^{n+1} + U_{jk}^{n}}{2} + \frac{\tau}{4} A_2^h \left(U_{jk}^{n+1} - U_{jk}^{n} \right). \tag{2.6}$$

Substituting this result into $(2.5)_2$, we derive

$$\frac{U_{jk}^{n+1} - U_{jk}^{n}}{\tau} + A_1^h \Big(\frac{U_{jk}^{n+1} + U_{jk}^{n}}{2} \Big) + A_2^h \Big(\frac{U_{jk}^{n+1} + U_{jk}^{n}}{2} \Big) + \frac{\tau^2}{4} A_1^h A_2^h \Big(\frac{U_{jk}^{n+1} - U_{jk}^{n}}{\tau} \Big) = f_{jk}^{n+\frac{1}{2}},$$

which is equivalent to the classical symmetrical finite difference scheme up to order $O(\tau^2)$ term. Therefore, provided that boundary conditions of intermediate time layers satisfy (2.6), the approximation error is of the same order as for the symmetrical finite difference scheme, which can be verified by substituting the Taylor expansions. □

It is interesting to note that the boundary values at intermediate time layers (as well as solution itself) generally do not necessarily represent physical conditions at corresponding times, they should be rather seen as a correction step, even if for the ADI method they are of physically reasonable values.

Although in the proof we have somewhat committed ourselves to use (2.6) for calculating intermediate-time Dirichlet boundary values, which is the so-called Fairweather-Mitchell type correction [30], from the numerical point of view this correction technique makes numerical approximations only a little more accurate, as dropping the second term of sum in (2.6) results in the same order of accuracy. This term increases the order in time of local errors, however, the global error remains of the same order. For an interesting discussion regarding this topic for the ADI method, we refer the reader to [30].

As will be seen later, since computations of this problem do not require values of intermediate time layers of g_2 and g_4, the Fairweather-Mitchell type correction only makes sense when applied to the left and right Dirichlet-type boundaries of Ω.

Next, one important issue is noncommuting operators A_1^h and A_2^h (e.g., consider the cell #2 in Figure 2.2), which leads to a more complicated stability analysis than in a commuting case. The first half-step of ADI scheme $(2.5)_1$ decreases the error growth factor in x direction and increases it in y direction, while the second half-step acts vice versa. After combining half-steps, the error growth multiplier does not increase in its absolute value (see, e.g., [49] or [81]). Overall, what matters is that in our case stability can be proved in a suitable norm.

To prove the next lemma, let us consider discrete functions $\hat{u}_j = \hat{u}(x_j)$, $\hat{v}_j = \hat{v}(x_j)$ defined on spatial mesh points, such that

$\hat{u}_0 = \hat{u}_J = 0$, $\hat{v}_0 = \hat{v}_J = 0$. Then the formulas

$$(\hat{u}, \hat{v})_x = \sum_{j=1}^{J-1} \hat{u}_j \hat{v}_j h, \quad \|u\|_x = \sqrt{(u,u)_x}$$

define an inner product and a norm in this vector space. We also define one more inner product

$$(\hat{u}, \hat{v}]_x = \sum_{j=1}^{J} \hat{u}_j \hat{v}_j h.$$

Analogously, for functions $\widetilde{u}_k = \widetilde{u}(y_k)$, $\widetilde{v}_k = \widetilde{v}(y_k)$ defined on spatial mesh points, such that $\widetilde{u}_0 = \widetilde{u}_K = 0$, $\widetilde{v}_0 = \widetilde{v}_K = 0$, the formulas

$$(\tilde{u}, \tilde{v})_y = \sum_{k=1}^{K-1} \tilde{u}_k \tilde{v}_k H, \ (\tilde{u}, \tilde{v}]_y = \sum_{k=1}^{K} \tilde{u}_k \tilde{v}_k H, \ \|u\|_y = \sqrt{(u,u)_y}$$

define two inner products and a norm in this vector space. In the next lemma below, the partial derivative is treated in a backward-step sense, see (2.3) for the definitions of ∂_x, ∂_y.

Lemma 2.2. *The discrete operators A_1^h and A_2^h are symmetric and positive semi-definite.*

Proof. Let us first analyse A_1^h and start with the intervals $k \in [1; K_1 - 1] \cup [K_2 + 1; K - 1]$. Applying the summation by parts (see, e.g., [66]) we get

$$\begin{aligned}
(A_1^h \hat{u}, \hat{v})_x &= \sum_{j=J_1}^{J_2} (A_1^h \hat{u})_j \hat{v}_j h = -\frac{\hat{u}_{J_1+1} - \hat{u}_{J_1}}{h} \hat{v}_{J_1} \\
&- \sum_{j=J_1+1}^{J_2-1} \left(\frac{\hat{u}_{j+1} - \hat{u}_j}{h} - \frac{\hat{u}_j - \hat{u}_{j-1}}{h} \right) \hat{v}_j + \frac{\hat{u}_{J_2} - \hat{u}_{J_2-1}}{h} \hat{v}_{J_2} \\
&= \frac{\hat{u}_{J_1+1} - \hat{u}_{J_1}}{h} (\hat{v}_{J_1+1} - \hat{v}_{J_1}) + \sum_{j=J_1+2}^{J_2-1} \frac{\hat{u}_j - \hat{u}_{j-1}}{h} (\hat{v}_j - \hat{v}_{j-1}) \\
&+ \frac{\hat{u}_{J_2} - \hat{u}_{J_2-1}}{h} (\hat{v}_{J_2} - \hat{v}_{J_2-1}) = (\partial_x \hat{u}, \partial_x \hat{v}]_x.
\end{aligned}$$

In an analogous way, for the case $k \in [K_1 + 1; K_2 - 1]$ we can confirm that

$$(A_1^h \hat{u}, \hat{v})_x = \sum_{j=1}^{J-1} (A_1^h \hat{u})_j \hat{v}_j h = (\partial_x \hat{u}, \partial_x \hat{v}]_x.$$

The same result also holds for the case $k \in \{K_1, K_2\}$. It follows that A_1^h is a symmetric operator. Furthermore, since $A_1^h \phi_l = \lambda_l \phi_l$ has only nonnegative eigenvalues λ_l [66], A_1^h is a positive semi-definite operator. These derivations can be repeated for A_2^h to get analogous results, thus both operators A_1^h and A_2^h are symmetric and positive semi-definite. □

Recall that A_1^h and A_2^h do not commute for the geometry of this problem, thus we cannot use the spectral stability analysis and we restrict ourselves to showing stability estimate in one particular energy norm. Note that the norm presented in the following lemma is 2D, having the form $\|u\|^2 = \sum_{j=0}^{J} \sum_{k=0}^{K} c_{jk}^2 u_{jk}^2$. The symmetry and positive semi-definiteness properties of A_1^h and A_2^h hold on each line of corresponding direction, thus these properties are preserved in the total discrete 2D sum of the norm and the analysis of operators on single lines provided in Lemma 2.2 is sufficient. The proof technique of Lemma 2.3 is a well known procedure, see, e.g., [31, 49].

Proposition 2.3. *If U^n is the solution of ADI scheme (2.5), when $f^n \equiv 0$ and $g_i^n \equiv 0$, $i = 1, \ldots, 4$, then the following stability estimate is valid*

$$\|(I + \frac{\tau}{2} A_2^h) U^n\| \leqslant \|(I + \frac{\tau}{2} A_2^h) U^0\|.$$

Proof. The ADI scheme equations (2.5) give $U^{n+1} = RU^n$ with

$$R = \Big(I + \frac{\tau}{2} A_2^h\Big)^{-1} \Big(I - \frac{\tau}{2} A_1^h\Big) \Big(I + \frac{\tau}{2} A_1^h\Big)^{-1} \Big(I - \frac{\tau}{2} A_2^h\Big)$$

We rewrite this relation as

$$\Big(I + \frac{\tau}{2} A_2^h\Big) U^{n+1} = \widetilde{R} \Big(I + \frac{\tau}{2} A_2^h\Big) U^n$$

with operator $\widetilde{R}$ defined by

$$\widetilde{R} = \Big(I - \frac{\tau}{2}A_1^h\Big)\Big(I + \frac{\tau}{2}A_1^h\Big)^{-1}\Big(I - \frac{\tau}{2}A_2^h\Big)\Big(I + \frac{\tau}{2}A_2^h\Big)^{-1}.$$

By induction we prove that

$$\Big(I + \frac{\tau}{2}A_2^h\Big)U^n = \widetilde{R}^n\Big(I + \frac{\tau}{2}A_2^h\Big)U^0.$$

It follows from Lemma 2.2 that $\|\widetilde{R}\| \leqslant 1$, thus

$$\|\widetilde{R}^n\| \leqslant \|\widetilde{R}\|^n \leqslant 1.$$

Therefore, the proposition is proved. □

2.4 A hybrid dimension model

In this section, a modified approximate problem is considered that approximates the classical heat conduction model (2.1). Further reasoning follows numerous works of G. Panasenko [51–53] that concern the method of asymptotic partial decomposition of the domain (MAPDD).

The motivation here is the same as in the previous chapter – it roots in the observation that when heat is conducted in a rod or a plate, the distribution of it along the radius tends to smooth-out after quite a short distance when diffusing through an externally unheated part. However, a sufficient space is needed for smoothing after "leaving" the heated area. In our model, we define this distance for smoothing by the parameter δ. After smoothing-out, 1D calculations are sufficient until another acting heat source is encountered.

To begin with, let us denote the reduced rods (reduced dimension zones) by

$$\begin{aligned}
L_1^\delta &= \{(x,y) : \delta \leqslant x \leqslant X_1 - \delta,\ Y_1 \leqslant y \leqslant Y_2\},\\
L_2^\delta &= \{(x,y) : X_1 \leqslant x \leqslant X_2,\ \delta \leqslant y \leqslant Y_1 - \delta\},\\
L_3^\delta &= \{(x,y) : X_2 + \delta \leqslant x \leqslant X - \delta,\ Y_1 \leqslant y \leqslant Y_2\},\\
L_4^\delta &= \{(x,y) : X_1 \leqslant x \leqslant X_2,\ Y_2 + \delta \leqslant y \leqslant Y - \delta\}
\end{aligned}$$

and let the union of reduced dimension domains be denoted by $\Omega^\delta = L_1^\delta \cup L_2^\delta \cup L_3^\delta \cup L_4^\delta$. Visual representation of Ω^δ corresponds to yellow zones in Figure 2.4. Here δ is taken the same for both sides of each rod only for the sake of simplicity and in practice can be adapted to each side and each rod uniquely.

It is assumed that the initial condition u^0 and the source function f do not depend on x in L_2 and L_4, also that they do not depend on y in L_1 and L_3:

$$u^0(x,y) = \widetilde{u}^0(y),\ f(x,y,t) = \widetilde{f}(y,t),\ (x,y,t) \in (L_2 \cup L_4) \times (0,T];$$
$$u^0(x,y) = \widetilde{u}^0(x),\ f(x,y,t) = \widetilde{f}(x,t),\ (x,y,t) \in (L_1 \cup L_3) \times (0,T].$$

Next, function U is called an approximate solution to (2.1) if it satisfies

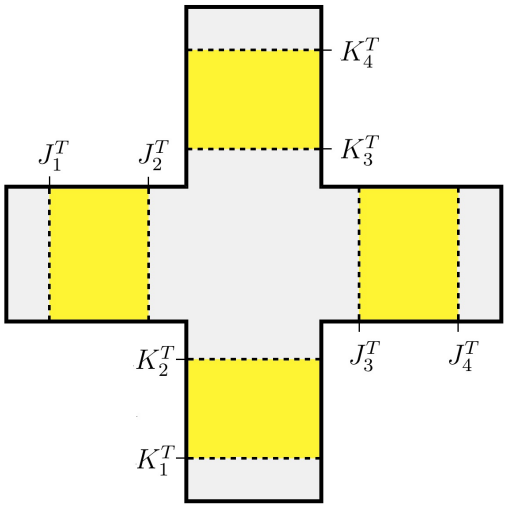

Figure 2.4: Domain Ω with indices of truncations and reduced dimension zones in yellow.

$$\begin{cases} \dfrac{\partial U}{\partial t} = \dfrac{\partial^2 U}{\partial x^2} + \dfrac{\partial^2 U}{\partial y^2} + f(x,y,t), & (x,y,t) \in (\Omega \setminus \Omega^\delta) \times (0,T], \\ \dfrac{\partial U}{\partial t} = \dfrac{\partial^2 U}{\partial x^2} + \widetilde{f}(x,t), & (x,y,t) \in (L_1^\delta \cup L_3^\delta) \times (0,T], \\ \dfrac{\partial U}{\partial t} = \dfrac{\partial^2 U}{\partial y^2} + \widetilde{f}(y,t), & (x,y,t) \in (L_2^\delta \cup L_4^\delta) \times (0,T], \\ U(0,y,t) = g_1(y,t), & (y,t) \in [Y_1,Y_2] \times (0,T], \\ U(x,0,t) = g_2(x,t), & (x,t) \in [X_1,X_2] \times (0,T], \\ U(X,y,t) = g_3(y,t), & (y,t) \in [Y_1,Y_2] \times (0,T], \\ U(x,Y,t) = g_4(x,t), & (x,t) \in [X_1,X_2] \times (0,T], \\ \dfrac{\partial U}{\partial \mathbf{n}} = 0, & (x,y,t) \in \partial_N \Omega \times (0,T], \\ U(x,y,0) = u^0(x,y), & (x,y) \in \Omega. \end{cases} \tag{2.7}$$

It has been shown in [3] that the H^1 norm of the difference of the exact solution and the approximate solution obtained by the MAPDD for a heat equation depends on the parameter δ. Thus the motivation of turning from (2.1) to (2.7), while balancing δ between being large enough for the accuracy justified by MAPDD and small enough for a considerable computational speed-up.

To be used at conjugations of 1D and 2D parts, let the averaging operators S_x and S_y be defined as

$$\begin{aligned} S_x(U) &= \frac{1}{X_2 - X_1} \int_{X_1}^{X_2} U(x,y,t) \mathrm{d}x, \\ S_y(U) &= \frac{1}{Y_2 - Y_1} \int_{Y_1}^{Y_2} U(x,y,t) \mathrm{d}y. \end{aligned} \tag{2.8}$$

Assuming continuity of U with conservation of full fluxes along each truncation line of reduced rods, we will use the following conjugation conditions:

$$
\begin{aligned}
U|_{x=\delta-0} = U|_{x=\delta+0}\,, \quad & \left.\frac{\partial S_y(U)}{\partial x}\right|_{x=\delta-0} = \left.\frac{\partial U}{\partial x}\right|_{x=\delta+0}\,,\\
U|_{x=X_1-\delta-0} = U|_{x=X_1-\delta+0}\,, \quad & \left.\frac{\partial S_y(U)}{\partial x}\right|_{x=X_1-\delta-0} = \left.\frac{\partial U}{\partial x}\right|_{x=X_1-\delta+0}\,,\\
U|_{x=X_2+\delta-0} = U|_{x=X_2+\delta+0}\,, \quad & \left.\frac{\partial S_y(U)}{\partial x}\right|_{x=X_2+\delta-0} = \left.\frac{\partial U}{\partial x}\right|_{x=X_2+\delta+0}\,,\\
U|_{x=X-\delta-0} = U|_{x=X-\delta+0}\,, \quad & \left.\frac{\partial S_y(U)}{\partial x}\right|_{x=X-\delta-0} = \left.\frac{\partial U}{\partial x}\right|_{x=X-\delta+0}\,,\\
U|_{y=\delta-0} = U|_{y=\delta+0}\,, \quad & \left.\frac{\partial S_x(U)}{\partial y}\right|_{y=\delta-0} = \left.\frac{\partial U}{\partial y}\right|_{y=\delta+0}\,,\\
U|_{y=Y_1-\delta-0} = U|_{y=Y_1-\delta+0}\,, \quad & \left.\frac{\partial S_x(U)}{\partial y}\right|_{y=Y_1-\delta-0} = \left.\frac{\partial U}{\partial y}\right|_{y=Y_1-\delta+0}\,,\\
U|_{y=Y_2+\delta-0} = U|_{y=Y_2+\delta+0}\,, \quad & \left.\frac{\partial S_x(U)}{\partial y}\right|_{y=Y_2+\delta-0} = \left.\frac{\partial U}{\partial y}\right|_{y=Y_2+\delta+0}\,,\\
U|_{y=Y-\delta-0} = U|_{y=Y-\delta+0}\,, \quad & \left.\frac{\partial S_x(U)}{\partial y}\right|_{y=Y-\delta-0} = \left.\frac{\partial U}{\partial y}\right|_{y=Y-\delta+0}\,.
\end{aligned}
\tag{2.9}
$$

In [57] the existence and uniqueness of an approximate solution U to the 2D heat equation set in a rod structure with partial asymptotic domain decomposition is proved. By analysing the weak form of heat equation, it is also shown that conditions (2.9) are valid at the truncations. In the following sections we seek to improve the reduction of computational cost of partial domain decomposition method used in [57] for solving problem (2.7) by proposing a different numerical strategy, also following the guidelines of [38].

Regarding previous sections, solving the main problem (2.1) numerically using the ADI scheme (2.5) is considered to be somewhat of a classical problem, while in this section solving the main problem (2.7) numerically requires additional methods originating from nonclassical conditions, namely, conjugations of hybrid dimensions.

Let the truncation lines between 2D and 1D parts be denoted by T_i^x and T_i^y, the corresponding grid indices at which the trun-

cations are applied be denoted by J_i^T for vertical and K_i^T for horizontal truncation lines, $i = 1, \ldots, 4$ (for a visual representation, see Figure 2.4). Recall that all grid points on any single truncation line (or any line parallel to it inside its reduced zone) are assumed to be of equal U values and can be used in calculations as one single point instead of a row/column, thus the index notation $*$ will be used for such cases.

Define the sets of grid points, corresponding to each reduced rod, by

$$\begin{aligned}
\omega_{L_1} &= \{(x_j, y_k) :\ J_1^T \leqslant j \leqslant J_2^T,\ K_1 \leqslant k \leqslant K_2\},\\
\omega_{L_2} &= \{(x_j, y_k) :\ J_1 \leqslant j \leqslant J_2,\ K_1^T \leqslant k \leqslant K_2^T\},\\
\omega_{L_3} &= \{(x_j, y_k) :\ J_3^T \leqslant j \leqslant J_4^T,\ K_1 \leqslant k \leqslant K_2\},\\
\omega_{L_4} &= \{(x_j, y_k) :\ J_1 \leqslant j \leqslant J_2,\ K_3^T \leqslant k \leqslant K_4^T\},\\
\omega_R &= \omega_{L_1} \cup \omega_{L_2} \cup \omega_{L_3} \cup \omega_{L_4}.
\end{aligned}$$

Instead of having 2 dimensions, here one of them is reduced, therefore, the sets of 2D grid points are replaced by 1D sets

$$\begin{aligned}
\tilde{\omega}_{L_1} &= \{x_j :\ J_1^T \leqslant j \leqslant J_2^T\}, \quad & \tilde{\omega}_{L_2} &= \{y_k :\ K_1^T \leqslant k \leqslant K_2^T\},\\
\tilde{\omega}_{L_3} &= \{x_j :\ J_3^T \leqslant j \leqslant J_4^T\}, \quad & \tilde{\omega}_{L_4} &= \{y_k :\ K_3^T \leqslant k \leqslant K_4^T\},\\
& & \tilde{\omega}_R &= \tilde{\omega}_{L_1} \cup \tilde{\omega}_{L_2} \cup \tilde{\omega}_{L_3} \cup \tilde{\omega}_{L_4},
\end{aligned}$$

so that the numerical grid with reduced dimension points is denoted by

$$\Omega_{h,RD} = \big((\overline{\omega}_x \times \overline{\omega}_y) \cap (\Omega \setminus \Omega^\delta)\big) \cup \tilde{\omega}_R. \tag{2.10}$$

Next, introducing the discrete analogue of averaging operators 2.8

$$S_x^h(U_k^n) = \frac{1}{X_2 - X_1} \sum_{j=J_1}^{J_2} U_{jk}^n s_{j,k+\frac{1}{2}}^k,$$

$$S_y^H(U_j^n) = \frac{1}{Y_2 - Y_1} \sum_{k=K_1}^{K_2} U_{jk}^n s_{j+\frac{1}{2},k}^j$$

and including conjugation conditions (2.9) in the ADI approximation of (2.7), we get the following problem (2.11) for the first

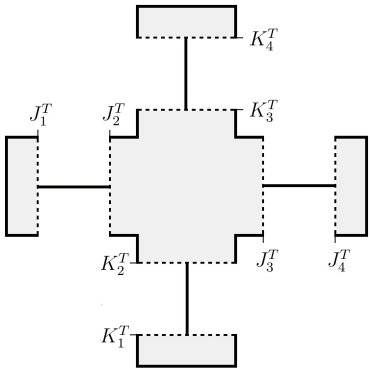

Figure 2.5: Domain Ω with indices of truncations and reduced dimension parts as 1D lines.

substep of (2.5). Here it is presented in a detailed form only for the sake of convenience of the next section. It is presented in a compact form in (2.19).

$$
\begin{cases}
\dfrac{U_{jk}^{n+\frac{1}{2}} - U_{jk}^{n}}{\tau/2} + A_1 U_{jk}^{n+\frac{1}{2}} + A_2 U_{jk}^{n} = f_{jk}^{n+\frac{1}{2}}, \ (x_j, y_k) \in \Omega_h \setminus \omega_R; \\
\dfrac{U_{j*}^{n+\frac{1}{2}} - U_{j*}^{n}}{\tau/2} + A_1 U_{j*}^{n+\frac{1}{2}} = f_{j*}^{n+\frac{1}{2}}, \ j \in (J_1^T, J_2^T) \cup (J_3^T, J_4^T); \\
\dfrac{U_{*k}^{n+\frac{1}{2}} - U_{*k}^{n}}{\tau/2} + A_2 U_{*k}^{n} = f_{*k}^{n+\frac{1}{2}}, \ k \in (K_1^T, K_2^T) \cup (K_3^T, K_4^T); \\
\dfrac{U_{j*}^{n+\frac{1}{2}} - U_{j*}^{n}}{\tau/2} + \dfrac{1}{h^2}\Big(- S_y^H(U_{j-1}^{n+\frac{1}{2}}) + 2U_{j*}^{n+\frac{1}{2}} - U_{j+1,*}^{n+\frac{1}{2}}\Big) = f_{j*}^{n+\frac{1}{2}}, \\
\qquad\qquad\qquad\qquad\qquad\qquad\qquad\qquad\qquad\qquad j \in \{J_1^T, J_3^T\}; \\
\dfrac{U_{j*}^{n+\frac{1}{2}} - U_{j*}^{n}}{\tau/2} + \dfrac{1}{h^2}\Big(- S_y^H(U_{j+1}^{n+\frac{1}{2}}) + 2U_{j*}^{n+\frac{1}{2}} - U_{j-1,*}^{n+\frac{1}{2}}\Big) = f_{j*}^{n+\frac{1}{2}}, \\
\qquad\qquad\qquad\qquad\qquad\qquad\qquad\qquad\qquad\qquad j \in \{J_2^T, J_4^T\}; \\
\dfrac{U_{*k}^{n+\frac{1}{2}} - U_{*k}^{n}}{\tau/2} + \dfrac{1}{H^2}\Big(- S_x^h(U_{k-1}^{n}) + 2U_{*k}^{n} - U_{*,k+1}^{n}\Big) = f_{*k}^{n+\frac{1}{2}}, \\
\qquad\qquad\qquad\qquad\qquad\qquad\qquad\qquad\qquad\qquad k \in \{K_1^T, K_3^T\}; \\
\dfrac{U_{*k}^{n+\frac{1}{2}} - U_{*k}^{n}}{\tau/2} + \dfrac{1}{H^2}\Big(- S_x^h(U_{k+1}^{n}) + 2U_{*k}^{n} - U_{*,k-1}^{n}\Big) = f_{*k}^{n+\frac{1}{2}}, \\
\qquad\qquad\qquad\qquad\qquad\qquad\qquad\qquad\qquad\qquad k \in \{K_2^T, K_4^T\}.
\end{cases}
\tag{2.11}
$$

To put it simply, we let the full heat transfer to take place in a neighbourhood of the central part of domain as well as near boundaries with Dirichlet conditions. In reduced regions, one of operators A_1^h or A_2^h vanishes and on the truncation lines we use special conjugation conditions to couple 1D and 2D regions. Whatever values are defined on outer boundaries, they tend to "smooth out" while diffusing through rods or plates. At some distance it becomes of little practical importance to keep solving full diffusion, thus we switch to 1D equations, losing a bit of accuracy but improving the speed of computations due to the reduced dimension zones. The truncation lines around the central part L_0 are designed to allow "smoothing-out" of the values of f defined in the central part, while the values of f in rods have to be defined as averaged.

Analogous system for the second substep is given by (2.12):

$$\begin{cases} \dfrac{U_{jk}^{n+1} - U_{jk}^{n+\frac{1}{2}}}{\tau/2} + A_1 U_{jk}^{n+\frac{1}{2}} + A_2 U_{jk}^{n+1} = f_{jk}^{n+\frac{1}{2}}, (x_j, y_k) \in \Omega_h \setminus \omega_R; \\ \dfrac{U_{*k}^{n+1} - U_{*k}^{n+\frac{1}{2}}}{\tau/2} + A_2 U_{*k}^{n+1} = f_{*k}^{n+\frac{1}{2}}, \ k \in (K_1^T, K_3^T) \cup (K_2^T, K_4^T); \\ \dfrac{U_{j*}^{n+1} - U_{j*}^{n+\frac{1}{2}}}{\tau/2} + A_1 U_{j*}^{n+\frac{1}{2}} = f_{j*}^{n+\frac{1}{2}}, \ j \in (J_1^T, J_2^T) \cup (J_3^T, J_4^T); \\ \dfrac{U_{*k}^{n+1} - U_{*k}^{n+\frac{1}{2}}}{\tau/2} + \dfrac{1}{H^2}\Big(- S_x^H(U_{k-1}^{n+1}) + 2U_{*k}^{n+1} - U_{*,k+1}^{n+1}\Big) = f_{*k}^{n+\frac{1}{2}}, \\ \qquad\qquad k \in \{K_1^T, K_3^T\}; \\ \dfrac{U_{*k}^{n+1} - U_{*k}^{n+\frac{1}{2}}}{\tau/2} + \dfrac{1}{H^2}\Big(- S_x^H(U_{k+1}^{n+1}) + 2U_{*k}^{n+1} - U_{*,k-1}^{n+1}\Big) = f_{*k}^{n+\frac{1}{2}}, \\ \qquad\qquad k \in \{K_2^T, K_4^T\}; \\ \dfrac{U_{j*}^{n+1} - U_{j*}^{n+\frac{1}{2}}}{\tau/2} + \dfrac{1}{h^2}\Big(- S_y^h(U_{j-1}^{n+\frac{1}{2}}) + 2U_{j*}^{n+\frac{1}{2}} - U_{j+1,*}^{n+\frac{1}{2}}\Big) = f_{j*}^{n+\frac{1}{2}}, \\ \qquad\qquad j \in \{J_1^T, J_3^T\}; \\ \dfrac{U_{j*}^{n+1} - U_{j*}^{n+\frac{1}{2}}}{\tau/2} + \dfrac{1}{h^2}\Big(- S_y^h(U_{j+1}^{n+\frac{1}{2}}) + 2U_{j*}^{n+\frac{1}{2}} - U_{j-1,*}^{n+\frac{1}{2}}\Big) = f_{j*}^{n+\frac{1}{2}}, \\ \qquad\qquad j \in \{J_2^T, J_4^T\}. \end{cases} \tag{2.12}$$

It is shown below that for each time half-step, a unique solution exists and it can be computed by using an effective algorithm which is obtained by modifying the classical Thomas algorithm for tridiagonal matrices. First, the values of U on implicit-valued truncation lines are found (e.g., $j \in \{J_1^T, J_2^T, J_3^T, J_4^T\}$ for the first half-step) and then the rest, moving to the next half-step afterwards.

2.5 Unique existence of the ADI numerical solution to the hybrid model

To prove the next theorem, let us analyse how the classical Thomas algorithm has to be modified due to nonclassical conjugation conditions. Equations $(2.11)_{1-2}$ and $(2.12)_{1-2}$ can be written in the following forms, respectively:

$$
\begin{gathered}
-a_{jk}U_{j-1,k}^{n+\frac{1}{2}} + b_{jk}U_{jk}^{n+\frac{1}{2}} - c_{jk}U_{j+1,k}^{n+\frac{1}{2}} = d_{jk}, \\
-\hat{a}_{jk}U_{j,k-1}^{n+1} + \hat{b}_{jk}U_{jk}^{n+1} - \hat{c}_{jk}U_{j,k+1}^{n+1} = \hat{d}_{jk}, \\
a_{jk}, b_{jk}, c_{jk}, \hat{a}_{jk}, \hat{b}_{jk}, \hat{c}_{jk} \geqslant 0,\ b_{jk} \geqslant a_{jk} + c_{jk},\ \hat{b}_{jk} \geqslant \hat{a}_{jk} + \hat{c}_{jk}.
\end{gathered}
$$

Recall that (2.11) is the first half-step in time and (2.12) is the second half-step in time. Each of them uses values of the previous half-step to advance in time by $\tau/2$. (2.11) and (2.12) are solved separately and the following procedure is analogous for both of them, therefore, here we will only present it in details for the first half-step.

With k such that $Y_1 \leqslant kH \leqslant Y_2$, consider $(2.11)_{1-2}$ for the following intervals:

1. For $j \in [0, J_1^T)$ the solution is presented as

$$
U_{jk}^{n+\frac{1}{2}} = \alpha_{jk}U_{j+1,k}^{n+\frac{1}{2}} + \gamma_{jk}, \tag{2.13}
$$

$$
\begin{gathered}
\alpha_{0,k} = 0,\ \alpha_{jk} = \frac{c_{jk}}{b_{jk} - a_{jk}\alpha_{j-1,k}}, \\
\gamma_{0,k} = g_1(y_k, t^{n+1}), \gamma_{jk} = \frac{d_{jk} + a_{jk}\gamma_{j-1,k}}{b_{jk} - a_{jk}\alpha_{j-1,k}}.
\end{gathered}
$$

It follows directly from the tridiagonal matrix factorization algorithm. By induction it can be proved that the estimate $0 \leqslant \alpha_{jk} \leqslant 1$ is valid.

2. For $j \in (J_1^T, J_2^T)$ the solution is presented as

$$U_{j*}^{n+\frac{1}{2}} = \alpha_{j*} U_{J_1^T *}^{n+\frac{1}{2}} + \beta_{j*} U_{J_2^T *}^{n+\frac{1}{2}} + \gamma_{j*}. \tag{2.14}$$

First, the solution is written as

$$U_{j*}^{n+\frac{1}{2}} = \widetilde{\alpha}_{j*} U_{J_1^T *}^{n+\frac{1}{2}} + \widetilde{\beta}_{j*} U_{j+1,*}^{n+\frac{1}{2}} + \widetilde{\gamma}_{j*}, \;\; J_1^T < j < J_2^T,$$

$$\widetilde{\alpha}_{J_1^T+1,*} = \frac{a_{J_1^T+1,*}}{b_{J_1^T+1,*}}, \;\; \widetilde{\beta}_{J_1^T+1,*} = \frac{c_{J_1^T+1,*}}{b_{J_1^T+1,*}}, \;\; \widetilde{\gamma}_{J_1^T+1,*} = \frac{d_{J_1^T+1,*}}{b_{J_1^T+1,*}},$$

$$\widetilde{\alpha}_{j*} = \frac{a_{j*}\widetilde{\alpha}_{j-1,*}}{b_{j*} - a_{j*}\widetilde{\beta}_{j-1,*}}, \widetilde{\beta}_{j*} = \frac{c_{j*}}{b_{j*} - a_{j*}\widetilde{\beta}_{j-1,*}}, \widetilde{\gamma}_{j*} = \frac{a_{j*}\widetilde{\gamma}_{j-1,*} + d_{j*}}{b_{j*} - a_{j*}\widetilde{\beta}_{j-1,*}}.$$

Let us assume that $0 \leqslant \widetilde{\alpha}_{j-1,*} \leqslant 1$, $0 \leqslant \widetilde{\beta}_{j-1,*} \leqslant 1$ and $\widetilde{\alpha}_{j-1,*} + \widetilde{\beta}_{j-1,*} \leqslant 1$. Then it follows from the formulae above that $0 \leqslant \widetilde{\beta}_{j*} \leqslant 1$ and $\widetilde{\alpha}_{j*} \geqslant 0$. It remains to prove that $\widetilde{\alpha}_{j*} \leqslant 1$ and $\widetilde{\alpha}_{j*} + \widetilde{\beta}_{j*} \leqslant 1$. It follows from the simple inequalities

$$\begin{aligned} &a_{j*}\widetilde{\alpha}_{j-1,*} + c_{j*} + a_{j*}\widetilde{\beta}_{j-1,*} \\ &= a_{j*}(\widetilde{\alpha}_{j-1,*} + \widetilde{\beta}_{j-1,*}) + c_{j*} \leqslant a_{j*} + c_{j*} \leqslant b_{j*}, \end{aligned}$$

that

$$a_{j*}\widetilde{\alpha}_{j-1,*} + c_{j*} \leqslant b_{j*} - a_{j*}\widetilde{\beta}_{j-1,*}.$$

Thus we get the estimate

$$0 \leqslant \widetilde{\alpha}_{j*} + \widetilde{\beta}_{j*} \leqslant 1.$$

Next, coefficients in (2.14) are computed by

$$\begin{aligned} &\alpha_{J_2^T-1,*} = \widetilde{\alpha}_{J_2^T-1,*}, \;\; \beta_{J_2^T-1,*} = \widetilde{\beta}_{J_2^T-1,*}, \;\; \gamma_{J_2^T-1,*} = \widetilde{\gamma}_{J_2^T-1,*}, \\ &\alpha_{j*} = \widetilde{\alpha}_{j*} + \widetilde{\beta}_{j*}\alpha_{j+1,*}, \;\; \beta_{j*} = \widetilde{\beta}_{j*}\beta_{j+1,*}, \;\; \gamma_{j*} = \widetilde{\gamma}_{j*} + \widetilde{\beta}_{j*}\gamma_{j+1,*}, \\ &j = J_2^T - 2, \ldots, J_1^T + 1. \end{aligned}$$

From these relations and estimates for $\widetilde{\alpha}_{j*}$ and $\widetilde{\beta}_{j*}$ it follows that the following estimates hold as well

$$0 \leqslant \alpha_{j*} \leqslant 1, \;\; 0 \leqslant \beta_{j*} \leqslant 1, \;\; 0 \leqslant \alpha_{j*} + \beta_{j*} \leqslant 1.$$

3. For $j \in (J_2^T, J_3^T)$ the solution is presented as

$$U_{jk}^{n+\frac{1}{2}} = \alpha_{jk} U_{J_2^T *}^{n+\frac{1}{2}} + \beta_{jk} U_{J_3^T *}^{n+\frac{1}{2}} + \gamma_{jk}. \tag{2.15}$$

Here each horizontal line is treated separately from each other. For each line, the derivation and estimates of coefficients are analogous to the previous part.

4. For $j \in (J_3^T, J_4^T)$ the solution is presented as

$$U_{j*}^{n+\frac{1}{2}} = \alpha_{j*} U_{J_3^T *}^{n+\frac{1}{2}} + \beta_{j*} U_{J_4^T *}^{n+\frac{1}{2}} + \gamma_{j*}, \tag{2.16}$$

here the derivation and estimates of coefficients are analogous as in the second interval.

5. For $j \in (J_4^T, J]$ the solution is presented as

$$U_{jk}^{n+\frac{1}{2}} = \beta_{jk} U_{j-1,k}^{n+\frac{1}{2}} + \gamma_{jk}, \tag{2.17}$$

$$\beta_{Jk} = 0, \ \beta_{jk} = \frac{a_{jk}}{b_{jk} - c_{jk}\beta_{j+1,k}},$$
$$\gamma_{Jk} = g_3(y_k, t^{n+1}), \ \gamma_{jk} = \frac{d_{jk} + c_{jk}\gamma_{j+1,k}}{b_{jk} - c_{jk}\beta_{j+1,k}}.$$

By induction it can be proved that the estimate $0 \leqslant \beta_{jk} \leqslant 1$ is valid.

Substituting (2.13)–(2.17) into $(2.11)_{4-5}$, we get the linear system

$$\begin{pmatrix} A_{11} & A_{12} & 0 & 0 \\ A_{21} & A_{22} & A_{23} & 0 \\ 0 & A_{32} & A_{33} & A_{34} \\ 0 & 0 & A_{43} & A_{44} \end{pmatrix} \begin{pmatrix} U_{J_1^T *}^{n+\frac{1}{2}} \\ U_{J_2^T *}^{n+\frac{1}{2}} \\ U_{J_3^T *}^{n+\frac{1}{2}} \\ U_{J_4^T *}^{n+\frac{1}{2}} \end{pmatrix} = \begin{pmatrix} B_1 \\ B_2 \\ B_3 \\ B_4 \end{pmatrix}, \tag{2.18}$$

with coefficients defined by

$$A_{11} = \frac{2}{\tau} + \frac{1}{h^2}\Big(2 - \alpha_{J_1^T+1,*} - \frac{1}{Y_2 - Y_1} \sum_{k=K_1}^{K_2} \alpha_{J_1^T-1,k} \ s^j_{J_1^T-\frac{1}{2},k}\Big),$$

$$A_{12} = -\frac{\beta_{J_1^T+1,*}}{h^2}, \ A_{21} = -\frac{\alpha_{J_2^T-1,*}}{h^2},$$

$$A_{22} = \frac{2}{\tau} + \frac{1}{h^2}\Big(2 - \beta_{J_2^T-1,*} - \frac{1}{Y_2 - Y_1}\sum_{k=K_1}^{K_2} \alpha_{J_2^T+1,k}\ s^j_{J_2^T+\frac{1}{2},k}\Big),$$

$$A_{23} = -\frac{1}{h^2(Y_2 - Y_1)}\sum_{k=K_1}^{K_2} \beta_{J_2^T+1,k}\ s^j_{J_2^T+\frac{1}{2},k},$$

$$A_{32} = -\frac{1}{h^2(Y_2 - Y_1)}\sum_{k=K_1}^{K_2} \alpha_{J_3^T-1,k}\ s^j_{J_3^T-\frac{1}{2},k},$$

$$A_{33} = \frac{2}{\tau} + \frac{1}{h^2}\Big(2 - \alpha_{J_3^T+1,*} - \frac{1}{Y_2 - Y_1}\sum_{k=K_1}^{K_2} \beta_{J_3^T-1,k}\ s^j_{J_3^T-\frac{1}{2},k}\Big),$$

$$A_{34} = -\frac{\beta_{J_3^T+1,*}}{h^2},\ A_{43} = -\frac{\alpha_{J_4^T-1,*}}{h^2},$$

$$A_{44} = \frac{2}{\tau} + \frac{1}{h^2}\Big(2 - \beta_{J_4^T-1,*} - \frac{1}{Y_2 - Y_1}\sum_{k=K_1}^{K_2} \beta_{J_4^T+1,k}\ s^j_{J_4^T+\frac{1}{2},k}\Big),$$

$$B_i = \frac{1}{h^2(Y_2 - Y_1)}\sum_{k=K_1}^{K_2} \gamma_{J_i^T-1,k}\ s^j_{J_i^T-\frac{1}{2},k} + \frac{2}{\tau}U^n_{J_i^T*} + f^{n+\frac{1}{2}}_{J_i^T*} + \frac{\gamma_{J_i^T+1,*}}{h^2} \text{ for } i \in \{1,3\},$$

$$B_i = \frac{1}{h^2(Y_2 - Y_1)}\sum_{k=K_1}^{K_2} \gamma_{J_i^T+1,k}\ s^j_{J_i^T+\frac{1}{2},k} + \frac{2}{\tau}U^n_{J_i^T*} + f^{n+\frac{1}{2}}_{J_i^T*} + \frac{\gamma_{J_i^T-1,*}}{h^2} \text{ for } i \in \{2,4\}.$$

Employing the estimates for α and β, we see that the coefficient matrix A in (2.18) is diagonally dominant. To briefly collaborate on it, note that only the diagonal elements are positive in A. Then consider, for example, the first row of A. As we have

$$0 \geqslant -\alpha_{J_1^T+1,*} - \beta_{J_1^T+1,*} \geqslant -1 \ \text{ and } \ \frac{1}{Y_2 - Y_1}\sum_{k=K_1}^{K_2} s_{J_1^T-\frac{1}{2},k} = 1,$$

evidently $|A_{11}| \geqslant |A_{12}|$.

Therefore, due to the diagonal dominance, unique solutions $U^{n+\frac{1}{2}}_{J_1^T*}$, $U^{n+\frac{1}{2}}_{J_2^T*}$, $U^{n+\frac{1}{2}}_{J_3^T*}$, $U^{n+\frac{1}{2}}_{J_4^T*}$ exist. Then the backward factorization is applied, computing the remaining values of U. The procedure is analogous to solve (2.12). Therefore, we conclude the latter results of this chapter into the following theorem.

Theorem 2.4. *A unique solution to* (2.11), (2.12) *exists and can be computed using the efficient factorization algorithm* (2.13)–(2.18).

Not only do results (2.13)–(2.18) serve as a proof of Theorem 2.4; they also define the constructive algorithm to solve (2.11), (2.12). Furthermore, in each time substep we first find values of solution on truncation lines and then in each segment between these lines independently from other segments, thus the proposed method might be promising in the sense of speed-up by parallel computing, but we leave analysis of this question for future works.

To briefly comment on the algorithmic extension to more reduced dimension zones, each additional reduced dimension zone increases the rank of coefficient matrix A in (2.18) by 2, while A remains tridiagonal.

Finally, from this section we see that the ADI method is well compatible with the MAPDD for heat conduction problems, as the implementation of the averaging operator that is used to truncate dimensions is a natural one on structured grids. Considering the ADI method for 3D cases, it does not have a natural extension, but similar ideas give rise to the method known as the stabilizing corrections (see, e.g., [28, 29]). However, it remains effective if the calculations can be reduced to 2D – given radial symmetry in a rod, for example (see Chapter 1 or [38]).

2.6 Convergence of the FVM ADI scheme for the hybrid model

Let us rewrite (2.11) and (2.12) in a compact form as

$$\begin{aligned} &\frac{U_{jk}^{n+\frac{1}{2}} - U_{jk}^{n}}{\tau/2} + \mathcal{A}_1^h U_{jk}^{n+\frac{1}{2}} + \mathcal{A}_2^h U_{jk}^{n} = f_{jk}^{n+\frac{1}{2}}, \\ &\frac{U_{jk}^{n+1} - U_{jk}^{n+\frac{1}{2}}}{\tau/2} + \mathcal{A}_1^h U_{jk}^{n+\frac{1}{2}} + \mathcal{A}_2^h U_{jk}^{n+1} = f_{jk}^{n+\frac{1}{2}} \end{aligned} \tag{2.19}$$

with the operators $\mathcal{A}_1^h$ and $\mathcal{A}_2^h$ defined by

$$\mathcal{A}_1^h U = \begin{cases} A_1^h U_{jk}, & (x_j, y_k) \in \Omega_h \setminus \omega_R, \\ A_1^h U_{j*}, & j \in (J_1^T, J_2^T) \cup (J_3^T, J_4^T), \\ 0, & k \in [K_1^T, K_2^T] \cup [K_3^T, K_4^T] \\ \dfrac{1}{h^2}\Big(- S_y^H(U_{j-1}) + 2U_{j*} - U_{j+1,*}\Big), & j \in \{J_1^T, J_3^T\}, \\ \dfrac{1}{h^2}\Big(- S_y^H(U_{j+1}) + 2U_{j*} - U_{j-1,*}\Big), & j \in \{J_2^T, J_4^T\}, \end{cases}$$

$$\mathcal{A}_2^h U = \begin{cases} A_2^h U_{jk}, & (x_j, y_k) \in \Omega_h \setminus \omega_R, \\ A_2^h U_{*k}, & k \in (K_1^T, K_2^T) \cup (K_3^T, K_4^T), \\ 0, & j \in [J_1^T, J_2^T] \cup [J_3^T, J_4^T] \\ \dfrac{1}{H^2}\Big(- S_x^h(U_{k-1}) + 2U_{*k} - U_{*,k+1}\Big), & k \in \{K_1^T, K_3^T\}, \\ \dfrac{1}{H^2}\Big(- S_x^h(U_{k+1}) + 2U_{*k} - U_{*,k-1}\Big), & k \in \{K_2^T, K_4^T\}. \end{cases}$$

Now let us consider discrete functions $U_{jk} = U(x_j, y_k)$, $V_{jk} = V(x_j, y_k)$ defined on the spatial mesh $\Omega_{h,RD}$ (for definition see (2.10)). Let us denote the set of such vectors by D_h.

For $U, V \in D_h$, such that $U_{0k} = U_{Jk} = 0$, $k \in [K_1, K_2]$, and $V_{j0} = V_{jK} = 0$, $j \in [J_1, J_2]$, the following formulas define an inner product and a norm in this vector space

$$\begin{aligned} (U,V) = &\sum_{j=1}^{J_1^T-1} \sum_{k=K_1}^{K_2} U_{jk} V_{jk} h s^k_{j,k-\frac{1}{2}} + (Y_2 - Y_1) \sum_{j=J_1^T}^{J_2^T} U_{j*} V_{j*} h \\ &+ \sum_{j=J_2^T+1}^{J_3^T-1} \sum_{k=K_1}^{K_2} U_{jk} V_{jk} h s^j_{j-\frac{1}{2},k} + (Y_2 - Y_1) \sum_{j=J_3^T}^{J_4^T} U_{j*} V_{j*} h \\ &+ \sum_{j=J_4^T+1}^{J-1} \sum_{k=K_1}^{K_2} U_{jk} V_{jk} h s^j_{j-\frac{1}{2},k} + \sum_{j=J_1}^{J_2} \sum_{k=1}^{K_1^T-1} U_{jk} V_{jk} H s^k_{j,k-\frac{1}{2}} \\ &+ (X_2 - X_1) \sum_{k=K_1^T}^{K_2^T} U_{*k} V_{*k} H + \sum_{j=J_1}^{J_2} \sum_{k=K_2^T+1}^{K_1-1} U_{jk} V_{jk} H s^k_{j,k-\frac{1}{2}} \end{aligned}$$

$$+\sum_{j=J_1}^{J_2}\sum_{k=K_2+1}^{K_3^T-1} U_{jk}V_{jk}Hs^k_{j,k-\frac{1}{2}} + (X_2-X_1)\sum_{k=K_3^T}^{K_4^T} U_{*k}V_{*k}H$$
$$+\sum_{j=J_1}^{J_2}\sum_{k=K_4^T+1}^{K-1} U_{jk}V_{jk}Hs^k_{j,k-\frac{1}{2}},$$
$$\|U\| = (U,U)^{1/2}.$$

Although the presented expanded form of this inner product is somewhat lengthy, this termwise representation proves to be useful for the next lemma.

Lemma 2.5. *The discrete operators $\mathcal{A}_1^h$ and $\mathcal{A}_2^h$ are symmetric and positive semi-definite operators.*

Proof. Let us consider $U, V \in D_h$, such that $U_{0k} = U_{Jk} = 0$, $k \in [K_1, K_2]$, and $V_{j0} = V_{jK} = 0$, $J \in [J_1, J_2]$

The investigation of operators $\mathcal{A}_1^h$ and $\mathcal{A}_2^h$ is analogous, thus we will only show these properties for $\mathcal{A}_1^h$. Let us analyse the terms of $(\mathcal{A}_1^h U, V)$. First, applying the summation by parts, we rewrite the term

$$\sum_{j=1}^{J_1^T-1}\sum_{k=K_1}^{K_2} \mathcal{A}_1^h U_{jk}V_{jk}hs^j_{j-\frac{1}{2},k}$$
$$= \sum_{k=K_1}^{K_2}\left(\sum_{j=1}^{J_1^T} \partial_x U_{jk}\partial_x V_{jk}hs^j_{j-\frac{1}{2},k} - \partial_x U_{J_1^T*}V_{J_1^T*}s^j_{J_1^T-\frac{1}{2},k}\right).$$

Analogously, we also rewrite

$$\sum_{j=J_3^T+1}^{J-1}\sum_{k=K_1}^{K_2} \mathcal{A}_1^h U_{jk}V_{jk}hs^j_{j-\frac{1}{2},k}$$
$$= \sum_{k=K_1}^{K_2}\left(\sum_{j=J_3^T+1}^{J} \partial_x U_{jk}\partial_x V_{jk}hs^j_{j-\frac{1}{2},k} + \partial_x U_{J_3^T+1,k}V_{J_3^T*}s^j_{J_3^T-\frac{1}{2},k}\right).$$

Inside the zones where the y dimension is reduced, we have, for example,

$$\sum_{j=J_1^T}^{J_2^T} \mathcal{A}_1^h U_{j*} V_{j*} h = \frac{1}{h}\left(-S_H^y(U_{J_1^T-1}) + 2U_{J_1^T*} - U_{J_1^T+1,*}\right) V_{J_1^T*}$$

$$+ \sum_{j=J_1^T+1}^{J_2^T-1} \mathcal{A}_1^h U_{j*} V_{j*} h + \frac{1}{h}\left(-S_H^y(U_{J_2^T+1}) + 2U_{J_2^T*} - U_{J_2^T-1,*}\right) V_{J_2^T*}$$

$$= \sum_{j=J_1^T+1}^{J_2^T} \partial_x U_{j*} \partial_x V_{j*} h - \partial_x U_{J_2^T*} V_{J_2^T*} + \partial_x U_{J_1^T+1,*} V_{J_1^T*}$$

$$- \partial_x U_{J_1^T+1,*} V_{J_1^T*} + \frac{U_{J_1^T*} - S_H^y U_{J_1^T-1}}{h} V_{J_1^T*} + \partial_x U_{J_2^T*} V_{J_2^T*}$$

$$- \frac{S_H^y U_{J_2^T+1} - U_{J_2^T*}}{h} V_{J_2^T*}.$$

Next, in the middle part we have

$$\sum_{j=J_2^T+1}^{J_3^T-1} \sum_{k=K_1}^{K_2} \mathcal{A}_1^h U_{jk} V_{jk} h s^j_{j-\frac{1}{2},k} = \sum_{j=J_2^T+1}^{J_3^T} \sum_{k=K_1}^{K_2} \partial_x U_{jk} \partial_x V_{jk} h s^j_{j-\frac{1}{2},k}$$

$$- \sum_{k=K_1}^{K_2} \partial_x U_{J_3^T*} V_{J_3^T} s^j_{j-\frac{1}{2},k} + \sum_{k=K_1}^{K_2} \partial_x U_{J_2^T*} V_{J_2^T*} s^j_{j-\frac{1}{2},k}.$$

Taking into consideration identities of type

$$\sum_{k=K_1}^{K_2} \partial_x U_{J_1^T*} V_{J_1^T*} s^j_{j-\frac{1}{2},k} = \frac{Y_2 - Y_1}{h}\Big(U_{J_1^T k} - S_H^y(U_{J_1^T-1})\Big) V_{J_1^T*},$$

we see that in the overall sum of the norm, the additional terms in the latter representations cancel out.

Finally, for $k \in (0, K_1^T) \cup (K_2^T, K_1) \cup (K_2, K_3^T) \cup (K_4^T, K)$, the summation by parts yields

$$\sum_{j=J_1}^{J_2} \mathcal{A}_1^h U_{jk} V_{jk} s^k_{j,k-\frac{1}{2}}$$

$$= \sum_{j=J_1+1}^{J_2} \partial_x U_{jk} \partial_x V_{jk} s^k_{j,k-\frac{1}{2}} = \sum_{j=J_1}^{J_2} U_{jk} \mathcal{A}_1^h V_{jk} s^k_{j,k-\frac{1}{2}}.$$

Therefore, we have that the symmetry property $(A_1^h U, V) = (U, A_1^h V)$ holds. Furthermore, since $(\mathcal{A}_1^h U, U) \geqslant 0$, the operator $\mathcal{A}_1^h$ is positive semi-definite. $\square$

Proposition 2.6. *If U^n is the solution of ADI scheme* (2.11), (2.12), *when $f^n \equiv 0$ and $g_i^n \equiv 0$, $i = 1, \ldots, 4$, then the following stability estimate is valid*

$$\|(I + \frac{\tau}{2}\mathcal{A}_2^h)U^n\| \leqslant \|(I + \frac{\tau}{2}\mathcal{A}_2^h)U^0\|.$$

The proof of Proposition 2.6 is analogous to the one of Proposition 2.3, as the operators $\mathcal{A}_1^h$, $\mathcal{A}_2^h$ have the same properties of symmetry and positive semi-definiteness as previously analysed A_1^h, A_2^h.

2.7 Computational experiments

The accuracy of time integration of ADI schemes

First, the time integration accuracy of ADI solver for a nonreduced model was tested. Consider (2.1) with the ADI scheme (2.5), solved on a uniform spatial grid Ω_h with parameters $T = 1$, $X = 1$, $Y = 1$, $X_1 = Y_1 = 1/3$, $X_2 = Y_2 = 2/3$. In the first test problem we have used functions $u^0 = 0$, $f(x, y, t) = 0$, $g_1(y, t) = (1 + 4t)e^{-y^2}$, $g_2(x, t) = 7te^{-4x^2}$, $g_3(y, t) = 3 - 50(y - Y_1)(y - Y_2)$, $g_4(x, t) = e^t e^{-20(x-X_1)(x-X_2)}$ and the benchmark solution $U(x_j, y_k, t_N)$ was computed using $\tau = 2.5 \cdot 10^{-5}$. The second order convergence rate is confirmed by the computational results, thus indicating that the ADI scheme accuracy agrees well with the theoretical prediction (see Table 2.1 below, displaying correspondence between a sequence of time steps τ, errors $e(\tau)$ and experimental convergence rates $\rho(\tau)$ for the discrete solution of the ADI scheme (2.5)).

Here the errors $e(\tau)$ and experimental convergence rates $\rho(\tau)$ at time $t = T$ are defined in the maximum norm

$$e(\tau) = \max_{(x_j, y_k) \in \Omega_h} \left| U_{j,k}^N - U(x_j, y_k, T) \right|, \ \rho(\tau) = \log_2 \left(\frac{e(2\tau)}{e(\tau)} \right).$$

Table 2.1: Results of errors $e(\tau)$ and experimental convergence rates $\rho(\tau)$ with corresponding τ for the first test problem with $J = K = 600$.

τ	$e(\tau)$	$\rho(\tau)$
0.0008	$6.9300 \cdot 10^{-4}$	6.2786
0.0004	$1.2685 \cdot 10^{-4}$	2.4497
0.0002	$3.1460 \cdot 10^{-5}$	2.0115
0.0001	$7.4977 \cdot 10^{-6}$	2.0690

The accuracy of reduced dimension model

For the second test problem, let us show the accuracy of reduced dimension model (2.7). Here we track the difference between solution to the full model and solution to the reduced dimension model, thus the following error definition is used

$$e(\delta) = \max_{(x_j, y_k) \in \omega} \left| U^N_{j,k} - U^N_{j,k}(\delta) \right|.$$

We also present the relative error

$$e_r = \frac{e(\delta)}{\left| U^N_{j^*,k^*} \right|} \cdot 100\%,$$

here j^*, k^* are indices of the grid point at which the error $e(\delta)$ is found. The results are presented in Table 2.2 below. All simulations are hardly visually distinguishable from each other.

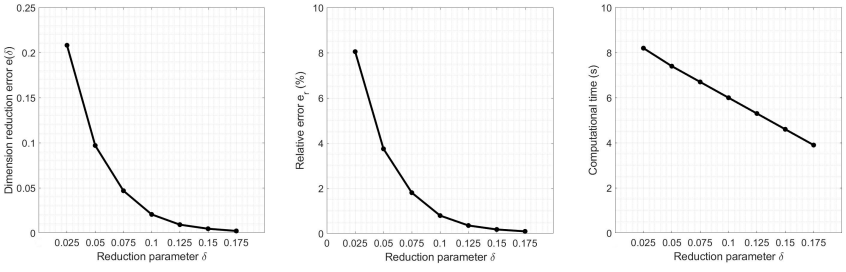

(a) δ *vs* $e(\delta)$ (b) δ *vs* e_r (c) δ *vs* CPU time

Figure 2.6: Graphs of results from Table 2.2, showing correspondence between δ and other data.

Table 2.2: Functions of the first test problem were used for the second test problem to investigate the error and speed-up with respect to reduction parameter δ. Here time is measured in seconds and notation $\delta = \delta^*$ corresponds to the full model.

δ	$e(\delta)$	e_r	time
δ^*	–	–	9.4
0.175	$2.242 \cdot 10^{-3}$	0.094%	8.2
0.150	$4.668 \cdot 10^{-3}$	0.178%	7.4
0.125	$9.194 \cdot 10^{-3}$	0.353%	6.7
0.100	$2.057 \cdot 10^{-2}$	0.792%	6.0
0.075	$4.682 \cdot 10^{-2}$	1.806%	5.3
0.050	$9.699 \cdot 10^{-2}$	3.747%	4.6
0.025	$2.082 \cdot 10^{-1}$	8.051%	3.9

The larger zones are reduced to 1D, the better is the computational speed-up, as in the reduced dimension zones it is sufficient to compute only one line/column of values. Therefore, the speed-up gained by shrinking the size of full-dimensional zones, presented in Table 2.2, is mostly due to a lesser amount of computational operations.

For the full model case of Table 2.2, the error of time discretization equals $e(\tau) = 2.279 \cdot 10^{-4}$ and was calculated using a benchmark solution with $\tau = 5 \cdot 10^{-5}$.

In this second test problem, we have used the same functions as in the first test problem, but with parameters $X_1 = Y_1 = 0.45$, $X_2 = Y_2 = 0.55$ and $J = K = 300$.

For the theoretical evaluation of the error in terms of δ, we refer the reader to [3, 57], where an effective asymptotic analysis method was applied to derive some estimates.

Visualisation of results

To get a better grasp of accuracy preserved by the reduced dimension model, let us compare results of the full model and results of the hybrid dimension model with $\delta = 0.05$, $\delta = 0.1$ and $\delta = 0.15$.

Let us take all functions equal to zero, except for f, which is set to $f(x, y, t) = 100e^t \cos(4\pi x) \cos(4\pi y)$ in the bottom-right quarter of the central part L_0 . This test was implemented using parameters $J = K = 300$, $\tau = 0.001$, $X_1 = Y_1 = 0.4$, $X_2 = Y_2 = 0.6$ and $T = 1$.

Figures 2.7, 2.8 below depict results of hybrid dimension model versus full model. In Figure 2.7, only the horizontal slice $(x, y) \in [0, X] \times [Y_1 - 1; Y_2 + 1]$ is represented.

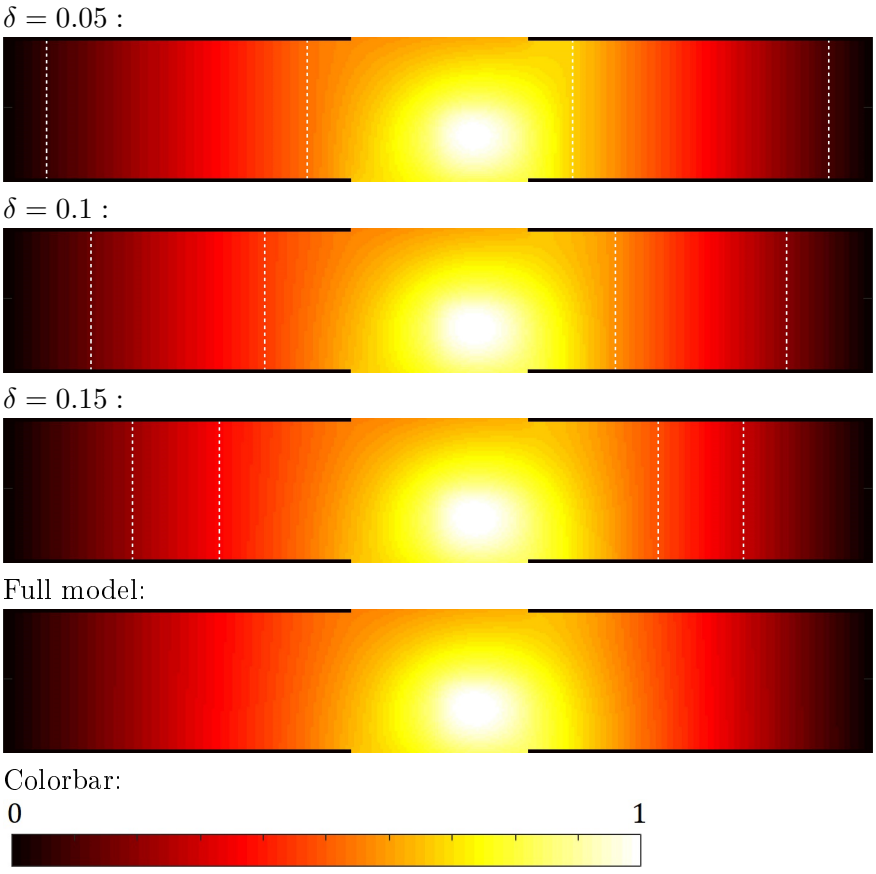

Figure 2.7: A visual comparison of full model and reduced dimension model in three cases of δ. The truncations are marked as white vertical dashed lines.

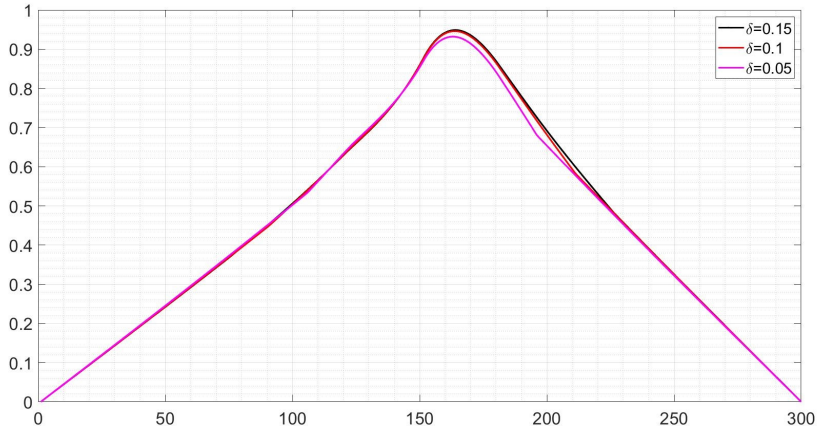

Figure 2.8: Values of solution to the hybrid dimension model with different values of δ at 1D cross section $k = 175$. The curve of $\delta = \delta^*$ is visually indistinguishable from $\delta = 0.15$.

2.8 Conclusions

A finite volume method is used to approximate space differential operators with nonclassical conjugation conditions between 2D and 1D parts. An ADI type scheme is applied to solve the hybrid dimension problem in time. An efficient modification of the basic factorization algorithm is developed to resolve nonlocal conjugation conditions. Results of numerical experiments confirm the theoretical conclusion that hybrid dimension models can be effectively used to simulate heat conduction models for a broad variety of domains and coefficients. Comparison of visualisations and computational times justifies the usage of proposed algorithm for many practical applications.

3 Viscous flow in elastic tube

In this chapter, one of the problems that were encountered in the project "Multiscale Mathematical and Computer Modeling for Flows in Networks: Application to Treatment of Cardiovascular Diseases"[1] is analysed from the perspective of numerical mathematics.

This problem was derived from [56] by team members and discussed together with colleagues Kristina Kaulakytė and Nikolajus Kozulinas under the supervision of professors Grigory Panasenko, Konstantinas Pileckas and Raimondas Čiegis. However, only the results that were derived solely by the author of this dissertation are presented here, unless provided otherwise.

The main target of this chapter is a fourth order PDE with constant coefficients

$$c_1 u_{tt} + c_2 u_{xxtt} + c_3 u_t + c_4 u_{xxt} + c_5 u_{xxxx} + c_6 u_{xx} + c_7 u = 0.$$

It is related to a specific case of viscous fluid flowing through a vessel with an elastic wall. Its solution corresponds to the averaged velocity of fluid at some longitudinal position of a vessel, where a 3D model has been reduced to 1D. Therefore, numerical results of this equation can significantly contribute to the progress of fluid-structure interaction problems, where two media with different physical characteristics are coupled.

As this equation was obtained by analysing the speed of fluid averaged over a cross-section instead of a full 3D solution, it also falls into the category of reduced dimension models. However, here the approach is different from the previous chapters, as the dimension has been reduced from 3D to 1D in the whole domain, thus there are no conjugation zones. Although for some processes a model with partially reduced dimensions might be

[1] Project No 09.3.3-LMT-K-712-17-0003, `www.hemodynamics.mif.vu.lt`

better (e.g., for a detailed consideration of bifurcations [20, 21]), the full dimension reduction from 3D to 1D for nonstationary models of flow in thin tubes was successfully applied in numerous works [8, 11, 12, 55].

The obtained fourth order PDE is far from being classical, however, from the perspective of operator splitting [31, 47], it includes equations such as the dissipation, vibration, heat conduction, hyperbolic heat conduction and pseudo-parabolic equations. Naturally, there is no universal discretization of derivatives to solve equations of all physical processes, thus the application of different schemes at distinct splitting steps might be an effective approach. Nonetheless, instead of using operator splitting, this chapter aims to suggest a single numerical scheme to ensure a numerical solution for a sufficiently broad variety of coefficients, within the range of applications of our interest.

In a more general sense, fourth order PDEs are used in mathematical models to describe processes such as elasticity, vibrations, geological and chemical transport phenomena [27, 45, 50, 64]. Some methods have been successfully applied to find analytical solutions, for example, the variational iteration method [9], the homotopy perturbation method [48] and the Adomian decomposition method [80]. However, these methods don't apply to our case due to some additional terms. As for most fourth order PDEs analytical solutions are unknown, numerical solutions are required.

For this PDE problem, under some conditions, the Fourier transform method could also be used and should be considered as a good competitor against numerical methods. However, due to some future interests for the solver, such as a wide class of applicable initial and boundary conditions, the inclusion of additional processes in some parts of domain or the possibility to return to fully 3D regions in some subdomains and couple parts of hybrid dimensions, the author's interest is to develop the current numerical approach.

It is interesting to note that from the theoretical point of view, very few studies focus on PDEs of order higher than two.

To give some sense about the voidness of the field, assume we want to know a general definition for elliptic, parabolic or hyperbolic PDEs. The short answer is: there is no general definition. The theory is well described only for the first and second order PDEs in terms of eigenvalues and discriminants of coefficients [17,62]. There are some nice descriptions only for specific cases of higher order equations and systems (e.g., [42]). Some classification in terms of quasi linearity was done in [32].

To reflect on the complexity behind this general classification problem, we invite the reader to consider the first definitions of elliptic, parabolic and hyperbolic PDEs that were given by Jacques Hadamard in 1926 (see [25]). However, the classification has been incomplete ever since, as some operators simply do not classify for either case.

Considering the fluid-structure interaction models, they are of natural importance in various biological and engineering fields [10, 44]. In [24] and [15] the existence of a solution for some fluid-structure interaction problems is studied. An up-to-date comprehensive model is given in [56].

This chapter is constructed in the following way. In Section 3.1, the PDE problem is formulated and a brief dimensional analysis is presented. In Section 3.2, a numerical scheme is constructed using forward and central finite differences. Its stability is analysed in Section 3.3 and accuracy is analysed in Section 3.4. Section 3.5 discusses some issues of initial and boundary conditions. Some computational tests are provided in Section 3.6. In Section 3.7 an alternative scheme constructed using only central finite differences is proposed. Its stability and accuracy are briefly analysed. Section 3.8 discusses some conclusions that arise from comparison of these two schemes, as well as comparison of different boundary conditions.

3.1 The PDE problem

Let us consider the following PDE with constant coefficients a_i:

$$a_1 v_{tt} + a_2 v_{xxtt} + a_3 v_t + a_4 v_{xxt} + a_5 v_{xxxx} + a_6 v_{xx} + a_7 v = 0. \quad (3.1)$$

Here the lower index of v denotes derivatives in space and time and we are interested in finding a solution at time T, given some initial and boundary conditions that will be discussed later.

First, let us note the importance of dimensional analysis from the perspective of numerical computations. To get some intuition behind its motivation, note that for practical problems the constants a_i include complicated combinations of numerous physical parameters. For applications at various scales, these constants might be of unreasonable orders of magnitude, thus causing difficulties in computations.

For example, consider a small human arteriole with length of order 10^{-3} m and an elastic wall with thickness of order 10^{-4} m. The constants a_i were found to be of the following orders and signs:

a_1	a_2	a_3	a_4	a_5	a_6	a_7
10^{-41}	-10^{-51}	10^{-5}	-10^{-8}	10^{-14}	-10^{-11}	10^{-7}

As the numerical calculations have to be implemented using a computational code, a very low order of coefficients gives rise to some challenges. For example, the variables with more decimal values use more memory and might reduce the speed of computations, which is quite the opposite of our interest.

Therefore, one natural way is to redefine the characteristic measures. For example, let us choose the length 0.1 mm and the time 1 s as the new characteristic values for computations. Including emerging multipliers of dimensional analysis in constants a_i, we derive the new set of constants c_i of the following sign and order:

c_1	c_2	c_3	c_4	c_5	c_6	c_7
10^{-41}	-10^{-43}	10^{-5}	-10^{0}	10^{2}	-10^{-3}	10^{-7}

With such constants, the effect of first two terms might only be seen for astronomically large times T, thus it would be natural to set c_1 and c_2 to zero in practical computations.

Next, note that the differential terms in (3.1) encode multiple physical phenomena. Therefore, by setting some of the co-

efficients a_i to zero, various processes can be encountered. Also, recall that from the perspective of operator splitting, these processes might require different discretizations to be applied at each splitting step.

For example, consider the differential equation of the form $u_t + \sigma u = 0$. If the constant σ is negative, it is the well-known differential equation for exponential growth, with one of the most popular applications to model bacterial growth [26]. With a positive σ, it encodes the decay process, which can be used to model the decay of population, as well as dissipation or absorption. Naturally, the latter is expected in our model, which is approved by the same sign of constants a_3 and a_7. From the numerical perspective, some simple schemes such as forward, central or backward differences are suitable to solve it.

Next, consider the classical parabolic equation $u_t = du_{xx}$. The constant d here is expected to be positive, as in the negative case it is considered to be not well-posed [59]. Thus is it natural that in our PDE the coefficients a_3 and a_6 are of different signs. One important aspect about this part is the cautious consideration of the Richardson scheme [4] (also known as the leapfrog scheme for the heat equation [5]), which is a well-known example of unconditionally unstable approximation for parabolic equations. However, as there are additional terms on the overall equation, they might regularize this instability to some extent.

The equation $(u - \alpha u_{xx})_t = du_{xx}$ with $\alpha > 0$ (and again $d > 0$) is an interesting pseudo-parabolic equation. The larger the coefficient α, the less the solution acts as in the heat equation problem (case $\alpha = 0$). As the corresponding constant a_4 is of considerably high order, the pseudo-parabolic behavior of solution is expected in our model. Some strategies to solve the pseudo-parabolic equation numerically were investigated in [35, 39].

The equation $u_{tt} + cu_{xxxx} = 0$ is a well-known Euler-Bernoulli beam equation [63]. The homogeneous case corresponds to an unforced beam, that is, without outer body forces being applied. Here c should be positive, thus we expect the constants a_1 and a_5 in our model to be of the same sign. Some finite difference

schemes to solve it are given in [16].

Considering $a_1 v_{tt} + a_6 v_{xx} = 0$ with different signs of a_1 and a_6, it is the classical hyperbolic wave equation. However, if the difference between orders of magnitude of coefficients a_1 and a_6 is large, visible vibrational effects are not to be expected, as it is in the example of blood flow in elastic arteriole.

Another interesting example that can be seen as built-in for our considered equation is the hyperbolic heat equation of the form $\epsilon u_{tt} + u_t = u_{xx}$ with a small positive constant ϵ. For this case, some robust finite difference schemes and their properties are analysed in [37]. The recommendations provided in the latter research can be applicable to (3.1), as we have $a_1 > 0$, $a_3 > 0$ and $a_6 < 0$.

Many more equations can be seen as included in the combined model (3.1). It is a complex task to provide a robust universal scheme for all possible cases, while the approach of operator splitting might require many intermediate stages for each time step with the risk of slowing down the overall solution. As our aim is to suggest a quick numerical solver, instead we make use of some information that is known about our cases of interest and the following approach is considered.

In fluid-structure interaction problems that arise from hemodynamics, some effects are very low (e.g., vibration), while some degree of others is expected (e.g., absorption). Therefore, the approach provided in this chapter reflects the practical applications of (3.1) to the cases of our interest, where the discretization of dominant terms can be performed using some simple central and forward differences. However, from the perspective of operator splitting we saw that the approximation of time derivative using central difference should be considered cautiously, as the corresponding Richardson scheme gives rise to a possible instability of numerical approximation.

3.2 Numerical scheme

Let us approximate the derivatives in

$$c_1 u_{tt} + c_2 u_{xxtt} + c_3 u_t + c_4 u_{xxt} + c_5 u_{xxxx} + c_6 u_{xx} + c_7 u = 0. \quad (3.2)$$

numerically using the finite difference method. See Figure 3.1 below for a simplified visualisation of proposed numerical approximations of these terms.

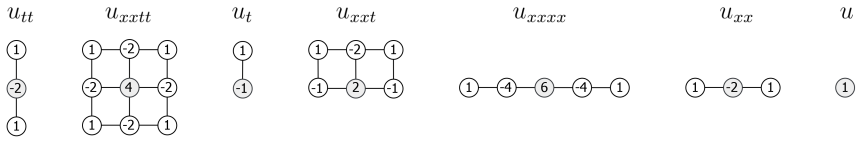

Figure 3.1: A schematic visualisation of numerical approximation of terms involved in (3.2), here the numbers inside circles correspond to the weights of coefficients of numerical points for approximations of differential terms

A uniform numerical grid is used, as no localized effects are of interest here and thus there is no need to thicken the mesh at some places. Let us denote by U_i^n the numerical solution to (3.2) at $(x_i, t_n) = (ih, n\tau)$, here h and τ are step sizes in space and time, respectively, with

$$i = 0, \ldots, N_h, \; h = L/N_h,$$
$$n = 0, \ldots, N_\tau, \; \tau = T/N_\tau,$$

where L is the length of spatial domain Ω and T is the length of time interval. The computational molecule applied at numerical mesh interior point U_i^n is visualised in Figure 3.2

For simplicity, the following notations will be used in this section:

$$m_1 = \frac{c_1}{\tau^2}, \; m_2 = \frac{c_2}{h^2\tau^2}, \; m_3 = \frac{c_3}{\tau}, \; m_4 = \frac{c_4}{h^2\tau},$$
$$m_5 = \frac{c_5}{h^4}, \; m_6 = \frac{c_6}{h^2}, \; m_7 = c_7.$$

Now, let us find the coefficients of each point of the computational molecule:

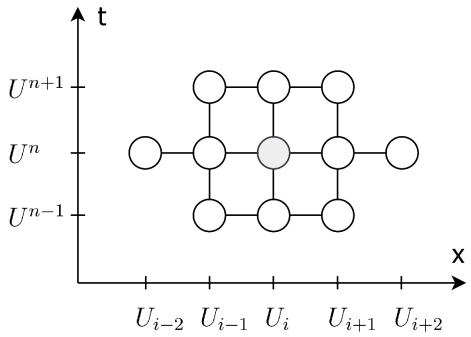

Figure 3.2: A computational molecule (stencil).

$$
\begin{aligned}
U_{i-i}^{n+1}: &\quad m_2 + m_4;\\
U_i^{n+1}: &\quad m_1 - 2m_2 + m_3 - 2m_4;\\
U_{i-1}^{n+1}: &\quad m_2 + m_4;\\
U_{i-2}^{n}: &\quad m_5;\\
U_{i-1}^{n}: &\quad -2m_2 - m_4 - 4m_5 + m_6;\\
U_{i}^{n}: &\quad -2m_1 + 4m_2 - m_3 + 2m_4 + 6m_5 - 2m_6 + m_7;\\
U_{i+1}^{n}: &\quad -2m_2 - m_4 - 4m_5 + m_6;\\
U_{i+2}^{n}: &\quad m_5;\\
U_{i-1}^{n-1}: &\quad m_2;\\
U_{i}^{n-1}: &\quad m_1 - 2m_2;\\
U_{i+1}^{n-1}: &\quad m_2.
\end{aligned}
$$

As there are three points in the unknown time layer U^{n+1}, at each time step the solution is implemented implicitly using the classical Thomas algorithm for tridiagonal matrices.

Note that in general, the expected accuracy of this scheme is $O(h^2 + \tau)$, as forward differences are used to approximate derivatives of first order in time, while the second and fourth order derivatives are approximated using central differences.

3.3 Stability

To prove the stability of proposed scheme, we use Fourier stability analysis. Using the standard notations of this method, we consider the solution in a form

$$U^n = G^n e^{ik_m x},$$

here k_m is the wavenumber and i is the imaginary unit $i^2 = -1$. Therefore, the Equation (3.2) results in a quadratic equation for the time amplification factor G

$$\begin{aligned} m_1(G - 2 + G^{-1}) + m_2(G - 2 + G^{-1})(e^{-i\theta} - 2 + e^{i\theta}) \\ +m_3(G - 1) + m_4(G - 1)(e^{-i\theta} - 2 + e^{i\theta}) \\ +m_5(e^{-2i\theta} - 4e^{-i\theta} + 6 - 4e^{i\theta} + e^{2i\theta}) \\ +m_6(e^{-i\theta} - 2 + e^{i\theta}) + m_7 = 0, \end{aligned} \tag{3.3}$$

here $\theta = k_m h$. Applying some standard trigonometric identities, namely,

$$\frac{e^{i\theta} - e^{-i\theta}}{2i} = \sin(\theta) \iff -\frac{1}{4}\left(e^{i\theta} - 2 + e^{-i\theta}\right) = \sin^2(\theta/2),$$

the Equation (3.3) results in

$$G^2 A + GB + C = 0 \tag{3.4}$$

with

$$\begin{aligned} A &= m_1 - 4m_2 \sin^2(\theta/2) + m_3 - 4m_4 \sin^2(\theta/2), \\ B &= -2m_1 + 8m_2 \sin^2(\theta/2) - m_3 + 4m_4 \sin^2(\theta/2) \\ &\quad + 16m_5 \sin^4(\theta/2) - 4m_6 \sin^2(\theta/2) + m_7, \\ C &= m_1 - 4m_2 \sin^2(\theta/2). \end{aligned}$$

Recall that $|G| \leqslant 1$ must hold for a scheme to be stable, thus the most straightforward way to check stability is to manually evaluate

$$G_{1,2} = \frac{-B \pm \sqrt{B^2 - 4AC}}{2A} \tag{3.5}$$

for specific cases of interest.

Let us recall that in practical calculations, the constants m_i include complicated combinations of parameters involved in the model, such as the radius of tube, elastic tube thickness, density of the elastic medium, Young's modulus, Poisson's ratio and dynamic viscosity, to name a few. Therefore, from the perspective of model parameters, a complete stability analysis is quite overcomplicated.

Let us denote $b := B/A$ and $c := C/A$, so that instead of (3.4) we have

$$G^2 + bG + c = 0. \tag{3.6}$$

In general, to indicate the criteria for stability, the well-known Hurwitz's criterion is a useful tool (see, e.g., [75]), which in our case of (3.6) states that for $b, c \in \mathbb{R}$, the following equivalence holds:

$$|G| \leqslant 1 \iff |c| \leqslant 1,\ |b| \leqslant c + 1.$$

Let us collaborate on the case of blood flow in a small elastic arteriole, where the leading constants are c_4 and c_5, thus let us make an assumption for a moment that the rest of c_i are equal to zero. Consequently, $c = 0$ and from (3.6) we have

$$G^2 + bG = G(G + b) = 0 \iff G_1 = 0,\ G_2 = -b.$$

Furthermore,

$$A = -4\frac{c_4}{h^2\tau}\sin^2(\theta/2),\ B = 4\frac{c_4}{h^2\tau}\sin^2(\theta/2) + 16\frac{c_5}{h^2\tau^2}\sin^4(\theta/2).$$

Therefore, for this assumption we have that $|-b|$ equals

$$\left|-\frac{B}{A}\right| = \left|\frac{4m_4\sin^2(\theta/2) + 16m_5\sin^4(\theta/2)}{4m_4\sin^2(\theta/2)}\right| = \left|1 + 4\frac{m_5}{m_4}\sin^2(\theta/2)\right|.$$

With regards to the test problems of blood flow presented in Subsection 3.6, let us take $c_5/c_4 = -4$, thus in this case we get

$$\left|\frac{B}{A}\right| = \left|1 - 16\frac{\tau}{h^2}\sin^2(\theta/2)\right| \leqslant 1.$$

For $\sin^2(\theta/2)$ close to 0, the latter inequality easily holds. Let us consider the maximum case (in the sense of sin function), that

is, $\theta = \pi$. We get the stability condition

$$\tau \leqslant \frac{h^2}{8}. \tag{3.7}$$

Therefore, (3.7) can be considered as a referential stability criteria for the example of blood flow in elastic arteriole even with all of c_i being nonzero. From the practical perspective, e.g. for the constants of Subsection 3.6, the time step τ was taken approximately equal to $0.9 \cdot \frac{h^2}{8}$ to achieve stable computations.

To sum up, it should be emphasized that with the current numerical scheme, in practice a good pair of h and τ can be easily found manually, followed by a reasonable accuracy. From the perspective of numerical simulations, we consider checking the condition (3.5) as a sufficient criteria to indicate stability for specific cases of interest and (3.7) as a referential criteria to choose step sizes.

3.4 Accuracy

The accuracy analysis is done using the standard Taylor expansions. As classical approximations are used, only the results of accuracy analysis are mentioned here. Namely, given that $u \in C^6(\Omega)$ and $u \in C^4(0,T)$ hold, the error of numerical approximations of u_{xx}, u_{xxxx} are of order $O(h^2)$, the error of approximation of u_{tt} is of order $O(\tau^2)$, for u_{xxtt} it is $O(h^2+\tau^2)$, for u_t it is $O(\tau)$ and for u_{xxt} it is $O(h^2+\tau)$.

Therefore, we conclude that the approximation error of the current scheme, visualised in Figure 3.1, is $O(h^2+\tau)$. However, including boundary conditions might affect the order of error.

3.5 Initial and boundary conditions

First, let us note that in general, various combinations of boundary conditions at $x = 0$ and $x = L$ can be implemented. Periodic boundary conditions are a natural choice for some cases of periodic flow, though due to the term u_{xxxx}, a second order derivative would be the most natural choice. However, in the original

derivation of this PDE problem, the Neumann boundary conditions were used. Therefore, we inspect both cases of boundary conditions (first and second derivatives). The errors corresponding to each case are compared in the second test problem of Section 3.6.

For now, let us consider the following initial and boundary conditions:

$$\begin{aligned} &U(x,0) = u_0(x),\ U_t(x,0) = u_1(x),\\ &U(0,t) = D_1(t),\ U(L,t) = D_2(t),\\ &U_{xx}(0,t) = N_1(t),\ U_{xx}(L,t) = N_2(t). \end{aligned}$$

When the numerical scheme is applied at $t = 0$, the bottom layer of computational molecule addresses nonexistent points U_i^{-1} that are also called *ghost points*. The initial condition of U_t can be used to eliminate them using an approximation of the derivative U_t, for example

$$U_t(x_i, t_0) = \frac{U_i^1 - U_i^{-1}}{2\tau} + O(\tau^2). \tag{3.8}$$

It can be useful in calculations for very small T, but in other cases a practical roundabout is to replicate the initial condition for the points at $t = \tau$ and start applying the scheme from there, as the error becomes practically invisible after some steps in time.

Also note that only the differential term U_{xxxx} addresses the boundary condition U_{xx}. For example, applying the computational molecule at (x_1, t_n), this term is approximated as

$$\begin{aligned} U_{xxxx}(x_1,t_n) =& \frac{U_{xx}(x_0,t_n) - 2U_{xx}(x_1,t_n) + U_{xx}(x_2,t_n)}{h^2}\\ =& \frac{N_1(t)}{h^2} + \frac{-2U(x_0,t_n) + 5U(x_1,t_n) - 4U(x_2,t_n) + U(x_3,t_n)}{h^4}. \end{aligned}$$

Instead of boundary conditions of the second order derivatives, the Neumann boundary conditions are also suitable. However, they require to deal with the so-called *ghost* points: for example, when the scheme presented in Figure 3.1 is applied at (x_1, t_n), the *ghost* point U_{-1}^n is addressed in calculations. It is

avoided when using the second order derivatives at boundaries, thus there is no need to incorporate *ghost* points, as seen above. However, these points can be eliminated by approximating the boundary conditions.

Take, for example, $u_0(x) = u_1(x) = 0$, $U(0,t) = \sin(t)$, $U(L,t) = e^t$, $U_x(0,t) = \cos(t)$, $U_x(L,t) = e^t$, the set of constants from Subsection 3.6 and eliminate the *ghost* points using the same type of approximation as in (3.8), namely,

$$U_x(x_i, t_n) = \frac{U_{i+1}^n - U_{i-1}^n}{2h} + O(h^2).$$

Table 3.1 below shows spatial errors and experimental convergence rates for this example (see their definitions in Subsection 3.6). Here we have used $\tau = 10^{-6} \cdot 2^{-2}$ and the benchmark solution was calculated using $h = 10^{-1} \cdot 2^{-6}$.

h	$e_h(h)$	$\rho_h(h)$
0.1	$1.4047 \cdot 10^{-4}$	1.9439
0.05	$3.6510 \cdot 10^{-5}$	2.0157
0.025	$9.0286 \cdot 10^{-6}$	2.0769

Table 3.1: Computational results of errors in space at $T = 0.1$ with Neumann boundary conditions.

Table 3.1 experimentally indicates that with the Neumann boundary condition, the spatial error is of order $O(h^2)$, while the test problems provided in Subsection 3.6 confirm that with U_{xx} boundary condition it is also of order $O(h^2)$.

3.6 Numerical tests

This section presents some test problems to investigate the accuracy of constructed numerical scheme.

To find the averaged velocity U in mm/s with characteristic measures 1 mm and 1 s, the equation (3.2) was solved with the following constants c_i (rounded up):

c_1	c_2	c_3	c_4	c_5	c_6	c_7
$9 \cdot 10^{-38}$	$-2 \cdot 10^{-42}$	$4 \cdot 10^{-2}$	$-2 \cdot 10^{1}$	$8 \cdot 10^{1}$	$-6 \cdot 10^{-2}$	$4 \cdot 10^{-4}$

However, c_1 and c_2 can be treated as zero in the test problems of this section, as they do not visibly contribute to the solutions.

In all test problems, the definitions of error $e(h, \tau)$, experimental convergence rates $\rho_\tau(\tau)$ and $\rho_h(h)$ at time $t = T$ will be used, that are defined in the maximum norm

$$e(h, \tau) = \max_i \left| U_i^{N_\tau} - U(x_i, T) \right|,$$

$$\rho_h(h) = \log_2 \left(\frac{e(2h, \tau)}{e_h(h, \tau)} \right), \rho_\tau(\tau) = \log_2 \left(\frac{e(h, 2\tau)}{e(h, \tau)} \right).$$

Here $U(x_i, T)$ is a benchmark solution.

First test problem

In the first test problem, the classical Runge test was applied to find experimental convergence rates in space and time. The following functions were used: $U(x, 0) = U_t(x, 0) = 0$, $U(0, t) = U(L, t) = 1 - \cos t$, $U_{xx}(0, t) = U_{xx}(L, t) = \sin t$.

Table 3.2 below shows spatial errors and experimental convergence rates for a series of decreasing space step sizes h. These calculations were performed using $\tau = 2^{-2} \cdot 10^{-6}$. Here the benchmark solution was calculated with $h = 2^{-6} \cdot 10^{-1}$.

h	$e(h)$	$\rho_h(h)$
0.1	$2.3394 \cdot 10^{-5}$	1.9983
0.05	$5.8555 \cdot 10^{-6}$	2.0007
0.025	$1.4632 \cdot 10^{-6}$	2.0047
0.0125	$3.6460 \cdot 10^{-7}$	2.0188

Table 3.2: Computational results of spatial errors and experimental convergence rates at $T = 0.1$ for the first test problem.

Table 3.3 below shows errors and experimental convergence rates in time for a series of decreasing time step sizes τ. Here

τ	$e(\tau)$	$\rho_\tau(\tau)$
0.0001	$2.3969 \cdot 10^{-7}$	1.0109
0.00005	$1.1894 \cdot 10^{-7}$	1.0228
0.000025	$5.8537 \cdot 10^{-8}$	1.0461
0.0000125	$2.8327 \cdot 10^{-8}$	1.0406

Table 3.3: Computational results of errors and experimental convergence rates in time at $T = 0.1$ for the first test problem.

we have used $h = 2^{-2} \cdot 10^{-1}$ and the benchmark solution was calculated with $\tau = 2^{-7} \cdot 10^{-4}$. We see that the experimental convergence rates agree well with the theoretical estimates.

Second test problem

In this test, an exact solution to (3.2) will be known. Let us assume that it possesses the complex-exponential form $\tilde{U} = e^{i(kx+t)} = \cos(kx + t) + i \sin(kx + t)$. From this form, corresponding initial and boundary conditions easily follow:

$$\tilde{U}(x,0) = e^{ikx},\ \tilde{U}_t(x,0) = ie^{ikx},$$
$$\tilde{U}(0,t) = e^{it},\ \tilde{U}(L,t) = e^{i(kL+t)},$$
$$\tilde{U}_{xx}(0,t) = -k^2 e^{it},\ \tilde{U}_{xx}(L,t) = -k^2 e^{i(kL+t)}.$$

The parameter k can be found by substituting $\tilde{U}$ into (3.2). We get

$$c_1\tilde{U}_{tt} + c_2\tilde{U}_{xxtt} + c_3\tilde{U}_t + c_4\tilde{U}_{xxt} + c_5\tilde{U}_{xxxx} + c_6\tilde{U}_{xx} + c_7\tilde{U} = 0.$$

By calculating derivatives and grouping terms, the following quartic equation is obtained

$$k^4 c_5 + k^2(c_2 - ic_4 - c_6) + (-c_1 + ic_3 + c_7) = 0,$$

thus giving four complex solutions k_1, k_2, k_3, k_4. Each of them corresponds to a different solution to (3.2). For example, our current choice of c_i gives approximately

$$k_1 = 0.3546 - 0.3526i = -k_2,$$
$$k_3 = 0.0004 + 0.0483i = -k_4.$$

As numerical experiments suggest, the solver constructed in this section works well with both real and complex numbers. It is interesting to note that we can also take the solely sine or cosine part of $\tilde{U}$ with corresponding sine or cosine part of initial and boundary conditions to get an exact known solution and compare it to a numerical solution obtained with the corresponding initial and boundary conditions. However, the same argument does not hold for solely real or imaginary parts of solution, as it is rare for k_i to be solely real or imaginary.

Figure 3.3 below visualizes the four numerical solutions V_1, V_2, V_3 and V_4 that were acquired using k_1, k_2, k_3 and k_4, respectively.

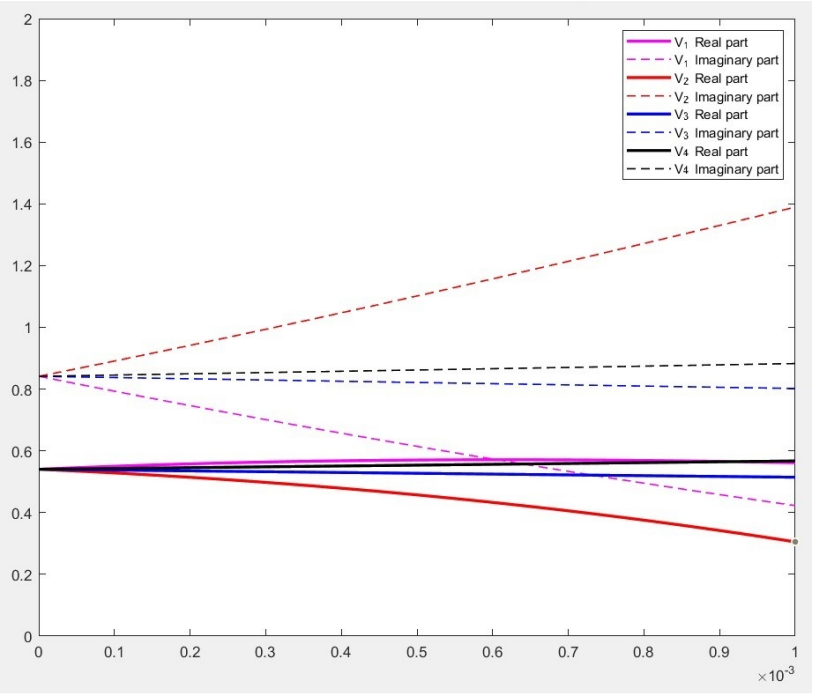

Figure 3.3: Solutions V_i at T=1.

Next, denote by V_1^* the numerical solution that was calculated using Neumann boundary conditions instead of second order derivatives at boundaries for corresponding complex-exponential solution of this test.

In Table 3.4 below, we compare the errors of V_1 and V_1^* at

some different times T. These solutions were acquired with $h = 2^{-1} \cdot 10^{-1}$ and $\tau = 2^{-2} \cdot 10^{-3}$

T	e of $Re(V_1)$	e of $Re(V_1^*)$	e of $Im(V_1)$	e of $Im(V_1^*)$
1	$6.4903 \cdot 10^{-7}$	$6.3309 \cdot 10^{-6}$	$1.8334 \cdot 10^{-6}$	$5.1999 \cdot 10^{-6}$
2	$1.1960 \cdot 10^{-6}$	$2.6706 \cdot 10^{-6}$	$1.5366 \cdot 10^{-6}$	$8.0973 \cdot 10^{-6}$
3	$1.9371 \cdot 10^{-6}$	$7.2964 \cdot 10^{-6}$	$1.3013 \cdot 10^{-7}$	$4.0185 \cdot 10^{-6}$
4	$9.0119 \cdot 10^{-7}$	$6.9911 \cdot 10^{-6}$	$1.7234 \cdot 10^{-6}$	$4.3136 \cdot 10^{-6}$
5	$9.6898 \cdot 10^{-7}$	$2.9784 \cdot 10^{-6}$	$1.6895 \cdot 10^{-6}$	$8.1424 \cdot 10^{-6}$
10	$1.3468 \cdot 10^{-6}$	$7.8812 \cdot 10^{-6}$	$1.4050 \cdot 10^{-6}$	$2.7121 \cdot 10^{-6}$

Table 3.4: Errors e of real and imaginary parts of numerical solutions V_1 and V_1^* at various times T.

We see that boundary conditions in form of U_{xx} instead of U_x give slightly lower errors.

3.7 Discussing an alternative scheme

In this section, a different approximation of derivatives involved in (3.2) is considered. The same problem is approached with a slightly different scheme. Namely, here we consider constructing a scheme having error in time of order $O(\tau^2)$. Therefore, the time derivatives of first order are approximated by central differences instead of forward differences.

The updated scheme is visualised in Figure 3.4 below.

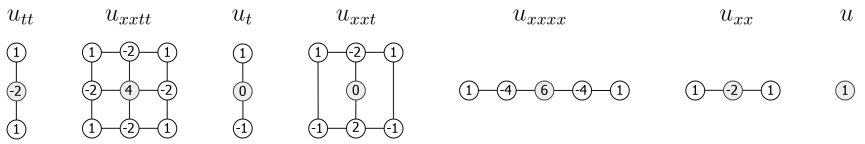

Figure 3.4: A schematic visualisation of numerical approximation of terms involved in (3.2), here the numbers inside circles correspond to the weight of coefficients of numerical points for approximations of differential terms

The shape of computational molecule remains the same as before (see Figure 3.2), however, some notations in this section

are different, namely m_3 and m_4:

$$m_1 = \frac{c_1}{\tau^2},\ m_2 = \frac{c_2}{h^2\tau^2},\ m_3 = \frac{c_3}{2\tau},\ m_4 = \frac{c_4}{2h^2\tau},$$
$$m_5 = \frac{c_5}{h^4},\ m_6 = \frac{c_6}{h^2},\ m_7 = c_7.$$

Let us also redefine the coefficients of each point of the computational molecule:

$$\begin{aligned}
U_{i-i}^{n+1}: &\quad m_2 + m_4;\\
U_{i}^{n+1}: &\quad m_1 - 2m_2 + m_3 - 2m_4;\\
U_{i-1}^{n+1}: &\quad m_2 + m_4;\\
U_{i-2}^{n}: &\quad m_5;\\
U_{i-1}^{n}: &\quad -2m_2 - 4m_5 + m_6;\\
U_{i}^{n}: &\quad -2m_1 + 4m_2 + 6m_5 - 2m_6 + m_7;\\
U_{i+1}^{n}: &\quad -2m_2 - 4m_5 + m_6;\\
U_{i+2}^{n}: &\quad m_5;\\
U_{i-1}^{n-1}: &\quad m_2 - m_4;\\
U_{i}^{n-1}: &\quad m_1 - 2m_2 - m_3 + 2m_4;\\
U_{i+1}^{n-1}: &\quad m_2 - m_4.
\end{aligned}$$

The classical method of Taylor expansions of derivatives was used to analyse the accuracy of updated scheme. Given that $u \in C^6(\Omega)$ and $u \in C^4(0,T)$ hold, the errors of numerical approximations of u_{xx} and u_{xxxx} are of order $O(h^2)$, the error of approximation of u_{tt} is of order $O(\tau^2)$, for u_{xxtt} it is $O(h^2+\tau^2)$, for u_t it is $O(\tau^2)$ and for u_{xxt} it is $O(h^2+\tau^2)$. Therefore, the overall order of accuracy for this scheme is $O(h^2+\tau^2)$.

Recall that the Richardson scheme, which is constructed using central difference for the first derivative in time, is unconditionally unstable for parabolic problems. As for our cases of interest parabolicity plays a significant role in Equation (3.2), this instability is treated as a cautious *a priori* concern here. In some cases the hyperbolic terms might regularize this instability to some extent, however, with the set of constants that emerges from the example of elastic arteriole, the hyperbolic

and parabolic terms differ by many orders of magnitude.

Numerical computations indicate that it is nearly impossible to experimentally find a stable pair of h and τ for this case. To briefly illustrate it, similarly as in the previous section, by using the standard Fourier stability analysis for Equation (3.2), we get

$$\begin{aligned} m_1(G-2+G^{-1})+m_2(G-2+G^{-1})(e^{-i\theta}-2+e^{i\theta}) \\ +m_3(G-G^{-1})+m_4(G-G^{-1})(e^{-i\theta}-2+e^{i\theta}) \\ +m_5(e^{-2i\theta}-4e^{-i\theta}+6-4e^{i\theta}+e^{2i\theta}) \\ +m_6(e^{-i\theta}-2+e^{i\theta})+m_7=0. \end{aligned} \tag{3.9}$$

which leads to

$$G^2A+GB+C=0 \tag{3.10}$$

with

$$\begin{aligned} A &= m_1-4m_2\sin^2(\theta/2)+m_3-4m_4\sin^2(\theta/2), \\ B &= -2m_1+8m_2\sin^2(\theta/2)+16m_5\sin^4(\theta/2) \\ &\quad -4m_6\sin^2(\theta/2)+m_7, \\ C &= m_1-4m_2\sin^2(\theta/2)-m_3+4m_4\sin^2(\theta/2). \end{aligned}$$

By denoting $b:=B/A$ and $c:=C/A$, instead of (3.10) we have

$$G^2+bG+c=0.$$

And the following equivalence holds:

$$|G|\leqslant 1 \iff |c|\leqslant 1,\ |b|\leqslant c+1.$$

For instance, let us suppose that $h=10^{-1}$ and the characteristic values are 1 mm and 1 s. Taking into account the positivity of A and B, instead of $|b|\leqslant c+1$ we can analyse $B\leqslant C+A$. Let us take the case $\sin(\theta/2)=1$, for which we get the following problem for τ (the terms were rounded up):

$$\frac{-2}{\tau^2}\cdot 10^{-37}-\frac{2}{\tau^2}10^{-41}+1\cdot 10^7+25+4\cdot 10^{-4}\leqslant \frac{2}{\tau^2}\cdot 10^{-37}+\frac{2}{\tau^2}10^{-41}.$$

It simplifies to, approximately,

$$\tau^2\leqslant 4\cdot 10^{-44},$$

but simulations with such τ are quite unpractical in terms of computational time. Note that this estimate was derived only for the case of a small elastic human arteriole and is only referential.

In this section it was illustrated that the warning from Section 3.1 to cautiously consider the Richardson scheme, which emerged from the analysis of equations that can be seen as included in (3.2), eventually proved to be worthy.

To avoid the instability caused by the Richardson scheme and still hold out the $O(h^2 + \tau^2)$ accuracy, we refer the reader, for example, to the Dufort–Frankel scheme [5]. It has the benefit of unconditional stability, however, in some cases it poses restrictions for the boundary conditions [73]. Furthermore, it suffers from being conditionally consistent. For more details on the fragility of consistency of Dufort-Frankel scheme, we refer the reader to [23].

Although it should be possible to construct some more complicated schemes to achieve $O(h^2 + \tau^2)$ accuracy, this interesting topic is left for future research. For now, the scheme constructed in Section 3.2 is considered to be sufficiently efficient for the problems of current interest.

3.8 Conclusions

For the 4th order PDE problem analysed in this chapter, the approximation of time derivative using symmetric difference gives the error in time of order $O(\tau^2)$, while the approximation of forward difference results in error of order $O(\tau)$. In general, the symmetric difference approximation seems better than forward difference due to its higher accuracy. However, schemes constructed from symmetric differences for parabolic PDEs raise some instability issues. As hyperbolic terms are also present, they regularize the instability to some extent, nonetheless, insufficiently for the applications of our interest.

The stability analysis revealed that the scheme constructed using forward difference approximation results in stability condition of the form $\tau \leqslant Ch^2$, which is easy to satisfy in prac-

tice. However, in cases of our interest, the stability of scheme constructed using symmetric difference approximation for the first order time derivative is almost impossible to satisfy in the sense of practical computations, as the size of time step τ has to be taken extremely small. Therefore, for CFD simulations our choice was the scheme with error in time of order $O(\tau)$ instead of $O(\tau^2)$, but with a more reasonable stability.

Overall, the error of scheme constructed in the first section is of order $O(h^2+\tau)$. It was confirmed experimentally in Subsection 3.6. Furthermore, it was shown that formulating the problem with boundary conditions of type U_{xx} instead of U_x results in smaller errors.

4 General conclusions

Summarizing the main results of this dissertation, the FVM ADI scheme was implemented to solve two hybrid dimension heat conduction models with nonclassical conjugation conditions between the zones of different dimensions. The finite volume method was used to approximate the differential operators in space and the alternating direction implicit scheme was used to solve the problems in time.

In both cases, an efficient modification of the Thomas algorithm was developed to resolve nonclassical conjugation conditions. Some stability estimates were proven. It was shown that unique numerical solutions exist to the FVM ADI schemes for the hybrid dimension models, also the properties of symmetry and positive semi-definiteness were proven for the modified spatial discretization operators.

Results of computational experiments confirmed the theoretical error analysis. The comparison of computational times confirmed the theoretical conclusion that hybrid dimension models can be effectively used to simulate heat conduction models for a broad variety of domains and coefficients. Visual representations of solutions justified the usage of proposed algorithm for practical applications.

Bibliography

[1] H. Amar and D. Givoli. Mixed-dimensional modeling of time-dependent wave problems using the Panasenko construction. *J. Theor. Comput. Acoust.*, **26**(03):1850034, 2018.

[2] H. Amar and D. Givoli. Mixed-dimensional coupling for time-dependent wave problems using the Nitsche method. *Comput. Methods Appl. Mech. Engrg.*, **349**:213–250, 2019.

[3] A. Amosov and G. Panasenko. Partial dimension reduction for the heat equation in a domain containing thin tubes. *Math. Methods Appl. Sci.*, **41**(18):9529–9545, 2018.

[4] D. Anderson, J. Tannehill, and R. Pletcher. *Computational Fluid Mechanics and Heat Transfer*. CRC Press, 2012.

[5] U. M. Ascher. *Numerical Methods for Evolutionary Differential Equations*. SIAM, Philadelphia, 2008.

[6] R. Astrauskas, F. Ivanauskas, I. Morkvėnaitė-Vilkončienė, and A. Ramanavičius. Mathematical modelling of the influence of ultra-micro electrode geometry on approach curves registered by scanning electrochemical microscopy. *Electroanalysis*, **31**(11):2214–2223, 2019.

[7] C. Bertoglio, C. Conca, D. Nolte, G. Panasenko, and K. Pileckas. Junction of models of different dimension for flows in tube structures by Womersley-type interface conditions. *SIAM J. Appl. Math.*, **79**(3):959–985, 2019.

[8] J. Březina, O. Kreml, and V. Mácha. Dimension reduction for the full Navier–Stokes–Fourier system. *J. Math. Fluid Mech.*, **19**:659–683, 2017.

[9] J. Biazar and H. Ghazvini. He's variational iteration method for fourth-order parabolic equations. *Comput. Math. with Appl.*, **54**(7):1047–1054, 2007.

[10] S. Canic and A. Mikelic. Effective equations modeling the flow of a viscous incompressible fluid through a long elastic tube arising in the study of blood flow through small arteries. *SIAM J. Appl. Dyn. Syst.*, **2**:431–463, 2003.

[11] E. Canon, F. Chardard, G. Panasenko, and O. Štikonienė. Numerical solution of viscous flows in a network of thin tubes: asymptotics and discretization in the cross-section. *HAL-02906473*, 2020.

[12] E. Canon, F. Chardard, G. Panasenko, and O. Štikonienė. Numerical solution of the viscous flows in a network of thin tubes: Equations on the graph. *J. Comput. Phys.*, **435**:110262, 2021.

[13] R. C. Cascaval, C. D'Apice, M. P. D'Arienzo, and R. Manzo. Flow optimization in vascular networks. *Math. Biosci. Eng.*, **14**(3):607–624, 2017.

[14] W. J. De Lange et al. An operational, multi-scale, multi-model system for consensus-based, integrated water management and policy analysis: The Netherlands hydrological instrument. *Environ. Model. Softw.*, **59**:98–108, 2014.

[15] B. Desjardins, M. Esteban, C. Grandmont, and P. Tallec. Weak solutions for a fluid-elastic structure interaction model. *Rev. Mat. Complut.*, **14**:523–538, 2000.

[16] M. Ducceschi and S. Bilbao. Conservative finite difference time domain schemes for the prestressed Timoshenko, shear and Euler-Bernoulli beam equations. *Wave Motion*, **89**:142–165, 2019.

[17] L. C. Evans. *Partial Differential Equations.* American Mathematical Society, 2010.

[18] R. Eymard, T. Gallouët, and R. Herbin. Finite volume methods. *Handb. Numer. Anal.*, **7**:713–1018, 2000.

[19] I. Faille. A control volume method to solve an elliptic equation on a two-dimensional irregular mesh. *Comput. Methods Appl. Mech. Eng.*, **100**(2):275–290, 1992.

[20] L. Formaggia, J. Gerbeau, F. Nobile, and A. Quarteroni. On the coupling of 3D and 1D Navier-Stokes equations for flow problems in compliant vessels. *Comput. Methods Appl. Mech. Eng.*, **191**:561–582, 2001.

[21] L. Formaggia, A. Quarteroni, and C. Vergara. On the physical consistency of the coupling between three-dimensional compliant and one-dimensional problems in haemodynamics. *J. Comput. Phys.*, **244**:97–112, 2013.

[22] G. P. Galdi, K. Pileckas, and A. L. Silvestre. On the unsteady Poiseuille flow in a pipe. *Z. angew. Math. Phys.*, **58**:994–1007, 2007.

[23] S. Gasparin, J. Berger, D. Dutykh, and N. Mendes. Stable explicit schemes for simulation of nonlinear moisture transfer in porous materials. *J. Build. Perform. Simul.*, **11**(2):129–144, 2018.

[24] C. Grandmont and Y. Maday. Existence for an unsteady fluid-structure interaction problem. *Math. Model. Numer. Anal.*, **34**(3):609–636, 2000.

[25] J. Hadamard and P. M. Morse. Lectures on Cauchy's problem in linear partial differential equations. *Phys. Today*, **6**(8), 1953.

[26] S. J. Hagen. Exponential growth of bacteria: Constant multiplication through division. *Am. J. Phys.*, **78**:1290–1296, 2010.

[27] D. Halpern, O. E. Jensen, and J. B. Grotberg. A theoretical study of surfactant and liquid delivery into the lung. *J. Appl. Physiol.*, **85**(1):333–352, 1998.

[28] W. H. Hundsdorfer. Accuracy and stability of splitting with stabilizing corrections. *Appl. Numer. Math.*, **42**(1):213–233, 2002.

[29] W. H. Hundsdorfer and K. I. Hout. On multistep stabilizing correction splitting methods with applications to the Heston model. *SIAM J. Sci. Comput.*, **40**, 2018.

[30] W. H. Hundsdorfer and J. G. Verwer. Stability and convergence of the Peaceman-Rachford ADI method for initial-boundary value problems. *Math. Comput.*, **53**(187):81–101, 1989.

[31] W. H. Hundsdorfer and J. G. Verwer. *Numerical Solution of Time-Dependent Advection-Diffusion-Reaction Equations*, volume **33**. Springer, Berlin, Heidelberg, New York, Tokyo, 2003.

[32] K. Hussain, F. Ismail, and N. Senu. Direct numerical method for solving a class of fourth-order partial differential equation. *Glob. J. Pure Appl. Math.*, **12**:1257–1272, 2016.

[33] R. Čiegis, A. Dement'ev, and G Jankevičiūtė. Numerical analysis of the hyperbolic two-temperature model. *Lith. Math. J.*, **48**:46–60, 2008.

[34] R. Čiegis, R. Čiegis, M. Meilūnas, G. Jankevičiutė, and V. Starikovičius. Parallel numerical algorithms for optimization of electrical cables. *Math. Model. Anal.*, **13**(4):471–482, 2008.

[35] R. Čiegis, G. Jankevičiūtė, T. Leonavičienė, and A. Mirinavičius. On stability analysis of finite-difference schemes for some parabolic problems with nonlocal boundary conditions. *Numer. Funct. Anal. Optim.*, **35**(10):1308–1327, 2014.

[36] R. Čiegis, G. Jankevičiūtė, and O. Suboč. Numerical simulation of the heat conduction in composite materials. *Math. Model. Anal.*, **15**(1):9–22, 2010.

[37] R. Čiegis and A. Mirinavičius. On some finite difference schemes for solution of hyperbolic heat conduction problems. *Open Math.*, **9**(5):1164–1170, 2011.

[38] R. Čiegis, G. Panasenko, K. Pileckas, and V. Šumskas. ADI scheme for partially dimension reduced heat conduction models. *Comput. Math. with Appl.*, **80**(5):1275–1286, 2020.

[39] R. Čiegis, O. Suboč, and A. Bugajev. Parallel algorithms for three-dimensional parabolic and pseudoparabolic problems with different boundary conditions. *Nonlinear Anal. Model. Control*, **19**(3):382–395, 2014.

[40] O. Ismail and G. Adewoye. Analyses and modeling of laminar flow in pipes using numerical approach. *J. Softw. Eng. Appl.*, **5**(9):653–658, 2012.

[41] F. Ivanauskas, I. Morkvėnaitė-Vilkončienė, and R. Astrauskas. Modelling of scanning electrochemical microscopy at redox competition mode using diffusion and reaction equations. *Electrochim. Acta*, **222**:347–354, 2016.

[42] V. Korzyuk, O. Konopel'ko, and E. Cheb. Boundary-value problems for fourth-order equations of hyperbolic and composite types. *J. Math. Sci.*, **171**, 2010.

[43] R. Kumar, A. Quateroni, L. Formaggia, and D. Lamponi. On parallel computation of blood flow in human arterial network based on 1-D modelling. *Computing*, **71**:321–351, 2003.

[44] Y. Kwon. *Fluid-Structure Interaction of Composite Structures.* Springer, 2020.

[45] E. Lifshitz and L. Landau. *Theory of elasticity: course of theoretical physics.* Oxford: Butterworth - Heinemann, 1986.

[46] V. D. Liseikin. *Grid Generation Methods.* Springer, Dordrecht, 2009.

[47] S. MacNamara and G. Strang. *Operator Splitting*. Springer, 2016.

[48] J. Manafian. The solution of the variable coefficients fourth-order parabolic partial differential equations by the homotopy perturbation method. *Z. Naturforsch.*, **64**:420–430, 2009.

[49] G. I. Marchuk. Splitting and alternating direction methods. *Handb. Numer. Anal.*, **1**:197–462, 1990.

[50] T. G. Myers and J. P. Charpin. A mathematical model for atmospheric ice accretion and water flow on a cold surface. *Int. J. Heat Mass Transf.*, **47**(25):5483–5500, 2004.

[51] A. Nachit, G. Panasenko, and A. Zine. Asymptotic partial domain decomposition in thin tube structures: Numerical experiments. *Int. J. Multiscale Comput. Eng.*, **11**:407–441, 2013.

[52] G. Panasenko. Method of asymptotic partial decomposition of domain. *Math. Models Methods Appl. Sci.*, **8**(1):139–156, 1998.

[53] G. Panasenko. *Multi-scale Modeling for Structures and Composites*. Springer Netherlands, Dordrecht, 2005.

[54] G. Panasenko and K. Pileckas. Asymptotic analysis of the non-steady Navier–Stokes equations in a tube structure. I. the case without boundary-layer-in-time. *Nonlinear Anal. Theory Methods Appl.*, **122**:125–168, 2015.

[55] G. Panasenko and K. Pileckas. Asymptotic analysis of the non-steady Navier–Stokes equations in a tube structure. II. general case. *Nonlinear Anal.*, **125**:582–607, 2015.

[56] G. Panasenko and R. Stavre. Three dimensional asymptotic analysis of an axisymmetric flow in a thin tube with thin stiff elastic wall. *J. Math. Fluid Mech.*, **22**(20), 2020.

[57] G. Panasenko and M. Viallon. Finite volume implementation of the method of asymptotic partial domain decomposition for the heat equation on a thin structure. *Russ. J. Math. Phys.*, **22**(2):237–263, 2015.

[58] D. W. Peaceman and H. H. Rachford. The numerical solution of parabolic and elliptic differential equations. *J. Soc. Indust. App. Math.*, **3**(1):28–41, 1955.

[59] B. Perthame. *Parabolic Equations in Biology: Growth, Reaction, Movement and Diffusion.* Springer, 2015.

[60] G. F. Pinder. *Numerical Methods for Solving Partial Differential Equations.* John Wiley & Sons, 2018.

[61] A. Quarteroni, F. Saleri, and A. Veneziani. Factorization methods for the numerical approximation of Navier–Stokes equations. *Comput. Methods. Appl. Mech. Eng.*, **188**(1):505–526, 2000.

[62] A. Rastegar. EPH-classifications in geometry, algebra, analysis and arithmetic. *arXiv: History and Overview*, 2015.

[63] N. Rehana and F. Mahomed. Dynamic Euler-Bernoulli beam equation: Classification and reductions. *Math. Probl. Eng.*, **2015**:1–7, 2015.

[64] W. C. Royster and S. D. Conte. Convergence of finite difference solutions to a solution of the equation of the vibrating rod. *Proc. Amer. Math. Soc.*, **7**:742–749, 1956.

[65] A. A. Samarskii. *Fundamentals of Numerical Reservoir Simulation.* Elsevier Science, Amsterdam - Oxford - New York, 1977.

[66] A. A. Samarskii. *The Theory of Difference Schemes.* Marcel Dekker, New York, 2001.

[67] M. Sapagovas, G. Kairytė, O. Štikonienė, and A. Štikonas. Alternating direction method for a two-dimensional

parabolic equation with a nonlocal boundary condition. *Math. Model. Anal.*, **12**(1):131–142, 2007.

[68] M. Sapagovas, A. Štikonas, and O. Štikonienė. Alternating direction method for the Poisson equation with variable weight coefficients in an integral condition. *Differ. Equ.*, **47**:1176–1187, 2011.

[69] M. Sapagovas and O. Štikonienė. Alternating-direction method for a mildly nonlinear elliptic equation with nonlocal integral conditions. *Nonlinear Anal. Model. Control*, **2**, 2011.

[70] Y. Shi, P. Lawford, and R. Hose. Review of zero-D and 1-D models of blood flow in the cardiovascular system. *BioMed. Eng. OnLine*, **10**(33), 2011.

[71] V. Skakauskas, P. Katauskis, and R. Čiegis. Modelling of the NO + CO reaction over inhomogeneous surfaces. *J. Math. Chem.*, **56**(9):2626–2642, 2018.

[72] A. Sood, E. Pop, M. Asheghi, and K. Goodson. The heat conduction renaissance. In *2018 17th IEEE Intersociety Conference on Thermal and Thermomechanical Phenomena in Electronic Systems (ITherm)*, pages 1396–1402, 2018.

[73] P. J. Taylor. The stability of the Du Fort-Frankel method for the diffusion equation with boundary conditions involving space derivatives. *Comput. J.*, **13**(1):92–97, 1970.

[74] J. F. Thompson, B. K. Soni, and N. P. Weatherill. *Handbook of Grid Generation*. CRC Press, 1998.

[75] A. Štikonas. The root condition for polynomial of the second order and a spectral stability of finite-difference schemes for Kuramoto-Tsuzuki equation. *Math. Model. Anal.*, **3**:214–226, 1998.

[76] O. Štikonienė and M. Sapagovas. Numerical investigation of alternating-direction method for Poisson equation

with weighted integral conditions. *Lietuvos matematikos rinkinys*, **51**, 2019.

[77] M. C. Viallon. Error estimate for a 1D–2D finite volume scheme. comparison with a standard scheme on a 2D non-admissible mesh. *Comptes Rendus Math.*, **351**(1):47–51, 2013.

[78] M. C. Viallon. Domain decomposition methods in a geometrical multiscale domain using finite volume schemes. *Int. J. Numer. Methods Fluids*, **92**(5):391–421, 2020.

[79] V. Volpert, N. Bessonov, A. Sequeira, S. Simakov, and Y. Vassilevskii. Methods of blood flow modelling. *Math. Model. Nat. Phenom.*, **11**(1):1–25, 2016.

[80] A. M. Wazwaz. Analytic treatment for variable coefficient fourth-order parabolic partial differential equations. *Appl. Math. Comput.*, **123**(2):219–227, 2001.

[81] N. N. Yanenko. *The Method of Fractional Steps*. Springer-Verlag Berlin Heidelberg, 1971.

[82] D. Zaheer, M. Ahsan, M. Ahmad, W. Khan, E. E. Mahmoud, and A. Abdel-Aty. Meshless analysis of nonlocal boundary value problems in anisotropic and inhomogeneous media. *Mathematics*, **8**(11):2045, 2020.

Santrauka (summary in Lithuanian)

Įvadas

Tyrimų sritis

Šios disertacijos tyrimų sritis – diferencialinių lygčių dalinėmis išvestinėmis modelių, kuriems pritaikyta dalinė dimensijos redukcija, sprendimas skaitiniais metodais. Šilumos laidumo modeliuose dalyje uždavinio srities dimensijų skaičius sumažinamas ir gaunamas hibridinės dimensijos modelis, tokiu būdu sumažinant laiką, per kurį bus rastas sprendinys, tačiau prarandant dalį sprendinio tikslumo. Pritaikomi efektyvūs skaitiniai algoritmai, paremti neišreikštinėmis kintamųjų krypčių schemomis, siekiant išspręsti hibridinės dimensijos modelius, kuriuose vienmatės (1D) sritys sujungiamos su 2D arba 3D sritimis.

Šalia pagrindinių rezultatų, sukonstruojamos bei aptariamos skaitinės schemos uždaviniui, kylančiam iš klampaus skysčio tekėjimo elastingu vamzdeliu modelio. Jame trimatis uždavinys buvo pilnai pakeistas į vienmatį visoje srityje. Gauta ketvirtos eilės diferencialinė lygtis dalinėmis išvestinėmis išspręsta skaitiniais metodais.

Aktualumas

Matematiniai modeliai, kuriuose nagrinėjami fizikiniai reiškiniai vamzdelių struktūrose, yra svarbūs medicininiuose bei industriniuose taikymuose [14, 40, 79]. Daug dėmesio sulaukia ir tokių modelių sprendimų greitinimo strategijos [13, 43, 61, 70], kadangi tikslūs skaičiavimai gali pareikalauti ypač didelių kompiuterinių resursų.

Yra plačiai žinoma, kad matematinio modelio išsprendžiamumui daug įtakos turi kraštinės sąlygos [5, 31]. Taip pat ir neklasikinės sąlygos – susidūrus su jomis tenka tirti, kaip keisti klasikinius sprendimo metodus. Šioje disertacijoje taikomas dalinės dimensijos redukcijos metodas, kurio įgyvendinimui naudojamos nelokalios, neklasikinės jungtinumo sąlygos. Jų įtaka sprendiniui – svarbi tyrimo dalis.

Dalinės dimensijos redukcijos metodo pradininku laikomas G. Panasenko [52]. Nors paties metodo efektyvumas patvirtintas [1], jo įgyvendinimas hibridinės dimensijos uždaviniams iš skaitinių metodų pusės – vis dar aktuali tyrimų sritis. Šioje disertacijoje ir tiriama viena iš tokių sprendyklių – kintamųjų krypčių schema nestacionariems šilumos laidumo modeliams.

Tikslai

Pagrindinis šios disertacijos tikslas yra išvystyti lengvai įgyvendinamus ir efektyvius skaitinius metodus hibridinės dimensijos uždaviniams, kuriuose mažesnė uždavinio dalis paliekama pilnos dimensijos, o pagrindinėje srities dalyje dimensija sumažinama iki vienmatės.

Metodai

Šilumos sklidimo procesas temperatūros kintamajam U modeliuojamas klasikine paraboline šilumos laidumo lygtimi dalinėmis išvestinėmis su šaltinio funkcija f.

Tuomet dalinės dimensijos redukcijos metodo pagrindu [57] suformuluojamas hibridinės dimensijos apytikslis uždavinys. Tokiu būdu kai kuriose srities dalyse Laplaso operatorius tampa vienmatis, t.y. į jį įeina išvestinė tik pagal vieną erdvinį kintamąjį.

Sričių su skirtingomis dimensijomis sąlyčio vietose suformuluojamos jungtinumo sąlygos, į kurias įeina klasikinė sprendinio tolydumo sąlyga bei neklasikinė srautų tvermės sąlyga (pavyzdžiui, taške $x = \delta$):

$$U|_{x=\delta-0} = U|_{x=\delta+0}\,, \quad \left.\frac{\partial S(U)}{\partial x}\right|_{x=\delta-0} = \left.\frac{\partial U}{\partial x}\right|_{x=\delta+0},$$

čia S – vidurkinimo operatorius, suvidurkinantis reikšmes didesnės dimensijos srities pjūvyje.

Hibridinės dimensijos modelio sprendinio radimui naudojami skaitiniai metodai. Erdvinės išvestinės aproksimuojamos naudojant baigtinių tūrių metodą (*angl. finite volume method – FVM* [18]), o laiko išvestinė aproksimuojama naudojant kintamųjų krypčių metodą (*angl. alternating direction implicit – ADI* [31]).

Taikant gautą baigtinių tūrių kintamųjų krypčių (FVM ADI) schemą, klasikinio modelio sprendinio radimas suvedamas į trijįstrižainės matricos uždavinio sprendimą klasikiniu perkelties algoritmu. Hibridinės dimensijos atveju klasikinis algoritmas modifikuojamas taip, kad būtų įtrauktos neklasikinės jungtinumo sąlygos. Tokiu būdu gaunamas matricinis uždavinys taškams ties sričių sandūromis, jo koeficientų matricai įrodoma diagonalinio vyravimo sąlyga. Iš čia gaunama, kad FVM ADI schemai, randančiai hibridinės dimensijos modelio sprendinį, egzistuoja vienintelis sprendinys.

Testiniai uždaviniai realizuoti naudojant MATLAB ir C++ programavimo kalbas. Integravimo laike tikslumo tyrimui atlikti Rungės testai. Dimensijos redukcijos metodo efektyvumas patvirtintas paklaidos analizėje naudojant maksimumo normą. Šioje normoje apskaičiuoti eksperimentiniai konvergavimo greičiai patvirtina teorinius schemos paklaidos įverčius.

Naujumas

Šioje disertacijoje pateikti rezultatai pratęsia pastaruosius dalinės dimensijos redukcijos šilumos laidumo modeliams tyrimus [3, 57], kurie pasuko link didesnę praktinę reikšmę turinčių skysčių dinamikos tyrimų krypties [7, 12, 54, 56].

Vienas svarbiausių šios disertacijos rezultatų – kintamųjų krypčių metodo pritaikymas hibridinės dimensijos modeliams. Baigtinių tūrių metodas erdvinių išvestinių diskretizacijai šioje srityje naudojamas kaip standartinis, tačiau metodai integravimui laike – viena einamųjų aktualių tyrimų sričių. Šiame darbe pasiektas $O(\tau^2)$ eilės tikslumas naudojant efektyvią kintamųjų

krypčių schemą. Redukuotos dimensijos geometrijose įrodytos svarbios diskrečiųjų išvestinių operatorių savybės.

Ginami teiginiai

1. Dalinė dimensijos redukcija yra efektyvus metodas sumažinti skaitinio sprendinio radimo trukmę šilumos laidumo modeliams, išlaikantis aukštą tikslumą.

2. Pateikta FVM ADI schema suderinama su dalinės dimensijos redukcijos metodu šilumos laidumo modeliams. Šiai schemai egzistuoja vienintelis skaitinis sprendinys, randamas efektyviai, kurio paklaida – antros eilės dydis pagal erdvės ir laiko žingsnius.

S.1 FVM ADI schema 3D modeliams cilindre su ašine simetrija

Šiame skyriuje pateikiamas šilumos laidumo uždavinys trimačiame cilindre. Dėl ašinės simetrijos prielaidos trimatis uždavinys pervedamas į dvimatį. Tuomet dalyje srities dimensija sumažinama iki vienmatės, taip prarandant dalį skaičiavimų tikslumo, tačiau sumažinant sprendinio radimo laiką.

Dimensijos redukcijos metodas išnagrinėtas bei pagrįstas G. Panasenko tyrimuose [3, 52, 57]. Šio darbo tikslas – efektyviai realizuoti jį skaitiniais metodais, naudojant kintamųjų krypčių metodą [31].

S.1.1 Klasikinis modelis

Nagrinėkime sritį $\mathcal{T} \subset \mathbb{R}^3$ cilindrinėse koordinatėse (r, ϕ, z): $\mathcal{T} = D \times (0, l)$. Čia D yra skritulys su spinduliu R: $D = \{(r, \phi) : 0 < r < R, 0 \leqslant \phi < 2\pi\}$, o l yra cilindro ilgis.

Srityje $\mathcal{T} \times (0, T)$ spręsime tiesinę šilumos laidumo lygtį. Tarkime, kad pradinė bei kraštinė sąlygos tenkina ašinės simetrijos sąlygą (t.y. nepriklauso nuo kintamojo ϕ). Gauname pagal

erdvę dvimatį uždavinį

$$\begin{cases} \dfrac{\partial u}{\partial t} = \dfrac{1}{r}\dfrac{\partial}{\partial r}\Big(r\dfrac{\partial u}{\partial r}\Big) + \dfrac{\partial^2 u}{\partial z^2} + f(r,z,t), \\ \qquad\qquad\qquad\qquad\qquad\qquad (r,z,t) \in Q_T = \Omega \times (0,T], \\ u(r,0,t) = g_1(r,t), \quad u(r,l,t) = g_2(r,t),\ (r,t) \in (0,R] \times (0,T], \\ r\dfrac{\partial u}{\partial r} = 0, \quad 0 < z < l, r = 0 \text{ ir } r = R,\ 0 < t \leqslant T, \\ u(r,z,0) = u^0(r,z), \quad (r,z) \in \Omega. \end{cases} \tag{S.1.1}$$

Čia $\Omega = \{(r,z) \in (0,R) \times (0,l)\}$.

Erdvinė diskretizacija atliekama pagal centrinį baigtinių tūrių metodą [31]. Tolygųjį erdvinį tinklą apibrėžia $\bar{\omega}_r \times \bar{\omega}_z$ su

$$\begin{aligned} \bar{\omega}_r &= \{r_j : \ \ r_j = jh, \ \ j = 0, \ldots, J\}, \quad r_J = R, \\ \bar{\omega}_z &= \{z_k : \ \ z_k = kH, \ \ k = 0, \ldots, K\}, \quad z_K = l. \end{aligned}$$

Čia h, H – erdvinio tinklo žingsniai. Apibrėžiame ir tolygųjį laiko tinklą

$$\bar{\omega}_t = \{t^n : \ \ t^n = n\tau, \qquad n = 0, \ldots, N\}, \quad t^N = T,$$

čia τ yra žingsnio dydis pagal laiką.

Tegul U^n_{jk} – skaitinė tikslaus sprendinio $u(r_j, z_k, t^n)$ aproksimacija uždaviniui (S.1.1) tinklo mazge (r_j, z_k, t^n). Funkcijoms, apibrėžtoms ant tinklo $\Omega_h \times \omega_t$, naudosime diskrečiuosius operatorius

$$\begin{aligned} \partial_z U^n_{jk} &:= \frac{U^n_{jk} - U^n_{j,k-1}}{H}, \\ A^h_2 U^n_{jk} &:= -\frac{1}{H}\Big(\partial_z U^n_{j,k+1} - \partial_z U^n_{jk}\Big). \\ \partial_r U^n_{jk} &:= \frac{U^n_{jk} - U^n_{j-1,k}}{h}, \\ A^h_1 U^n_{jk} &:= -\frac{1}{\widetilde{r}_j h}\Big(r_{j+\frac{1}{2}}\partial_r U^n_{j+1,k} - r_{j-\frac{1}{2}}\partial_r U^n_{jk}\Big), \end{aligned}$$

čia

$$\widetilde{r}_0 = \frac{1}{8}h,\ \widetilde{r}_j = r_j,\ 1 \leqslant j < J,\ \widetilde{r}_J = \frac{1}{2}\big(R - \frac{h}{4}\big), r_{-\frac{1}{2}} = 0, r_{J+\frac{1}{2}} = 0.$$

Tuomet šilumos laidumo uždavinys (S.1.1) aproksimuojamas Peaceman - Rachford ADI [31] schema

$$\frac{U_{jk}^{n+\frac{1}{2}} - U_{jk}^{n}}{\tau/2} + A_1^h U_{jk}^{n+\frac{1}{2}} + A_2^h U_{jk}^{n} = f_{jk}^{n+\frac{1}{2}}, \quad (r_j, z_k) \in \bar{\omega}_r \times \omega_z,$$
$$\frac{U_{jk}^{n+1} - U_{jk}^{n+\frac{1}{2}}}{\tau/2} + A_1^h U_{jk}^{n+\frac{1}{2}} + A_2^h U_{jk}^{n+1} = f_{jk}^{n+\frac{1}{2}}, \quad (r_j, z_k) \in \bar{\omega}_r \times \omega_z. \tag{S.1.2}$$

Toliau pateikiami keli gerai žinomi rezultatai, galiojantys klasikinio modelio atveju.

Lema 1.1. *Jei uždavinio* (S.1.1) *sprendinys pakankamai glodus, tuomet ADI schemos* (S.1.2) *tikslumo eilė yra* $O(\tau^2 + h^2 + H^2)$.

Lema 1.2. *Diskretieji operatoriai* A_1^h *ir* A_2^h *yra simetriniai bei atitinkamai neneigiamai ir teigiamai apibrėžti.*

Teiginys 1.3. *ADI schema* (S.1.2) *yra besąlygiškai stabili.*

Pabrėžtina, kad pastarojo teiginio įrodymui naudojama klasikinė Furjė stabilumo analizė, kadangi operatoriai A_1^h ir A_2^h komutuoja.

S.1.2 Hibridinės dimensijos modelis

Remiantis A. Amosov ir G. Panasenko rezultatais [3], šiame poskyryje nagrinėjamas apytikslis uždavinys, kuris dalyje srities sumažina erdvinę dimensiją iki vienmatės, tokiu būdu aproksimuojant klasikinį šilumos laidumo modelį (S.1.1).

Cilindrinėse koordinatėse vidurkinimo operatorius $S(u)$ išvedamas suintegruojant u reikšmes skerspjūvyje ir padalinant iš jo ploto, taip randant vidutinę u reikšmę cilindro skerspjūvyje:

$$S(u) = \frac{2}{R^2} \int_0^R ru(r, z, t)\mathrm{d}r.$$

Toliau darykime prielaidą, kad pradinė sąlyga u^0 ir šaltinio funkcija f nepriklauso nuo r srityje $\mathcal{T}$. Pažymėkime redukuotą sritį $\mathcal{T}_\delta = D \times (\delta, l - \delta)$ ir $\Omega_\delta = \{(r, z) \in (0, R) \times (\delta, l - \delta)\}$.

Funkciją U vadinsime apytiksliu sprendiniu uždaviniui (S.1.1), jeigu ji tenkina uždavinį (pagrindimui žr. [3])

$$\begin{cases} \dfrac{\partial U}{\partial t} = \dfrac{1}{r}\dfrac{\partial}{\partial r}\Big(r\dfrac{\partial U}{\partial r}\Big) + \dfrac{\partial^2 U}{\partial z^2} + f(z,t), (r,z,t) \in (\Omega \setminus \Omega_\delta) \times (0,T], \\ \dfrac{\partial U}{\partial t} = \dfrac{\partial^2 U}{\partial z^2} + f(z,t), \quad (r,z,t) \in \Omega_\delta \times (0,T], \\ U(r,0,t) = g_1(r,t), U(r,l,t) = g_2(r,t), \ (r,t) \in (0,R] \times (0,T], \\ r\dfrac{\partial U}{\partial r} = 0, \quad z \in (0,\delta) \cup (l-\delta, l), r = 0 \text{ ir } r = R, \ 0 < t \leqslant T, \\ U(r,z,0) = u^0(r,z), \quad (r,z) \in \Omega. \end{cases} \tag{S.1.3}$$

Srityje $\Omega_\delta \times (0,T]$ sprendinys U nepriklauso nuo r, todėl čia pakanka ieškoti vienmatės erdvinės dimensijos sprendinio $U(0,z,t)$.

Analizuojant silpnąją šilumos laidumo lygties formą, [3] buvo parodyta, kad ties skirtingų dimensijų sričių sandūromis galioja jungtinumo sąlygos

$$\begin{gathered} U\big|_{z=\delta-0} = U\big|_{z=\delta+0}, \quad U\big|_{z=l-\delta-0} = U\big|_{z=l-\delta+0}, \\ \frac{\partial S(U)}{\partial z}\Big|_{z=\delta-0} = \frac{\partial U}{\partial z}\Big|_{z=\delta+0}, \quad \frac{\partial U}{\partial z}\Big|_{z=l-\delta-0} = \frac{\partial S(U)}{\partial z}\Big|_{z=l-\delta+0}. \end{gathered} \tag{S.1.4}$$

Sąlygos $(\text{S.1.4})_1$ yra klasikinės ir nurodo U tolydumą, o $(\text{S.1.4})_2$ yra nelokalios ir nurodo srauto konservatyvumą per skirtingų dimensijų sričių sandūras.

Tegul indeksai K_1 ir K_2 žymi tuos srities taškus, ties kuriais keičiasi uždavinio dimensija, t.y. $z_{K_1} = \delta$, $z_{K_2} = l - \delta$. Tuomet kintamojo z tinklas ω_z padalinamas į tris dalis:

$$\begin{aligned} \omega_{z1} &= \{z_k : \ z_k = kH, \ k = 1, \ldots, K_1 - 1\}, \\ \omega_{z2} &= \{z_k : \ z_k = kH, \ k = K_1 + 1, \ldots, K_2 - 1\}, \\ \omega_{z3} &= \{z_k : \ z_k = kH, \ k = K_2 + 1, \ldots, K - 1\}. \end{aligned}$$

Taip pat apibrėžkime du diskrečiuosius tinklus $\Omega_{h,RD} = (\bar{\omega}_r \times (\omega_{z1} \cup \omega_{z3})) \cup \bar{\omega}_{z2}$ ir $\bar{\Omega}_{h,RD} = \Omega_{h,RD} \cup \big(\bar{\omega}_r \times (z_0 \cup z_K)\big)$. Pastebėkime, kad ω_{z2} kiekvienam k pakanka vieno taško pagal j, kadangi vienas taškas reprezentuoja visą taškų sperspjūvį. Tokiems atvejams vietoje j naudosime indekso žymėjimą $*$.

Tuomet argumentams U, apibrėžtiems ant tinklo $\bar{\Omega}_{h,RD}$, apibrėžkime du operatorius:

$$\mathcal{A}_1^h U = \begin{cases} A_1^h U_{jk}, & (r_j, z_k) \in \bar{\omega}_r \times (\omega_{z1} \cup \omega_{z3}), \\ 0, & z_k \in \bar{\omega}_{z2}, \end{cases}$$

$$\mathcal{A}_2^h U = \begin{cases} A_2^h U_{jk}, & (r_j, z_k) \in \bar{\omega}_r \times (\omega_{z1} \cup \omega_{z3}), \\ A_2^h U_{*k}, & z_k \in \omega_{z2}, \\ \frac{1}{H^2}\big(- S_h(U_{K_1-1}) + 2U_{*K_1} - U_{*,K_1+1}\big), & k = K_1, \\ \frac{1}{H^2}\big(- S_h(U_{K_2+1}) + 2U_{*K_2} - U_{*,K_2-1}\big), & k = K_2. \end{cases}$$

Lema 1.4. *Diskretieji operatoriai $\mathcal{A}_1^h$ ir $\mathcal{A}_2^h$ yra simetriniai ir atitinkamai neneigiamai bei teigiamai apibrėžti.*

Su šiais operatoriais diskrečiojo tinklo mazguose $(r_j, z_k) \in \Omega_{h,RD}$ uždavinį (S.1.3)–(S.1.4) aproksimuojame ADI schema:

$$\frac{U^{n+\frac{1}{2}} - U^n}{\tau/2} + \mathcal{A}_1^h U^{n+\frac{1}{2}} + \mathcal{A}_2^h U^n = f^{n+\frac{1}{2}},$$
$$\frac{U^{n+1} - U^{n+\frac{1}{2}}}{\tau/2} + \mathcal{A}_1^h U^{n+\frac{1}{2}} + \mathcal{A}_2^h U^{n+1} = f^{n+\frac{1}{2}}.$$

Patogumo dėlei pateikiamas ir išplėstinis pavidalas:

$$\begin{cases} \frac{U_{jk}^{n+\frac{1}{2}} - U_{jk}^n}{\tau/2} + A_1^h U_{jk}^{n+\frac{1}{2}} + A_2^h U_{jk}^n = f_{jk}^{n+\frac{1}{2}}, \\ \qquad\qquad (r_j, z_k) \in \bar{\omega}_r \times (\omega_{z1} \cup \omega_{z3}), \\ \frac{U_{*k}^{n+\frac{1}{2}} - U_{*k}^n}{\tau/2} + A_2^h U_{*k}^n = f_{*k}^{n+\frac{1}{2}}, \quad z_k \in \omega_{z2}, \\ \frac{U_{*K_1}^{n+\frac{1}{2}} - U_{*K_1}^n}{\tau/2} + \frac{1}{H^2}\Big(- S_h(U_{K_1-1}^n) + 2U_{*K_1}^n - U_{*,K_1+1}^n\Big) = f_{*K_1}^{n+\frac{1}{2}}, \\ \frac{U_{*K_2}^{n+\frac{1}{2}} - U_{*K_2}^n}{\tau/2} + \frac{1}{H^2}\Big(- S_h(U_{K_2+1}^n) + 2U_{*K_2}^n - U_{*,K_2-1}^n\Big) = f_{*K_2}^{n+\frac{1}{2}}, \\ \frac{U_{jk}^{n+1} - U_{jk}^{n+\frac{1}{2}}}{\tau/2} + A_1^h U_{jk}^{n+\frac{1}{2}} + A_2^h U_{jk}^{n+1} = f_{jk}^{n+\frac{1}{2}}, \\ \qquad\qquad (r_j, z_k) \in \bar{\omega}_r \times (\omega_{z1} \cup \omega_{z3}), \\ \frac{U_{*k}^{n+1} - U_{*k}^{n+\frac{1}{2}}}{\tau/2} + A_2^h U_{*k}^{n+1} = f_{*k}^{n+\frac{1}{2}}, \quad z_k \in \omega_{z2}, \\ \frac{U_{*K_1}^{n+1} - U_{*K_1}^{n+\frac{1}{2}}}{\tau/2} + \frac{1}{H^2}\Big(- S_h(U_{K_1-1}^{n+1}) + 2U_{*K_1}^{n+1} - U_{*,K_1+1}^{n+1}\Big) = f_{*K_1}^{n+\frac{1}{2}}, \\ \frac{U_{*K_2}^{n+1} - U_{*K_2}^{n+\frac{1}{2}}}{\tau/2} + \frac{1}{H^2}\Big(- S_h(U_{K_2+1}^{n+1}) + 2U_{*K_2}^{n+1} - U_{*,K_2-1}^{n+1}\Big) = f_{*K_2}^{n+\frac{1}{2}}. \end{cases} \tag{S.1.5}$$

Norint išspręsti gautas 1D subproblemas $(\text{S.1.5})_{1-4}$ ir $(\text{S.1.5})_{5-8}$, dėl nelokalių jungtinumo sąlygų $(\text{S.1.5})_{3,4,7,8}$ klasikinis perkelties algoritmas turi būti modifikuotas.

Teorema 1.5. *Uždaviniui* (S.1.5) *egzistuoja vienintelis sprendinys. Jį galima apskaičiuoti efektyvia perkelties algoritmo modifikacija.*

Šios teoremos įrodymas tuo pačiu yra ir konstruktyvus algoritmas, kaip išspręsti (S.1.5). Pavyzdžiui, sistemos lygtis $(\text{S.1.5})_{5,6}$ užrašę pavidalu

$$
\begin{aligned}
&-a_{jk}U^{n+1}_{j,k-1} + c_{jk}U^{n+1}_{jk} - b_{jk}U^{n+1}_{j,k+1} = d_{jk},\\
&a_{jk},\ b_{jk},\ c_{jk} \geqslant 0,\ \ c_{jk} \geqslant a_{jk} + b_{jk},
\end{aligned}
$$

antrajam laiko pusžingsniui srityse ω_{z1}, ω_{z2} ir ω_{z3} galime užrašyti tokias rekurenčiąsias formules (pirmajam pusžingsniui įrodymas ana- logiškas)

1. *Sritis* ω_{z1}. Sprendinys pateikiamas pavidalu

$$
\begin{aligned}
&U^{n+1}_{jk} = \alpha_{jk}U^{n+1}_{j,k+1} + \gamma_{jk}, \quad 0 \leqslant k < K_1, \qquad \text{(S.1.6)}\\
&\alpha_{j0} = 0,\ \alpha_{jk} = \frac{b_{jk}}{c_{jk} - a_{jk}\alpha_{j,k-1}},\\
&\gamma_{j0} = g_1(r_j, t^{n+1}),\ \ \gamma_{jk} = \frac{d_{jk} + a_{jk}\gamma_{j,k-1}}{c_{jk} - a_{jk}\alpha_{j,k-1}}.
\end{aligned}
$$

Naudojantis indukcija parodoma, kad galioja $0 \leqslant \alpha_{jk} \leqslant 1$.

2. *Sritis* ω_{z2}. Sprendinys pateikiamas pavidalu

$$
U^{n+1}_{*k} = \alpha_{*k}U^{n+1}_{*K_1} + \beta_{*k}U^{n+1}_{*K_2} + \gamma_{*k}, \quad K_1 < k < K_2. \qquad \text{(S.1.7)}
$$

Faktorizacija susideda iš dviejų dalių. Visų pirma, sprendinys užrašomas pavidalu

$$
\begin{aligned}
&U^{n+1}_{*k} = \widetilde{\alpha}_{*k}U^{n+1}_{*K_1} + \widetilde{\beta}_{*k}U^{n+1}_{*,k+1} + \widetilde{\gamma}_{*k}, \quad K_1 < k < K_2,\\
&\widetilde{\alpha}_{*,K_1+1} = \frac{a_{*,K_1+1}}{c_{*,K_1+1}},\ \ \widetilde{\alpha}_{*k} = \frac{a_{*k}}{c_{*k} - a_{*k}\widetilde{\beta}_{*,k-1}}\widetilde{\alpha}_{*,k-1},\\
&\widetilde{\beta}_{*,K_1+1} = \frac{b_{*,K_1+1}}{c_{*,K_1+1}},\ \ \widetilde{\beta}_{*k} = \frac{b_{*k}}{c_{*k} - a_{*k}\widetilde{\beta}_{*,k-1}},\\
&\widetilde{\gamma}_{*,K_1+1} = \frac{d_{*,K_1+1}}{c_{*,K_1+1}},\ \ \widetilde{\gamma}_{*k} = \frac{a_{*k}\widetilde{\gamma}_{*,k-1} + d_{*k}}{c_{*k} - a_{*k}\widetilde{\beta}_{*,k-1}}.
\end{aligned}
$$

Antrajame faktorizacijos žingsnyje randami koeficientai α_{*k}, β_{*k} ir γ_{*k}:

$$\alpha_{*,K_2-1} = \widetilde{\alpha}_{*,K_2-1}, \quad \beta_{*,K_2-1} = \widetilde{\beta}_{*,K_2-1}, \quad \alpha_{*k} = \widetilde{\alpha}_{*k} + \widetilde{\beta}_{*k}\alpha_{*,k+1},$$
$$\beta_{*k} = \widetilde{\beta}_{*k}\beta_{*,k+1}, \quad \gamma_{*k} = \widetilde{\gamma}_{*k} + \widetilde{\beta}_{*k}\gamma_{*,k+1}, \quad k = K_2-2, \ldots, K_1+1.$$

Taip pat įrodomi įverčiai

$$0 \leqslant \alpha_{*k}, \beta_{*k} \leqslant 1, \quad 0 \leqslant \alpha_{*k} + \beta_{*k} \leqslant 1.$$

3. *Sritis* ω_{z3}. Sprendinys pateikiamas pavidalu

$$\begin{aligned} &U_{jk}^{n+1} = \beta_{jk}U_{j,k-1}^{n+1} + \gamma_{jk}, \quad K_2 < k \leqslant K, \\ &\beta_{jK} = 0, \quad \beta_{jk} = \frac{a_{jk}}{c_{jk} - b_{jk}\beta_{j,k+1}}, \\ &\gamma_{jK} = g_2(r_j, t^{n+1}), \quad \gamma_{jk} = \frac{d_{jk} + b_{jk}\gamma_{j,k+1}}{c_{jk} - b_{jk}\beta_{j,k+1}}. \end{aligned} \tag{S.1.8}$$

Naudojantis indukcija parodoma, kad galioja $0 \leqslant \beta_{jk} \leqslant 1$.

Įstačius išraiškas (S.1.6)–(S.1.8) į lygtis $(S.1.5)_{7,8}$, gaunama dviejų tiesinių lygčių sistema $U_{*K_1}^{n+1}$, $U_{*K_2}^{n+1}$ radimui

$$\begin{cases} A_{11}U_{*K_1}^{n+1} + A_{12}U_{*K_2}^{n+1} = B_1 \\ A_{21}U_{*K_1}^{n+1} + A_{22}U_{*K_2}^{n+1} = B_2. \end{cases} \tag{S.1.9}$$

Įrodoma, kad sistemos (S.1.9) koeficientų matricos determinantas yra teigiamas, taigi, egzistuoja vienintelis sprendinys $U_{*K_1}^{n+1}$, $U_{*K_2}^{n+1}$.

Toliau, kadangi operatoriai $\mathcal{A}_1^h$ ir A_2^h nekomutuoja, negalime taikyti spektrinės stabilumo analizės, kuri buvo naudota klasikiniu atveju. Todėl stabilumo įvertis įrodomas specialioje energinėje normoje.

Teiginys 1.6. *Jei* U^n *yra ADI schemos* (S.1.5) *sprendinys, kai* $f^n \equiv 0$ *ir* $g_1^n = g_2^n \equiv 0$, *tuomet galioja stabilumo įvertis*

$$\|(I + \frac{\tau}{2}\mathcal{A}_2^h)U^n\| \leqslant \|(I + \frac{\tau}{2}\mathcal{A}_2^h)U^0\|.$$

Lentelė S.1.1. Diskrečiojo ADI schemos (S.1.2) sprendinio paklaidos $e(\tau)$ ir eksperimentiniai konvergavimo greičiai $\rho(\tau)$ su laiko žingsniais τ.

τ	$e(\tau)$	$\rho(\tau)$
0,0025	$5{,}215{\cdot}10^{-3}$	1,631
0,00125	$1{,}334{\cdot}10^{-3}$	1,958
0,000625	$3{,}343{\cdot}10^{-4}$	2,006
0,0003125	$8{,}194{\cdot}10^{-5}$	2,028

S.1.3 Testiniai uždaviniai

Viena redukuotos dimensijos sritis

Pirmajame testiniame uždavinyje su viena redukuotos dimensijos sritimi, nagrinėsime uždavinį (S.1.1) vamzdelyje su parametrais $l = 1$, $R = 0,1$. Uždavinys sprendžiamas iki $T = 1$ su funkcijomis

$$u^0(r,z) = 0,\ g_1(r,t) = (1+3t)e^{-(r/R)^2},$$
$$g_2(r,t) = te^{-(2r/R)^2},\ f(r,z,t) = 0.$$

ADI schemos integravimo laike tikslumas

Visų pirma, ištirtas ADI schemos integravimo laike tikslumas pilnos dimensijos modeliui, naudojant tolygųjį tinklą Ω_h su $J = 100$ ir $K = 400$. Lentelėje S.1.1 pateikiamas sąryšis tarp mažėjančių laiko žingsnių τ, paklaidų $e(\tau)$ ir eksperimentinių konvergavimo greičių $\rho(\tau)$ diskrečiajam ADI schemos sprendiniui maksimumo normoje:

$$e(\tau) = \max_{(r_j,z_k)\in\Omega_h} \left|U^N_{jk} - U(r_j,z_k,T)\right|, \quad \rho(\tau) = \log_2\left(e(2\tau)/e(\tau)\right),$$

čia $U(r_j,z_k,T)$ suskaičiuotas naudojant labai mažą žingsnį $\tau = 5\cdot 10^{-5}$.

Iš Lentelėje S.1.1 pateiktų rezultatų matome, kad eksperimentiškai rastas ADI schemos konvergavimo greitis atitinka teorinius įverčius.

Redukuotos dimensijos modelio tikslumas

Toliau tiriamas redukuotos dimensijos modelio (S.1.3) tikslumas. Erdvinei diskretizacijai naudojamas tolygusis tinklas Ω_h su $J = 100$, $K = 1600$. Integravimas laike atliekamas su $\tau = 0,0005$. Lentelėje S.1.2 pateikiamos redukuotos dimensijos modelio (S.1.3) sprendinio paklaidos $e(\delta)$ maksimumo normoje

$$e(\delta) = \max_{(r_j,z_k)\in\Omega_h h} \left| U_{jk}^N - U_{jk}^N(\delta) \right|$$

bei santykinės paklaidos e_r

$$e_r = \frac{e(\delta)}{\left|U_{j^*k^*}^N\right|} \cdot 100\%$$

įvairioms redukcijos parametro δ reikšmėms. Čia j^*, k^* – indeksai tinklo taško, kuriame rasta paklaida.

Lentelė S.1.2. Diskrečiojo redukuotos dimensijos modelio (1.3) paklaidos $e(\delta)$, santykinės paklaidos e_r ir skaičiavimų trukmė (sekundėmis) įvairiems redukcijos parametrams δ. Žymėjimas $\delta = \delta^*$ atitinka pilną modelį.

δ	$e(\delta)$	e_r	trukmė
δ^*	–	–	11,4
0,25	0,00013	0,0070%	5,9
0,20	0,00083	0,0421%	4,8
0,15	0,0056	0,2653%	3,7
0,10	0,0377	1,6537%	2,5
0,05	0,2471	9,3954%	1,4

Dvi redukuotos dimensijos sritys

Antrajame testiniame uždavinyje su $0 \leqslant z \leqslant 2$ nagrinėjamas atvejis, kai turime tris pilnos dimensijos ir dvi redukuotos dimensijos sritis. Papildomoje pilnos dimensijos srityje tiriamas šaltinio funkcijos f poveikis.

Tegul šiuo atveju redukuota sritis atitinka $\mathcal{T}_\delta = D \times (\delta; 0,9-\delta) \cup (1, 1+\delta; l-\delta)$ ir $\Omega_\delta = \{(r,z) \in (0,R) \times (\delta; 0,9-\delta) \cup (1, 1+$

$\delta; l-\delta)\}$. Šiame pavyzdyje centrinėje srities dalyje $0,9 \leqslant z \leqslant 1,1$ funkciją f apibrėžkime taip:

$$f(r,z,t) = 150t\exp(-(r/R)^2)\exp\big(-((z-1)/0,05)^2\big).$$

ADI schemos realizavimas išlieka toks pat. Naujoje pilnos dimensijos srityje su kiekvienu $j = 0,\ldots,J$ sprendinys užrašomas pavidalu

$$U_{jk}^{n+1} = \alpha_{jk}U_{jK_2}^{n+1} + \beta_{jk}U_{jK_3}^{n+1} + \gamma_{jk}, \quad K_2 < k < K_3.$$

Tuomet tiesinių lygčių sistema $U_{*K_1}^{n+1}$, $U_{*K_2}^{n+1}$, $U_{*K_3}^{n+1}$, $U_{*K_4}^{n+1}$ radimui susideda iš keturių lygčių, jos koeficientų matrica yra trijstrižainė.

ADI schemos integravimo laike tikslumas redukuotos dimensijos modeliui

Toliau pateikiamas ADI schemos (S.1.5) integravimo laike tikslumas redukuotos dimensijos modeliui. Erdvinei diskretizacijai naudojamas tolygusis tinklas Ω_h su $J = 100$, $K = 1600$ ir redukcijos parametru $\delta = 0,1$.

Lentelėje S.1.3 pateikiamas sąryšis tarp mažėjančių laiko žingsnių τ, paklaidų $e(\tau)$ ir eksperimentinių konvergavimo greičių $\rho(\tau)$ diskrečiajam ADI schemos (S.1.5) sprendiniui maksimumo normoje. Čia sprendinys $U(r_j, z_k, T)$ apskaičiuotas su labai mažu erdvės žingsniu $\tau = 5 \cdot 10^{-5}$.

Lentelė S.1.3. ADI schemos (S.1.5) sprendinio paklaidos $e(\tau)$ ir eksperimentiniai konvergavimo greičiai $\rho(\tau)$ įvairiems laiko žingsniams τ su $\delta = 0,1$.

τ	$e(\tau)$	$\rho(\tau)$
0,0025	$6{,}997{\cdot}10^{-3}$	1,279
0,00125	$2{,}106{\cdot}10^{-3}$	1,732
0,000625	$5{,}368{\cdot}10^{-4}$	1,972
0,0003125	$1{,}337{\cdot}10^{-4}$	2,005

Iš lentelėje S.1.3 pateiktų rezultatų matome antros eilės konvergavimo greitį. Be to, sprendinio paklaidos $e(\delta)$ artimos atvejo

su dviem pilnos dimensijos sritimis paklaidoms. Lentelėje S.1.4 pateikiamos skaičiavimų trukmės su įvairiais redukcijos parametrais δ.

Lentelė S.1.4. Redukuotos dimensijos modelio (S.1.3) sprendinio skaičiavimų trukmės priklausomumas nuo redukcijos parametro δ. Žymėjimas $\delta = \delta^*$ atitinka pilną modelį.

	$\delta = \delta^*$	$\delta = 0,25$	$\delta = 0,2$	$\delta = 0,15$	$\delta = 0,1$
Trukmė (s)	24,9	17,0	14,6	12,2	9,8

Antrojo testinio uždavinio sprendimui panaudoti tie patys duom- enys kaip ir pirmajame testiniame uždavinyje, išskyrus $K = 400$ ir f reikšmę.

S.1.4 Išvados

Hibridinės dimensijos šilumos laidumo uždaviniui sukonstruota ADI tipo schema. Baigtinių tūrių metodu aproksimuojami erdviniai diferencialiniai operatoriai ir neklasikinės jungtinumo sąlygos. Gautos vienmačių tiesinių lygčių sistemos išsprendžiamos perkelties algoritmu. Klasikinis perkelties algoritmas modifikuojamas, kad įtrauktų nelokalias jungtinumo sąlygas. Įrodomas pateikiamos schemos besąlyginis stabilumas. Skaitinių eksperimentų rezultatai patvirtina teorinius paklaidų įverčius bei teorinę išvadą, kad hibridiniai matematiniai modeliai gali būti naudojami šilumos laidumo modeliavimui plačiai sričių ir koeficientų klasei (taip pat žr. [3] įdomiai diskusijai šia tema).

S.2 FVM ADI schema 2D modeliams kryžiaus formos sritims

Šiame skyriuje šilumos laidumo uždavinys nagrinėjamas dvimatėje kryžiaus formos srityje (žr. pav. S.2.1). Taikant tą pačią ideologiją kaip ir ankstesniame skyriuje, šios geometrijos atveju susiduriama su naujais iššūkiais. Iš baigtinių tūrių metodo per-

spektyvos, ties vidiniais srities kampais atsiranda naujas kontrolinio elemento tipas (#3 paveikslėlyje S.2.2). Diskretieji išvestinių operatoriai aplink šiuos kampus nekomutuoja. Be to, vienose uždavinio srities dalyse dimensija redukuojama x kryptimi, kitose y kryptimi. Taigi, norint gauti panašius rezultatus, reikalingos naujos idėjos.

S.2.1 Klasikinis modelis

Nagrinėkime kryžiaus formos sritį $\Omega \subset \mathbb{R}^2$. Išoriniuose srities kraštuose naudojama pirmojo tipo (*Dirichlet*) kraštinė sąlyga, ši srities krašto dalis žymima $\partial_D\Omega$. Likusioje krašto dalyje naudojama antrojo tipo (*Neumann*) kraštinė sąlyga, ši srities krašto dalis žymima $\partial_N\Omega = \partial\Omega \setminus \partial_D\Omega$. Tegul srities plotis lygus X, o aukštis Y. Tuomet pirmojo tipo srities kraštas apibrėžiamas kaip $\partial_D\Omega = \partial_1\Omega \cup \partial_2\Omega \cup \partial_3\Omega \cup \partial_4\Omega$ (taip pat žr. pav. S.2.1 žemiau)

$$\begin{aligned}
\partial_1\Omega &= \{(x,y) : x = 0,\ Y_1 \leqslant y \leqslant Y_2\},\\
\partial_2\Omega &= \{(x,y) : y = 0,\ X_1 \leqslant x \leqslant X_2\},\\
\partial_3\Omega &= \{(x,y) : x = X,\ Y_1 \leqslant y \leqslant Y_2\},\\
\partial_4\Omega &= \{(x,y) : y = Y,\ X_1 \leqslant x \leqslant X_2\},
\end{aligned}$$

čia X_1, X_2, Y_1 ir Y_2 – realiosios konstantos, tenkinančios $0 < X_1 < X_2 < X$ ir $0 < Y_1 < Y_2 < Y$.

Srities Ω šakos žymimos L_1, L_2, L_3 ir L_4, o centrinė dalis L_0, tuomet $\Omega = L_0 \cup L_1 \cup L_2 \cup L_3 \cup L_4$:

$$\begin{aligned}
L_1 &= \{(x,y) : 0 \leqslant x \leqslant X_1,\ Y_1 \leqslant y \leqslant Y_2\},\\
L_2 &= \{(x,y) : X_1 \leqslant x \leqslant X_2,\ 0 \leqslant y \leqslant Y_1\},\\
L_3 &= \{(x,y) : X_2 \leqslant x \leqslant X,\ Y_1 \leqslant y \leqslant Y_2\},\\
L_4 &= \{(x,y) : X_1 \leqslant x \leqslant X_2,\ Y_2 \leqslant y \leqslant Y\},\\
L_0 &= \{(x,y) : X_1 < x < X_2,\ Y_1 < y < Y_2\}.
\end{aligned}$$

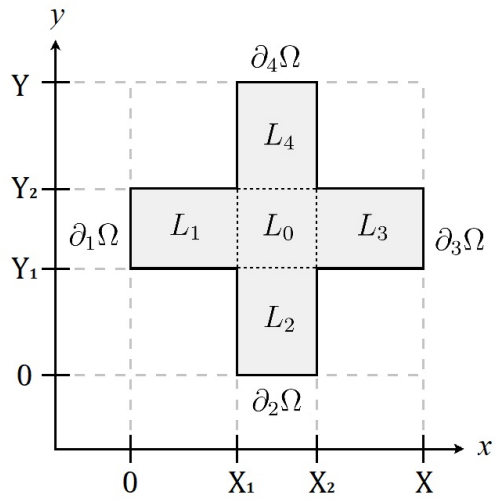

Paveikslėlis S.2.1. Sritis Ω (pilka) su pažymėtomis išorinėmis krašto dalimis ir šakomis.

Srityje $\Omega_T = \Omega \times (0, T]$ sprendžiama tiesinė šilumos laidumo lygtis:

$$\begin{cases} \dfrac{\partial u}{\partial t} = \dfrac{\partial^2 u}{\partial x^2} + \dfrac{\partial^2 u}{\partial y^2} + f(x,y,t), & (x,y,t) \in \Omega_T, \\ u(0,y,t) = g_1(y,t), & (y,t) \in [Y_1, Y_2] \times (0,T], \\ u(x,0,t) = g_2(x,t), & (x,t) \in [X_1, X_2] \times (0,T], \\ u(X,y,t) = g_3(y,t), & (y,t) \in [Y_1, Y_2] \times (0,T], \\ u(x,Y,t) = g_4(x,t), & (x,t) \in [X_1, X_2] \times (0,T], \\ \dfrac{\partial u}{\partial \mathbf{n}} = 0, & (x,y,t) \in \partial_N \Omega \times (0,T], \\ u(x,y,0) = u^0(x,y), & (x,y) \in \Omega, \end{cases} \tag{S.2.1}$$

čia f – šaltinio funkcija, $\mathbf{n}$ žymi išorinę normalę kraštui $\partial_N \Omega$. Modelis pateikiamas bedimensiniu pavidalu.

Kaip ir praeitame skyriuje, naudojamas baigtinių tūrių metodas [31]. Kiekvienas diskretusis nežinomasis apibrėžiamas mazge (x_j, y_k) ir asocijuojamas su kontroliniu elementu $\mathcal{K}_{jk}$. Žingsnio dydį kryptimi x žymint h, o kryptimi y žymint H, turime tinklą $\Omega_h = (\overline{\omega}_x \times \overline{\omega}_y) \cap \Omega$ su

$$\overline{\omega}_x = \{x_j : x_j = jh,\ j = 0,\ \ldots, J\},\ x_J = X,$$
$$\overline{\omega}_y = \{y_k : y_k = kH,\ k = 0,\ \ldots, K\},\ y_K = Y.$$

Be to, naudojami žymėjimai $x_{J_1} = X_1$, $x_{J_2} = X_2$ ir $y_{K_1} = Y_1$, $y_{K_2} = Y_2$. Taigi, kryžminei sričiai gaunami trijų tipų kontroliniai elementai (žr. pav. S.2.2). Patogumo dėlei apibrėžiamas ir tolygusis laiko tinklas:

$$\overline{\omega}_t = \{t^n : t^n = n\tau,\ n = 0,\ \ldots, N\},\ t^N = T.$$

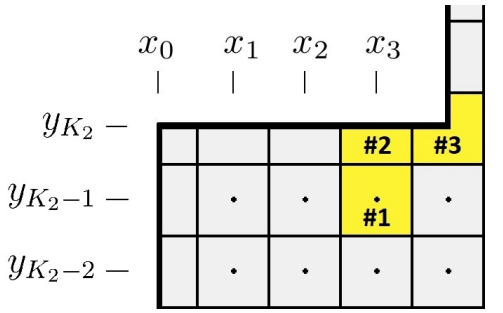

Paveikslėlis S.2.2. Viršutinio L_1 krašto diskretizacijos pavyzdys.

Toliau apibrėžiami šie matai: kontrolinio elemento plotas žymimas $V_{jk} = m(\mathcal{K}_{jk})$, o jo krašto σ_{jk} ilgis žymimas $s_{\alpha\beta} = m(\sigma_{\alpha\beta})$. Paveikslėlyje S.2.3 pavaizduota, kaip šios reikšmės skiriasi trims kontrolinių elementų tipams.

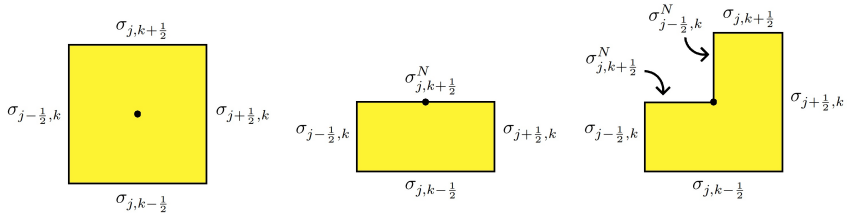

(a) #1 tipas:$V_{jk} = hH$ (b) #2 tipas:$V_{jk} = h\dfrac{H}{2}$ (c) #3 tipas:$V_{jk} = \dfrac{3hH}{4}$

Paveikslėlis S.2.3. Trijų tipų kontrolinių elementų $\mathcal{K}_{jk}$, apibrėžtų taške (x_j, y_k), kraštai. Viršutinis indeksas N žymi antrojo tipo kraštinę sąlygą.

Tegul U_{jk}^n – uždavinio (S.2.1) tikslaus sprendinio skaitinė aproksimacija. Naudodami standartinius baigtinių tūrių metodo žymėjimus gauname, kad šilumos laidumo lygtis užrašoma

$$\frac{\mathrm{d}U_{jk}}{\mathrm{d}t} = -A_1^h U_{jk} - A_2^h U_{jk} + f_{jk}, \tag{S.2.2}$$

čia diskretieji išvestinių operatoriai A_1^h ir A_2^h apibrėžiami kaip

$$\begin{aligned}
\partial_x U_{jk}^n &= \frac{U_{jk}^n - U_{j-1,k}^n}{h}, \\
A_1^h U_{jk} &= \frac{1}{V_{jk}} \left(-s_{j+\frac{1}{2},k}^j \partial_x U_{j+1,k}^n + s_{j-\frac{1}{2},k}^j \partial_x U_{jk}^n \right), \\
\partial_y U_{jk}^n &= \frac{U_{jk}^n - U_{j,k-1}^n}{H}, \\
A_2^h U_{jk} &= \frac{1}{V_{jk}} \left(-s_{j,k+\frac{1}{2}}^k \partial_y U_{j,k+1}^n + s_{j,k-\frac{1}{2}}^k \partial_y U_{jk}^n \right),
\end{aligned}$$

o koeficientai s:

$$\begin{aligned}
s_{j-\frac{1}{2},k}^j &= \frac{H}{2} \text{ jei } k \in \{K_1, K_2\} \text{ ir } j \in [1, J_1] \cup [J_2 + 1, J], \\
s_{j-\frac{1}{2},k}^j &= H \text{ kitur srityje } \Omega_h, \\
s_{j,k-\frac{1}{2}}^k &= \frac{h}{2} \text{ jei } j \in \{J_1, J_2\} \text{ ir } k \in [1, K_1] \cup [K_2 + 1, K], \\
s_{j,k-\frac{1}{2}}^k &= h \text{ kitur srityje } \Omega_h.
\end{aligned}$$

Koeficientai s laikomi lygūs nuliui, jei nepatenka į sritį Ω_h.

Taikant ADI metodą integravimui laike, taškams $(x_j, y_k) \in \Omega_h \setminus \partial_D$ iš (S.2.2) gaunama ADI schema

$$\begin{aligned}
\frac{U_{jk}^{n+\frac{1}{2}} - U_{jk}^n}{\tau/2} + A_1^h U_{jk}^{n+\frac{1}{2}} + A_2^h U_{jk}^n &= f_{jk}^{n+\frac{1}{2}}, \\
\frac{U_{jk}^{n+1} - U_{jk}^{n+\frac{1}{2}}}{\tau/2} + A_1^h U_{jk}^{n+\frac{1}{2}} + A_2^h U_{jk}^{n+1} &= f_{jk}^{n+\frac{1}{2}}.
\end{aligned} \tag{S.2.3}$$

Lema 2.1. *Jei uždavinio* (S.2.1) *sprendinys pakankamai glodus, tuomet ADI schemos* (S.2.3) *aproksimacijos paklaida yra* $O(\tau^2 + h^2 + H^2)$.

Kadangi operatoriai A_1^h ir A_2^h nekomutuoja, negalime taikyti klasikinės spektrinės stabilumo analizės. Lema 2.2 įrodoma konstruojant diskrečiąją skaliarinę sandaugą ir įrodant tolimesnes savybes joje.

Lema 2.2. *Diskretieji operatoriai A_1^h ir A_2^h yra simetriniai ir neneig- iamai apibrėžti.*

Teiginys 2.3. *Jei U^n yra ADI schemos* (S.2.3) *sprendinys, kai $f^n \equiv 0$ ir $g_i^n \equiv 0$, $i = 1, \ldots, 4$, tuomet galioja stabilumo įvertis*

$$\|(I + \frac{\tau}{2}A_2^h)U^n\| \leqslant \|(I + \frac{\tau}{2}A_2^h)U^0\|.$$

S.2.2 Hibridinės dimensijos modelis

Remiantis G. Panasenko rezultatais [51–53], šiame poskyryje nagrinėjamas apytikslis uždavinys (S.2.4), aproksimuojantis klasikinį šilumos laidumo uždavinį (S.2.1).

Žymėkime redukuotos dimensijos sritis

$$\begin{aligned}
L_1^\delta &= \{(x,y) : \delta \leqslant x \leqslant X_1 - \delta,\ Y_1 \leqslant y \leqslant Y_2\},\\
L_2^\delta &= \{(x,y) : X_1 \leqslant x \leqslant X_2,\ \delta \leqslant y \leqslant Y_1 - \delta\},\\
L_3^\delta &= \{(x,y) : X_2 + \delta \leqslant x \leqslant X - \delta,\ Y_1 \leqslant y \leqslant Y_2\},\\
L_4^\delta &= \{(x,y) : X_1 \leqslant x \leqslant X_2,\ Y_2 + \delta \leqslant y \leqslant Y - \delta\},
\end{aligned}$$

o jų sąjungą $\Omega^\delta = L_1^\delta \cup L_2^\delta \cup L_3^\delta \cup L_4^\delta$ (geltona sritis paveikslėlyje S.2.4).

Tarkime, kad pradinė sąlyga u^0 bei šaltinio funkcija f nepriklauso nuo x šakose L_2 ir L_4 bei nepriklauso nuo y šakose L_1 ir L_3:

$$\begin{aligned}
&u^0(x,y) = \widetilde{u}^0(y),\ \ f(x,y,t) = \widetilde{f}(y,t), (x,y,t) \in (L_2 \cup L_4) \times (0,T];\\
&u^0(x,y) = \widetilde{u}^0(x),\ \ f(x,y,t) = \widetilde{f}(x,t), (x,y,t) \in (L_1 \cup L_3) \times (0,T].
\end{aligned}$$

Tuomet U vadinsime apytiksliu (S.2.1) sprendiniu, jei tenkinama

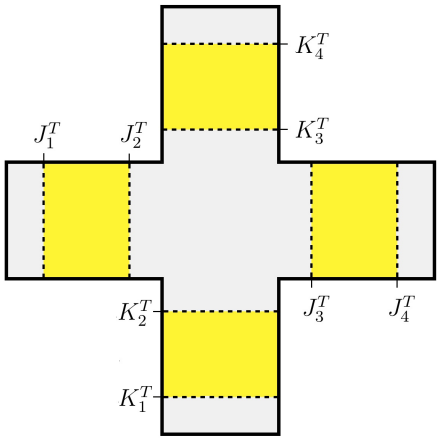

Paveikslėlis S.2.4. Sritis Ω su nurodytais dimensijos redukcijos indeksais ir geltonai pažymėtomis redukuotos dimensijos sritimis.

$$\begin{cases} \dfrac{\partial U}{\partial t} = \dfrac{\partial^2 U}{\partial x^2} + \dfrac{\partial^2 U}{\partial y^2} + f(x,y,t), & (x,y,t) \in (\Omega \setminus \Omega^\delta) \times (0,T], \\ \dfrac{\partial U}{\partial t} = \dfrac{\partial^2 U}{\partial x^2} + \widetilde{f}(x,t), & (x,y,t) \in (L_1^\delta \cup L_3^\delta) \times (0,T], \\ \dfrac{\partial U}{\partial t} = \dfrac{\partial^2 U}{\partial y^2} + \widetilde{f}(y,t), & (x,y,t) \in (L_2^\delta \cup L_4^\delta) \times (0,T], \\ U(0,y,t) = g_1(y,t), & (y,t) \in [Y_1,Y_2] \times (0,T], \\ U(x,0,t) = g_2(x,t), & (x,t) \in [X_1,X_2] \times (0,T], \\ U(X,y,t) = g_3(y,t), & (y,t) \in [Y_1,Y_2] \times (0,T], \\ U(x,Y,t) = g_4(x,t), & (x,t) \in [X_1,X_2] \times (0,T], \\ \dfrac{\partial U}{\partial \mathbf{n}} = 0, & (x,y,t) \in \partial_N \Omega \times (0,T], \\ U(x,y,0) = u^0(x,y), & (x,y) \in \Omega. \end{cases} \tag{S.2.4}$$

A. Amosov ir G. Panasenko darbe [3] įrodoma, kad šilumos laidumo modeliui tikslaus (gauto iš (S.2.1)) ir apytikslio (gauto iš (S.2.4)) sprendinio skirtumo H^1 norma priklauso nuo parametro δ. Tuo remiamasi ir šiame darbe, pereinant nuo (S.2.1) į (S.2.4), balansuojant δ tarp pakankamai didelio (tikslumui) ir pakankamai mažo (pagreitėjimui).

Toliau, ties 1D ir 2D sričių sandūromis naudojami šie vidurkinimo operatoriai:

$$S_x(U) = \frac{1}{X_2 - X_1} \int_{X_1}^{X_2} U(x, y, t) \mathrm{d}x,$$
$$S_y(U) = \frac{1}{Y_2 - Y_1} \int_{Y_1}^{Y_2} U(x, y, t) \mathrm{d}y, \tag{S.2.5}$$

taip pat ir šios jungtinumo sąlygos, nusakančios U tolydumą bei srautų konservatyvumą:

$$\begin{aligned}
U|_{x=\delta-0} &= U|_{x=\delta+0}, & \left.\frac{\partial S_y(U)}{\partial x}\right|_{x=\delta-0} &= \left.\frac{\partial U}{\partial x}\right|_{x=\delta+0}, \\
U|_{x=X_1-\delta-0} &= U|_{x=X_1-\delta+0}, & \left.\frac{\partial S_y(U)}{\partial x}\right|_{x=X_1-\delta-0} &= \left.\frac{\partial U}{\partial x}\right|_{x=X_1-\delta+0}, \\
U|_{x=X_2+\delta-0} &= U|_{x=X_2+\delta+0}, & \left.\frac{\partial S_y(U)}{\partial x}\right|_{x=X_2+\delta-0} &= \left.\frac{\partial U}{\partial x}\right|_{x=X_2+\delta+0}, \\
U|_{x=X-\delta-0} &= U|_{x=X-\delta+0}, & \left.\frac{\partial S_y(U)}{\partial x}\right|_{x=X-\delta-0} &= \left.\frac{\partial U}{\partial x}\right|_{x=X-\delta+0}, \\
U|_{y=\delta-0} &= U|_{y=\delta+0}, & \left.\frac{\partial S_x(U)}{\partial y}\right|_{y=\delta-0} &= \left.\frac{\partial U}{\partial y}\right|_{y=\delta+0}, \\
U|_{y=Y_1-\delta-0} &= U|_{y=Y_1-\delta+0}, & \left.\frac{\partial S_x(U)}{\partial y}\right|_{y=Y_1-\delta-0} &= \left.\frac{\partial U}{\partial y}\right|_{y=Y_1-\delta+0}, \\
U|_{y=Y_2+\delta-0} &= U|_{y=Y_2+\delta+0}, & \left.\frac{\partial S_x(U)}{\partial y}\right|_{y=Y_2+\delta-0} &= \left.\frac{\partial U}{\partial y}\right|_{y=Y_2+\delta+0}, \\
U|_{y=Y-\delta-0} &= U|_{y=Y-\delta+0}, & \left.\frac{\partial S_x(U)}{\partial y}\right|_{y=Y-\delta-0} &= \left.\frac{\partial U}{\partial y}\right|_{y=Y-\delta+0}.
\end{aligned} \tag{S.2.6}$$

Darbe [57], remiantis MAPDD metodu, įrodytas teorinio sprendinio U egzistavimas ir vienatis apytiksliam hibridinės dimensijos šilumos laidumo uždaviniui, apibrėžtam dvimačių sričių šakinėje struktūroje, taip pat įrodytas jungtinumo sąlygų (S.2.6) validumas.

Pažymėkime skirtingų dimensijų sričių sandūros linijas T_i^x ir T_i^y, o jų pozicijos indeksus J_i^T vertikalioms sandūroms ir K_i^T horizontalioms sandūroms, $i = 1, \ldots, 4$ (žr. pav. S.2.4). Bet kurios

į vienmatę redukuotos srities viduje vienas taškas reprezentuoja visą stulpelį ar eilutę tos pačios reikšmės taškų (dvimatėje perspektyvoje), tokiems atvejams naudojamas indekso žymėjimas $*$.

Redukuotos dimensijos sritis atitinkančius taškus žymėkime

$$\begin{aligned}
\omega_{L_1} &= \{(x_j, y_k) :\ J_1^T \leqslant j \leqslant J_2^T,\ K_1 \leqslant k \leqslant K_2\},\\
\omega_{L_2} &= \{(x_j, y_k) :\ J_1 \leqslant j \leqslant J_2,\ K_1^T \leqslant k \leqslant K_2^T\},\\
\omega_{L_3} &= \{(x_j, y_k) :\ J_3^T \leqslant j \leqslant J_4^T,\ K_1 \leqslant k \leqslant K_2\},\\
\omega_{L_4} &= \{(x_j, y_k) :\ J_1 \leqslant j \leqslant J_2,\ K_3^T \leqslant k \leqslant K_4^T\},\\
\omega_R &= \omega_{L_1} \cup \omega_{L_2} \cup \omega_{L_3} \cup \omega_{L_4}.
\end{aligned}$$

Kadangi dvimatė dimensija čia redukuojama į vienmatę, atitinkami dvimačiai tinklo taškų poaibiai pakeičiami vienmačiais

$$\begin{aligned}
\tilde{\omega}_{L_1} &= \{x_j :\ J_1^T \leqslant j \leqslant J_2^T\}, \quad \tilde{\omega}_{L_2} = \{y_k :\ K_1^T \leqslant k \leqslant K_2^T\},\\
\tilde{\omega}_{L_3} &= \{x_j :\ J_3^T \leqslant j \leqslant J_4^T\}, \quad \tilde{\omega}_{L_4} = \{y_k :\ K_3^T \leqslant k \leqslant K_4^T\},\\
&\qquad\qquad \tilde{\omega}_R = \tilde{\omega}_{L_1} \cup \tilde{\omega}_{L_2} \cup \tilde{\omega}_{L_3} \cup \tilde{\omega}_{L_4},
\end{aligned}$$

tuomet diskretusis uždavinio taškų tinklas hibridinės dimensijos atveju žymimas

$$\Omega_{h,RD} = \left((\overline{\omega}_x \times \overline{\omega}_y) \cap (\Omega \setminus \Omega^\delta)\right) \cup \tilde{\omega}_R.$$

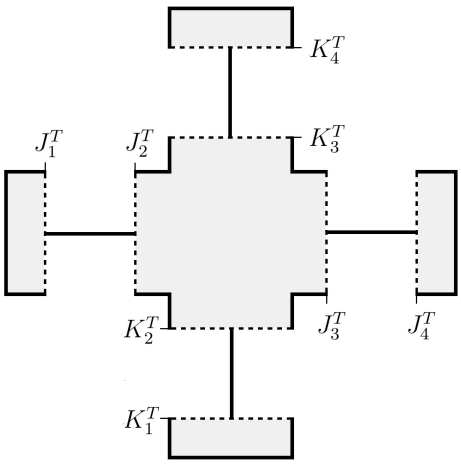

Paveikslėlis S.2.5. Sritis Ω su pažymėtais redukcijos indeksais bei redukuotos dimensijos sritimis kaip linijomis.

Vidurkinimo operatoriams (S.2.5) naudojamas jų diskretusis analogas

$$S_x^h(U_k^n) = \frac{1}{X_2 - X_1} \sum_{j=J_1}^{J_2} U_{jk}^n s_{j,k+\frac{1}{2}}^k,$$

$$S_y^H(U_j^n) = \frac{1}{Y_2 - Y_1} \sum_{k=K_1}^{K_2} U_{jk}^n s_{j+\frac{1}{2},k}^j.$$

Įtraukdami jungtinumo sąlygas (S.2.6) į ADI aproksimaciją uždaviniui (S.2.4), sukonstruotą schemą galima užrašyti kompaktine forma

$$\begin{aligned} &\frac{U_{jk}^{n+\frac{1}{2}} - U_{jk}^n}{\tau/2} + \mathcal{A}_1^h U_{jk}^{n+\frac{1}{2}} + \mathcal{A}_2^h U_{jk}^n = f_{jk}^{n+\frac{1}{2}}, \\ &\frac{U_{jk}^{n+1} - U_{jk}^{n+\frac{1}{2}}}{\tau/2} + \mathcal{A}_1^h U_{jk}^{n+\frac{1}{2}} + \mathcal{A}_2^h U_{jk}^{n+1} = f_{jk}^{n+\frac{1}{2}} \end{aligned} \tag{S.2.7}$$

su operatoriais $\mathcal{A}_1^h$ ir $\mathcal{A}_2^h$ apibrėžtais kaip

$$\mathcal{A}_1^h U = \begin{cases} A_1^h U_{jk}, & (x_j, y_k) \in \Omega_h \setminus \omega_R, \\ A_1^h U_{j*}, & j \in (J_1^T, J_2^T) \cup (J_3^T, J_4^T), \\ 0, & k \in [K_1^T, K_2^T] \cup [K_3^T, K_4^T] \\ \dfrac{1}{h^2}\Big(- S_y^H(U_{j-1}) + 2U_{j*} - U_{j+1,*}\Big), & j \in \{J_1^T, J_3^T\}, \\ \dfrac{1}{h^2}\Big(- S_y^H(U_{j+1}) + 2U_{j*} - U_{j-1,*}\Big), & j \in \{J_2^T, J_4^T\}, \end{cases}$$

$$\mathcal{A}_2^h U = \begin{cases} A_2^h U_{jk}, & (x_j, y_k) \in \Omega_h \setminus \omega_R, \\ A_2^h U_{*k}, & k \in (K_1^T, K_2^T) \cup (K_3^T, K_4^T), \\ 0, & j \in [J_1^T, J_2^T] \cup [J_3^T, J_4^T] \\ \dfrac{1}{H^2}\Big(- S_x^h(U_{k-1}) + 2U_{*k} - U_{*,k+1}\Big), & k \in \{K_1^T, K_3^T\}, \\ \dfrac{1}{H^2}\Big(- S_x^h(U_{k+1}) + 2U_{*k} - U_{*,k-1}\Big), & k \in \{K_2^T, K_4^T\}. \end{cases}$$

Perkelties algoritmo modifikacija atliekama tuo pačiu principu kaip ir praeitame skyriuje.

Reikšmėms ant skirtingų dimensijų sandūrų gaunamas uždavinys

$$\begin{pmatrix} A_{11} & A_{12} & 0 & 0 \\ A_{21} & A_{22} & A_{23} & 0 \\ 0 & A_{32} & A_{33} & A_{34} \\ 0 & 0 & A_{43} & A_{44} \end{pmatrix} \begin{pmatrix} U_{J_1^T *}^{n+\frac{1}{2}} \\ U_{J_2^T *}^{n+\frac{1}{2}} \\ U_{J_3^T *}^{n+\frac{1}{2}} \\ U_{J_4^T *}^{n+\frac{1}{2}} \end{pmatrix} = \begin{pmatrix} B_1 \\ B_2 \\ B_3 \\ B_4 \end{pmatrix}. \qquad \text{(S.2.8)}$$

Toliau turime, kad uždavinio (S.2.8) koeficientų matrica A yra diagonaliai vyraujanti. Taigi, egzistuoja vieninteliai sprendiniai $U_{J_1^T *}^{n+\frac{1}{2}}$, $U_{J_2^T *}^{n+\frac{1}{2}}$, $U_{J_3^T *}^{n+\frac{1}{2}}$, $U_{J_4^T *}^{n+\frac{1}{2}}$. Tuomet iš jų galima rasti likusias srities reikšmes ir pereiti prie kito pusžingsnio. Taigi, pastaruosius rezultatus apibendriname į žemiau pateiktą teoremą 2.4.

Teorema 2.4. *Uždaviniui* (S.2.7) *egzistuoja vienintelis sprendinys. Jį galima rasti efektyvia perkelties algoritmo modifikacija.*

Didinant redukuotos dimensijos sričių skaičių, kiekviena iš jų dvejetu padidina koeficientų matricos A rangą uždavinyje (S.2.8), o koeficientų matrica lieka trijįstrižainė.

Naudojant panašias skaliarines sandaugas bei normas kaip ir praeitame skyriuje, įrodoma, kad operatoriams $\mathcal{A}_1^h$ ir $\mathcal{A}_2^h$ galioja tolimesnės savybės.

Lema 2.5. *Diskretieji operatoriai $\mathcal{A}_1^h$ ir $\mathcal{A}_2^h$ yra simetriniai ir neneigiamai apibrėžti.*

Dėka šių savybių, įrodomas ir stabilumo įvertis specialioje energinėje normoje.

Teiginys 2.6. *Jei U^n yra ADI schemos* (S.2.7) *sprendinys, kai $f^n \equiv 0$ ir $g_i^n \equiv 0$, $i = 1, \ldots, 4$, tuomet galioja stabilumo įvertis*

$$\|(I + \frac{\tau}{2}\mathcal{A}_2^h)U^n\| \leqslant \|(I + \frac{\tau}{2}\mathcal{A}_2^h)U^0\|.$$

.

S.2.3 Testiniai uždaviniai

ADI schemos integravimo laike tikslumas

Visų pirma, ištirtas ADI schemos (S.2.3) integravimo laike tikslumas pilnam modeliui (S.2.1), naudojant tolygųjį tinklą Ω_h su parametrais $T = 1$, $X = 1$, $Y = 1$, $X_1 = Y_1 = 1/3$, $X_2 = Y_2 = 2/3$.

Pirmajame testiniame uždavinyje panaudotos funkcijos $u^0 = 0$, $f = 0$, $g_1(y,t) = (1+4t)e^{-y^2}$, $g_2(x,t) = 7te^{-4x^2}$, $g_3(y,t) = 3 - 50(y-Y_1)(y-Y_2)$, $g_4(x,t) = e^t e^{-20(x-X_1)(x-X_2)}$, o sprendinys $U(x_j, y_k, t_N)$ rastas naudojant labai mažą laiko žingsnį $\tau = 2,5 \cdot 10^{-5}$. Iš skaičiuojamųjų eksperimentų rezultatų matome antros eilės konvergavimo greitį, taigi, ADI schemos tikslumas atitinka teorinius įverčius (žr. lentelę S.2.1). Čia paklaida $e(\tau)$ ir eksperimentinis konvergavimo greitis $\rho(\tau)$ laiko momentu $t = T$ apibrėžti maksimumo normoje:

$$e(\tau) = \max_{(x_j,y_k)\in\omega} \left| U^N_{j,k} - U(x_j, y_k, T) \right|, \ \rho(\tau) = \log_2 \left(\frac{e(2\tau)}{e(\tau)} \right).$$

Lentelė S.2.1. ADI schemos sprendinio paklaidos $e(\tau)$ ir ekeperimentiniai konvergavimo greičiai $\rho(\tau)$ mažėjantiems laiko žingsniams τ pirmajam testiniam uždaviniui su $J = K = 600$.

τ	$e(\tau)$	$\rho(\tau)$
0,0008	$6,9300 \cdot 10^{-4}$	6,2786
0,0004	$1,2685 \cdot 10^{-4}$	2,4497
0,0002	$3,1460 \cdot 10^{-5}$	2,0115
0,0001	$7,4977 \cdot 10^{-6}$	2,0690

Redukuotos dimensijos modelio tikslumas

Antrajame testiniame uždavinyje tiriamas redukuotos dimensijos modelio (S.2.4) tikslumas. Nagrinėjamas skirtumas tarp pilno modelio sprendinio ir redukuotos dimensijos modelio sprendinio, kai jie abu rasti naudojant ADI schemą. Paklaida na-

grinėjama maksimumo normoje

$$e(\delta) = \max_{(x_j, y_k) \in \omega} \left| U^N_{j,k} - U^N_{j,k}(\delta) \right|.$$

Taip pat nagrinėjamos ir santykinės paklaidos

$$e_r = \frac{e(\delta)}{\left| U^N_{j^*,k^*} \right|} \cdot 100\%,$$

čia j^*, k^* – indeksai tinklo taško, kuriame rasta paklaida. Lentelėje S.2.2 pateikiami antrojo testinio uždavinio rezultatai.

Lentelė S.2.2. Antrojo testinio uždavinio rezultatams gauti panaudotos pirmojo testinio uždavinio funkcijos bei parametrai. Čia laikas pateikiamas sekundėmis, o žymėjimas $\delta = \delta^*$ atitinka pilną modelį.

δ	$e(\delta)$	e_r	laikas
δ^*	–	–	9.4
0,175	$2,242 \cdot 10^{-3}$	0,094%	8,2
0,150	$4,668 \cdot 10^{-3}$	0,178%	7,4
0,125	$9,194 \cdot 10^{-3}$	0,353%	6,7
0,100	$2,057 \cdot 10^{-2}$	0,792%	6,0
0,075	$4,682 \cdot 10^{-2}$	1,806%	5,3
0,050	$9,699 \cdot 10^{-2}$	3,747%	4,6
0,025	$2,082 \cdot 10^{-1}$	8,051%	3,9

Kuo didesnėje srities dalyje sumažinamas dimensijų skaičius, tuo didesnį pagreitėjimą matome, kadangi vienmatėse dalyse pakanka apskaičiuoti vienos eilutės/stulpelio reikšmes. Taigi, lentelėje S.2.2 matomo pagreitėjimo pagrindinė priežastis – mažesnis operacijų kiekis. Išsamesnei diskusijai apie teorinius paklaidos pagal δ įverčius žr. [3, 57].

S.2.4 Išvados

Baigtinių tūrių metodu aproksimuoti erdviniai diferencialiniai operatoriai ir neklasikinės jungtinumo sąlygos tarp 2D ir 1D sričių. ADI schema pritaikyta hibridinės dimensijos uždavinio

integravimui laike. Uždavinio skaitiniam išsprendimui išvesta efektyvi perkelties algoritmo modifikacija. Skaitinių eksperimentų rezultatai patvirtina teorinius įverčius bei išvadą, kad hibridinės dimensijos modeliai gali būti efektyviai pritaikyti simuliuoti šilumos laidumo modelius plačio- je sričių ir koeficientų klasėje.

S.3 Klampaus skysčio tekėjimas elastingu vamzdeliu

S.3.1 Uždavinio aptarimas

Šiame skyriuje iš skaitinių metodų pusės analizuojamas vienas iš uždavinių, su kuriais susidurta projekte "Daugiaskalis matematinis ir kompiuterinis srautų modeliavimas tinkluose: taikymai širdies ir kraujagyslių ligų gydymui"[1].

Sprendžiama ketvirtos eilės dalinių išvestinių lygtis su pastoviais koeficientais c_i:

$$c_1 v_{tt} + c_2 v_{xxtt} + c_3 v_t + c_4 v_{xxt} + c_5 v_{xxxx} + c_6 v_{xx} + c_7 v = 0, \quad \text{(S.3.1)}$$

čia v indeksas žymi dalinę išvestinę. Ieškomas sprendinys laiko momentu T, panaudojant pradines ir kraštines sąlygas, kurios bus pateiktos vėliau.

Ši lygtis gauta iš [56], nagrinėjant klampaus skysčio tekėjimą vamzdeliu su elastinga sienele. Jos sprendinys aproksimuoja vidutinį skysčio tekėjimo greitį per vamzdelio skerspjūvį, taigi, modelio erdvinė dimensija yra vienmatė. Nors šį modelį irgi galima laikyti redukuotos dimensijos modeliu, čia ideologija skiriasi nuo ankstesnių skyrių – dimensija vienmatė visoje srityje, todėl nelieka jungtinumo sąlygų.

S.3.2 Schemos sudarymas ir jos savybės

Lygties (S.3.1) tikslaus sprendinio skaitinę aproksimaciją taške

[1] Projekto nr. 09.3.3-LMT-K-712-17-0003, www.hemodynamics.mif.vu.lt

$(x_i, t_n) = (ih, n\tau)$ žymėsime U_i^n, čia h ir τ – žingsnių dydžiai, kuriems galioja

$$i = 0, \ldots, N_h,\ h = L/N_h,$$
$$n = 0, \ldots, N_\tau,\ \tau = T/N_\tau,$$

kai L – uždavinio srities Ω ilgis.

Diferencialinius narius lygtyje (S.3.1) aproksimuokime taip: lyginės eilės išvestines centriniais skirtumais, o pirmosios eilės išvestines vienpusiais priekiniais skirtumais. Paveikslėlyje S.3.1 vaizduojama supaprastinta šios diskretizacijos vizualizacija.

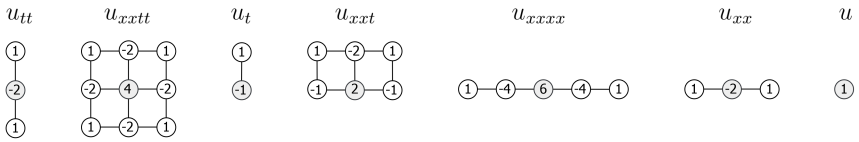

Paveikslėlis S.3.1. Lygties (S.3.1) diferencialinių narių diskretizacijos vizualizacija. Apskritimuose esantys skaičiai atitinka tinklo taškų svorinius koeficientus aproksimacijoje.

Skaičiuojamoji molekulė (šablonas) taške U_i^n vaizduojama pav. S.3.2.

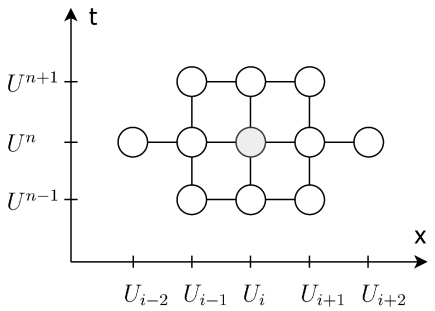

Paveikslėlis S.3.2. Skaičiuojamoji molekulė (schemos šablonas).

Paprastumo dėlei naudojami šie žymėjimai:

$$m_1 = \frac{c_1}{\tau^2},\ m_2 = \frac{c_2}{h^2\tau^2},\ m_3 = \frac{c_3}{\tau},\ m_4 = \frac{c_4}{h^2\tau},$$
$$m_5 = \frac{c_5}{h^4},\ m_6 = \frac{c_6}{h^2},\ m_7 = c_7.$$

Pritaikę skaičiuojamąją molekulę laiko sluoksnio U^n taške, gauname sąryšį tarp trijų naujojo laiko sluoksnio U^{n+1} taškų. Taigi, perėjimas nuo vieno laiko sluoksnio į kitą susiveda į trijstrižainės matricos sprendimą.

Schemos stabilumas nagrinėjamas naudojant klasikinę Furjė stabilumo analizę. Į stabilumo įverčius įeina sudėtinga koeficientų c_i kombinacija, todėl informatyvias stabilumo sąlygas galima išvesti nebent atskiriems modelio atvejams. Pavyzdžiui, projekte nagrinėj- amam kraujo tekėjimo elastinga arteriole uždaviniui pagrindžiamas referentinis stabilumo įvertis $\tau \leqslant h^2/8$, kai charakteristiniai erdvės ir laiko dydžiai – 0,1 mm ir 1 s.

Taikant klasikinį Teiloro skleidinių metodą parodoma, kad schemos aproksimacijos paklaida yra $O(h^2 + \tau)$ dydis.

Naudojamos šios pradinės ir kraštinės sąlygos:

$$\begin{aligned} &U(x,0) = u_0(x),\ U_t(x,0) = u_1(x), \\ &U(0,t) = D_1(t),\ U(L,t) = D_2(t), \\ &U_{xx}(0,t) = N_1(t),\ U_{xx}(L,t) = N_2(t). \end{aligned} \tag{S.3.2}$$

Ant krašto, vietoje antrosios eilės išvestinės taip pat galima formuluoti ir pirmosios eilės išvestinės sąlygą, abiem atvejais schemos tikslumas išlieka $O(h^2 + \tau)$. Skaitiniai eksperimentai parodė, kad su antrosios eilės išvestine sprendinio paklaida yra šiek tiek mažesnė nei su pirmosios eilės išvestine.

Toliau pateikiami du testiniai uždaviniai, pagrindžiantys sukonstruotos schemos tikslumą. Šiuose testuose vidutinis greitis U ieškomas su charakteristiniais dydžiais 1 mm ir 1 s. Pavyzdžiui, kraujo tekėjimui vieno milimetro ilgio arteriole su elastinga sienele rasti tokie koeficientai (pateikiami suapvalinti):

c_1	c_2	c_3	c_4	c_5	c_6	c_7
$9 \cdot 10^{-38}$	$-2 \cdot 10^{-42}$	$4 \cdot 10^{-2}$	$-2 \cdot 10^{1}$	$8 \cdot 10^{1}$	$-6 \cdot 10^{-2}$	$4 \cdot 10^{-4}$

Šiuo atveju galime laikyti, kad koeficientai c_1 ir c_2 lygūs nuliui, kadangi jų indėlis į sprendinį nereikšmingas.

Testiniuose uždaviniuose naudojami paklaidos $e(h,\tau)$ ir eksperimentinių konvergavimo greičių $\rho_\tau(\tau)$, $\rho_h(h)$ apibrėžimai mak-

simumo normoje:

$$e(h,\tau) = \max_i \left| U_i^{N_\tau} - U(x_i, T) \right|,$$

$$\rho_h(h) = \log_2 \left(\frac{e(2h,\tau)}{e_h(h,\tau)} \right), \rho_\tau(\tau) = \log_2 \left(\frac{e(h,2\tau)}{e(h,\tau)} \right).$$

Čia $U(x_i, T)$ – palyginamasis tikslus sprendinys, rastas su mažais žingsnių dydžiais.

Pirmas testinis uždavinys

Pirmajame testiniame uždavinyje atliktas Rungės testas, siekiant apskaičiuoti eksperimentinius konvergavimo greičius pagal erdvę ir laiką. Naudojamos funkcijos $U(x,0) = U_t(x,0) = 0$, $U(0,t) = U(L,t) = 1 - \cos t$, $U_{xx}(0,t) = U_{xx}(L,t) = \sin t$. Lentelėje S.3.1 pateikiamas sąryšis tarp paklaidų $e(h,\tau)$ ir eksperimentinių konvergavimo greičių $\rho_h(h)$ su mažėjančiais erdvės žingsniais h. Šie skaičiavimai atlikti naudojant $\tau = 2^{-2} \cdot 10^{-6}$. Palyginamasis sprendinys $U(x_i, T)$ rastas su $h = 2^{-6} \cdot 10^{-1}$.

h	$e(h)$	$\rho_h(h)$
0,1	$2,3394 \cdot 10^{-5}$	1,9983
0,05	$5,8555 \cdot 10^{-6}$	2,0007
0,025	$1,4632 \cdot 10^{-6}$	2,0047
0,0125	$3,6460 \cdot 10^{-7}$	2,0188

Lentelė S.3.1. Pirmojo testinio uždavinio paklaidos ir eksperimentiniai konvergavimo greičiai pagal erdvę laiko momentu $T = 0,1$ su įvairiais h.

Lentelėje S.3.2 pateikiamos paklaidos ir eksperimentiniai konvergavimo greičiai pagal laiko kintamąjį su įvairiais τ. Šie skaičiavimai atlikti su $h = 2^{-2} \cdot 10^{-1}$, palyginamasis sprendinys rastas su $\tau = 2^{-7} \cdot 10^{-4}$.

Iš lentelėse S.3.1 ir S.3.2 pateiktų rezultatų matome, kad eksperimentiniai konvergavimo greičiai atitinka teorinius tikslumo įverčius.

τ	$e(\tau)$	$\rho_\tau(\tau)$
0,0001	$2,3969 \cdot 10^{-7}$	1,0109
0,00005	$1,1894 \cdot 10^{-7}$	1,0228
0,000025	$5,8537 \cdot 10^{-8}$	1,0461
0,0000125	$2,8327 \cdot 10^{-8}$	1,0406

Lentelė S.3.2. Pirmojo testinio uždavinio paklaidos ir eksperimentiniai konvergavimo greičiai pagal laiką laiko momentu $T = 0,1$ su įvairiais τ.

Antras testinis uždavinys

Šiame teste uždavinio (S.3.1), (S.3.2) tikslus sprendinys žinomas. Tarkime, kad jis užrašomas eksponentine trigonometrine forma $\tilde{U} = e^{i(kx+t)} = \cos(kx+t) + i\sin(kx+t)$. Iš čia seka pradinės ir kraštinės sąlygos:

$$\tilde{U}(x,0) = e^{ikx},\ \tilde{U}_t(x,0) = ie^{ikx},$$
$$\tilde{U}(0,t) = e^{it},\ \tilde{U}(L,t) = e^{i(kL+t)},$$
$$\tilde{U}_{xx}(0,t) = -k^2e^{it},\ \tilde{U}_{xx}(L,t) = -k^2e^{i(kL+t)}.$$

Parametras k apskaičiuojamas įstatant $\tilde{U}$ į (S.3.1). Jo radimui gauname lygtį

$$k^4c_5 + k^2(c_2 - ic_4 - c_6) + (-c_1 + ic_3 + c_7) = 0$$

su keturiais kompleksiniais sprendiniais k_1, k_2, k_3, k_4. Nagrinėjamam koeficientų c_i rinkiniui turėsime

$$k_1 = 0.3546 - 0.3526i = -k_2,$$
$$k_3 = 0.0004 + 0.0483i = -k_4.$$

Žymėkime V_i^* uždavinio (S.3.1) sprendinius, gautus su atitinkamais k_i, tačiau ant krašto vietoje antrosios eilės išvestinės užduokime pirmosios eilės išvestinės kraštinę sąlygą. Lentelėje S.3.3 palyginamos V_1 ir V_1^* paklaidos skirtingais laiko momentais. Šie sprendiniai apskaičiuoti naudojant $h = 2^{-1} \cdot 10^{-1}$ ir $\tau = 2^{-2} \cdot 10^{-3}$.

Lentelėje S.3.3 matome, kad formuluojant antrosios eilės išvestinės kraštinę sąlygą vietoje pirmosios eilės išvestinės, paklaidos mažesn-ės.

T	e: $Re(V_1)$	e: $Re(V_1^*)$	e: $Im(V_1)$	e: $Im(V_1^*)$
1	$6,4903 \cdot 10^{-7}$	$6,3309 \cdot 10^{-6}$	$1,8334 \cdot 10^{-6}$	$5,1999 \cdot 10^{-6}$
2	$1,1960 \cdot 10^{-6}$	$2,6706 \cdot 10^{-6}$	$1,5366 \cdot 10^{-6}$	$8,0973 \cdot 10^{-6}$
3	$1,9371 \cdot 10^{-6}$	$7,2964 \cdot 10^{-6}$	$1,3013 \cdot 10^{-7}$	$4,0185 \cdot 10^{-6}$
4	$9,0119 \cdot 10^{-7}$	$6,9911 \cdot 10^{-6}$	$1,7234 \cdot 10^{-6}$	$4,3136 \cdot 10^{-6}$
5	$9,6898 \cdot 10^{-7}$	$2,9784 \cdot 10^{-6}$	$1,6895 \cdot 10^{-6}$	$8,1424 \cdot 10^{-6}$
10	$1,3468 \cdot 10^{-6}$	$7,8812 \cdot 10^{-6}$	$1,4050 \cdot 10^{-6}$	$2,7121 \cdot 10^{-6}$

Lentelė S.3.3. Sprendinių V_1 ir V_1^* paklaidų e realiosios ir menamasios dalys įvairiais laiko momentais T.

S.3.3 Alternatyvios schemos aptarimas

Nagrinėkime kitokią lygties (S.3.1) diferencialinių narių diskretizaciją – pirmosios eilės išvestinėms naudokime centrinių skirtumų formulę vietoje vienpusių skirtumų (žr. paveikslėlį S.3.3).

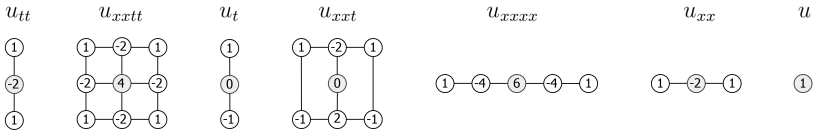

Paveikslėlis S.3.3. Lygties (S.3.1) diferencialinių narių alternatyvios diskretizacijos vizualizacija. Apskritimuose esantys skaičiai atitinka tinklo taškų svorinius koeficientus aproksimacijoje.

Skaičiuojamosios molekulės forma išlieka ta pati kaip ir pav. S.3.2.

Taikydami klasikinį Teiloro skleidinių metodą nesunkiai gauname, kad šios schemos aproksimacijos tikslumas yra $O(h^2+\tau^2)$, taigi, pagal laiką eilė vienetu aukštesnė nei ankstesnės schemos atveju. Tačiau taikydami klasikinę Furjė stabilumo analizę gauname, kad stabilumo apribojimai žymiai griežtesni. Pavyzdžiui, 1 mm ilgio arteriolei su erdvės žingsniu $h = 0,1$ mm reiktų naudoti $\tau < 10^{-22}$ s, kad schema būtų stabili.

Nesunkiai galime pastebėti to priežastį – yra gerai žinoma, kad Ričardsono schema paraboliniams uždaviniams yra besąlygiškai nestabili. Mūsų atveju turime ir parabolinius, ir hiperbolinius narius. Bendrai hiperboliniai nariai gali iš dalies regu-

liarizuoti šį nestabilumą, tačiau mūsų nagrinėjamuose uždaviniuose ši įtaka nėra pakankamai didelė, kadangi hiperboliniai ir paraboliniai nariai skiriasi net keliomis eilėmis.

Siekiant išvengti Ričardsono schemos kuriamo nestabilumo ir išlaikyti $O(h^2 + \tau^2)$ aproksimacijos tikslumą, vienas iš gerų kandidatų galėtų būti Diuforto-Frankelio schema [5]. Ji turi besąlyginio stabilumo privalumą, tačiau kai kuriais atvejais kelia papildomus reikalavimus kraštinėms sąlygoms. Be to, jos aproksimacijos tikslumas sąlyginis [23].

Pasiekti $O(h^2+\tau^2)$ tikslumą turėtų būti įmanoma ir sudėtingesnėmis schemomis, tačiau šis įdomus klausimas paliekamas ateities tyrimams. Poskyryje S.3.2 sukonstruota schema yra laikoma pakankamai efektyvia šiuometiniams praktiniams taikymams.

S.3.4 Išvados

Šiame skyriuje nagrinėjamam ketvirtos eilės dalinių išvestinių lygties uždaviniui parodyta, kad laiko išvestinę aproksimuodami centriniais skirtumais gauname $O(\tau^2)$ paklaidą, o aproksimuodami vienpusiais priekiniais skirtumais gauname $O(\tau)$ paklaidą. Tačiau tuo atveju, kai dominuoja paraboliniai nariai, naudodami centrinius skirtumus susiduriame su žymiai didesniais stabilumo apribojimais. Hiperboliniai nariai šį nestabilumą iš dalies reguliarizuoja, tačiau nepakankamai praktiniams taikymams. Aktualioms skysčių dinam-ikos simuliacijoms pasirinkome mažiau tikslią, tačiau mažesnių stabilumo apribojimų schemą.

Eksperimentiškai patvirtinta, kad ant srities krašto formuluojant antrosios eilės išvestinės kraštinę sąlygą, gaunama mažesnė paklaida nei formuluojant pirmosios eilės išvestinės kraštinę sąlygą.

S.4 Bendrosios išvados

Apibendrinant pagrindinius disertacijos rezultatus, dviems hibridinės dimensijos šilumos laidumo modeliams su neklasikinėmis jungtinumo sąlygomis buvo sukonstruota ir pagrįsta baigtinių tūrių kintamųjų krypčių schema. Baigtinių tūrių metodas pri-

taikytas erdvinei diskretizacijai, o kintamųjų krypčių metodas – integravimui laike.

Siekiant išspręsti hibridinės dimensijos (3D-1D ir 2D-1D) šilumos laidumo modelius skaitiniais metodais ir įtraukti neklasikines jungtinumo sąlygas, modifikuotas klasikinis perkelties algoritmas. Įrodyta, kad hibridinės dimensijos modeliams, sprendžiamiems sukonstruota schema, egzistuoja vienintelis skaitinis sprendinys. Hibridinės dimensijos atveju įrodytos kelios svarbios diskrečiųjų diferencialinių operatorių savybės.

Skaitinių eksperimentų rezultatai patvirtino teorinę paklaidų analizę. Skaičiavimo trukmės palyginimas patvirtino teorinę išvadą, kad hibridinės dimensijos modeliai gali būti efektyviai pritaikoi šilumos laidumo lygties modeliams plačioje sričių bei koeficientų klasėje. Įvairiems dimensijos redukcijos parametrams palyginti vaizdiniai rezultatai patvirtino pateikto algoritmo tinkamumą praktiniam panaudojimui.

Acknowledgements

Reflecting on the path that led to this dissertation, I am glad to have an opportunity to express my gratitude to people that played a characteristic role in shaping it.

I am mostly grateful to my supervisor Raimondas Čiegis for showing the ways of a professional mathematician and to coauthors Konstantinas Pileckas and Grigory Panasenko for opening me a door to their scientific field.

I am sincerely grateful to Mindaugas Skujus, Kristina Kaulakytė, Paulius Drungilas and Ramūnas Garunkštis for keeping my motivation for Mathematics prior to the PhD studies.

Finally, I wish to thank my closest relatives Jūra, Gintaras, Lina, Gediminas, Virgis, Angelė and friends Mindaugas, Greta for their continuous love and support.

Vytenis Šumskas
Vilnius
February 2022

Curriculum Vitae

Vytenis Šumskas

vytenis.sumskas@gmail.com

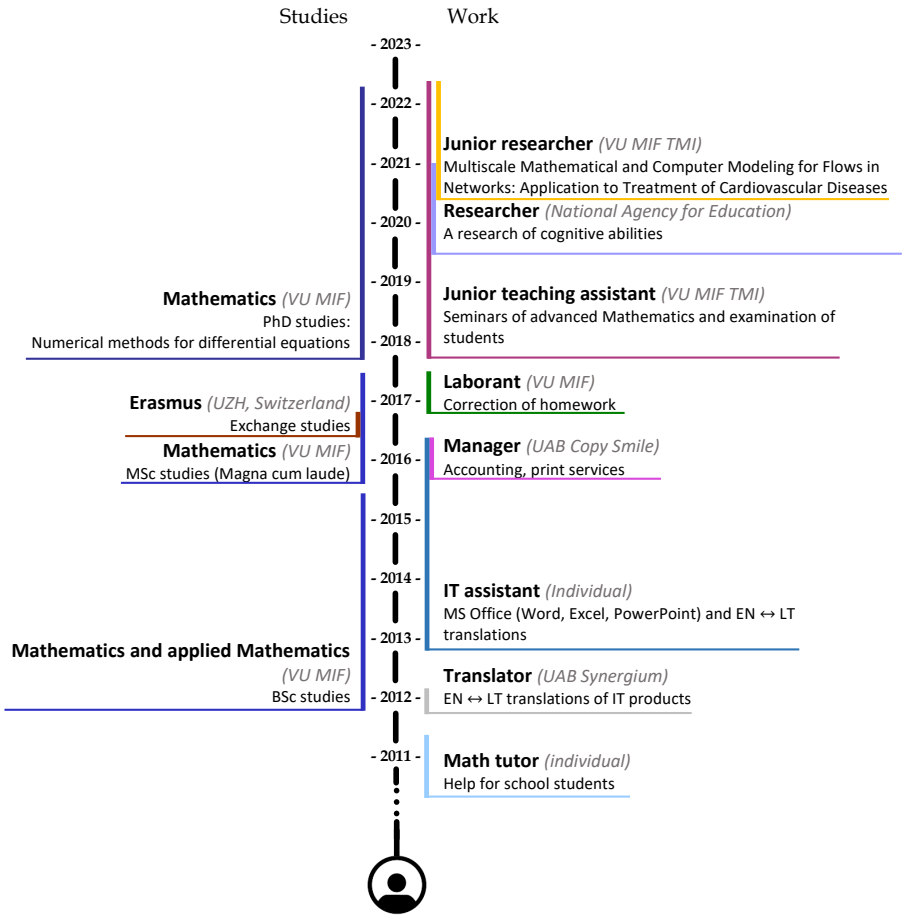

1992.11.26, Panevėžys

Languages: English – C1, German – A2, Lithuanian – native.
Certificates: Leadership and teamwork (61 h.), Public speaking (6 h.), Responsible conduct of research (30 h.), Integrity in academic publishing (15 h.), Activation of inner powers (8 h.), Lucid dreaming (50 h.).

Publications by the author

1. R. Čiegis, G. Panasenko, K. Pileckas, V. Šumskas. ADI scheme for partially dimension reduced heat conduction models. *Computers and Mathematics with Applications*, **80**:1275-1286, 2020, https://doi.org/10.1016/j.camwa.2020.06.012.

2. V. Šumskas, R. Čiegis. Finite volume ADI scheme for hybrid dimension heat conduction problems set in a cross-shaped domain. *Lithuanian Mathematical Journal*, 2022, https://doi.org/10.1007/s10986-022-09561-0.

Vilnius University Press
9 Saulėtekio Ave., Building III, LT-10222 Vilnius
Email: info@leidykla.vu.lt, www.leidykla.vu.lt
bookshop.vu.lt, journals.vu.lt
Print run of 20 copies